Optimization of purification and characterisation of over-expressed rotavirus capsid protein VP6

by

SAMUEL MAPHALLE KGOKOLO

submitted in accordance with the requirements
for the degree of

MASTER OF SCIENCE

in the subject

LIFE SCIENCES

at the

UNIVERSITY OF SOUTH AFRICA

SUPERVISOR: PROF S GILDENHUYS

CO-SUPERVISOR: DR N PARBHOO

DECEMBER 2017

Dedication

To my mother, who made all good things in my life possible, and taught me to believe that in God everything is possible.

UNISA | college of agriculture and environmental sciences

Declaration

Name: Samuel Maphalle Kgokolo___

Student number: __55765726__

Degree: Master in Life Sciences_

Optimization of purification and characterisation of over-expressed rotavirus capsid protein VP6.

I, Samuel Maphalle Kgokolo hereby declare that the dissertation which I hereby submit for the degree of MSc in Life Sciences at the University of South Africa, is my own work and has not previously been submitted by me for a degree at this or any other institution.

I declare that the dissertation does not contain any written work presented by other persons whether written, pictures, graphs or data or any other information without acknowledging the source.

I declare that where words from a written source have been used the words have been paraphrased and referenced and where exact words from a source have been used the words have been placed inside quotation marks and referenced.

I declare that I have not copied and pasted any information from the Internet, without specifically acknowledging the source and have inserted appropriate references to these sources in the reference section of the dissertation.

I declare that during my study I adhered to the Research Ethics Policy of the University of South Africa, received ethics approval for the duration of my study prior to the commencement of data gathering, and have not acted outside the approval conditions.

I declare that the content of my dissertation has been submitted through an electronic plagiarism detection program before the final submission for examination.

Student signature: _____ Date: 6 December 2017_

Acknowledgements

I would like to express my sincere gratitude to my supervisor Prof. Samantha Gildenhuys for her patience and infinite support over the last few years.

I would like to give thanks to Dr. Nishal Parbhoo for extending knowledge and skill on the project and beyond.

To my family, for the love and support I needed to get through the toughest times.

To Bonnie Russell and Tonny Mathebula for being there when I needed help, and providing a second opinion on protocols and techniques.

To Prof. SL Lebelo, for his support and understanding

To UNISA's department of life and consumer sciences staff who are always willing to give advice and support, and

To CAES laboratory staff, for assistance in providing a safe and clean lab area with well-maintained equipment.

Fellow

THANK YOU.

Abstract

Rotavirus is responsible for the death of many children annually, and current vaccines have lower efficiency in developing countries. A reverse translated consensus gene sequence of the rotavirus VP6 cloned into a pET-28a(+) plasmid was used to transform BL21 and KRX *Escherichia coli* cells. Optimal expression of soluble protein was induced in KRX cells by adding 0.05% *L*-rhamnose and 0.0001 M IPTG, with an incubation temperature of 25ºC for 6 h. VP6 was purified by combining anion exchange chromatography followed by affinity chromatography. Far-UV circular dichroism and intrinsic fluorescence were used as probes to assess the native structure of VP6 and structural in the presence of a denaturant, high sodium chloride concentrations and varying temperatures. The 0.2 M sodium chloride had an impact on the VP6's tertiary structure and also influenced the proteins conformational changes as detected during thermal unfolding to 90ºC. Although treatment with 3 M urea showed tertiary structural changes no secondary structural loss occurred due to the presence of a denaturant.

Key words: chromatography, circular dichroism, *Escherichia coli,* fluorescence, plasmid, protein conformation, protein expression, purification, rotavirus, VP6.

Table of contents

Abbreviations ..... *viii*

List of figures ..... *x*

List of buffers and composition ..... *xii*

Chapter 1: Introduction *1*

1.1. Rotavirus structure and genome composition **1**

1.2. Rotavirus replication cycle **3**

1.3. Rotavirus capsid proteins and non-structural proteins **6**

1.3.1. Outer layer proteins 6

1.3.2. Middle layer protein 6

1.3.3. Inner core proteins 6

1.3.4. Non-structural proteins 7

1.4. Rotavirus serotype and subgroup classification **7**

1.5. Structure of the VP6 protein **8**

1.6. Rotavirus vaccines **10**

1.7. Expression and purification of recombinant VP6 protein **11**

1.8. Aims and objectives **14**

Chapter 2: Experimental procedure *15*

2.1. Materials **15**

2.2. Bioinformatics **15**

2.3. Cell transformation and over-expression of VP6 ..... **18**

2.4. SDS-PAGE **19**

2.5. Ammonium sulphate protein precipitation. **20**

2.6. Protein purification **20**

2.6.1. HisTag affinity chromatography 20

2.6.2. Ion exchange chromatography 21

2.7 Absorbance spectroscopy **21**

2.8. Fluorescence **22**

2.9 Circular dichroism **22**

2.10. Thermal unfolding. **23**

2.11. Software and equations used for structural analysis, sequence analysis and data fitting **23**

2.11.1. Calibration curve 23

2.11.2 Mean residue ellipticity 23

2.11.3 Software 24

Chapter 3: Results *25*

3.1. Protein over-expression **25**

3.1.1. Optimizing inducer concentration 25

3.1.2 Optimisation of post-induction incubation temperature 29

3.1.3 Assessment of optimum induction growth time for protein over-expression 30

3.2. Protein purification **34**

3.2.1 Nickel affinity (HisTag) chromatography 36

3.2.2 Salting out 39

3.2.3 Anion exchange chromatography 39

3.2.4 Purification using affinity and ion exchange chromatography 51

3.3. Protein concentration determination **61**

3.4. Purification of VP6 with removal of nucleotides **61**

3.5. Structural characterisation of purified VP6 ..... **65**

3.6 Thermal unfolding **69**

3.7 Effect of urea and sodium chloride on the secondary and tertiary structure of VP6 ..... **71**

Chapter 4: Discussion *75*

Chapter 5: Conclusion *80*

Chapter 6: References *81*

Chapter 7: Appendices *96*

Abbreviations

A_{280}	absorbance at 280 nm
Ab	antibody
APS	ammonium persulphate
AS	ammonium sulphate
bp	base pair
CD	circular dichroism
CV	column volume
kDa	kiloDalton
DEAE	diethylaminoethyl
DLP	double layered particle
DNase I	deoxyribonuclease I
ds	double-stranded
DTT	dithiothreitol
ε	molar extinction coefficient
Far-UV CD	far-ultraviolet circular dichroism
IFN	interferon
Ig	immunoglobulin
IPTG	isopropyl β-D-1-thiogalactopyranoside
LB	Luria-Bertani
MCS	multiple cloning sites
MOPS	3-(N-morpholino) propanesulfonic acid
MWM	molecular weight marker
NSP	non-structural proteins
OD_{600}	optical density at 600 nm
PDB	protein data bank
pI	isoelectric point
RER	rough endoplasmic reticulum
rpm	revolutions per minute
RV	rotavirus
RVA	group A rotavirus
SDS-PAGE	sodium-dodecyl sulphate polyacrylamide gel electrophoresis
SUMO	small ubiquitin-like modifier

TEMED	*N, N, N', N'*-tetramethylethylenediamine
VLP	virus-like particle
VP	viral protein

The IUBMB-IUPAC abbreviations were used.

List of figures

Figure 1-1: Rotavirus structure and composition 2

Figure 1-2: Electrophoresis gel migration pattern of 11 rotavirus dsRNA genome segments and the proteins that they form 4

Figure 1-3: Rotavirus replication cycle 5

Figure 1-4: Ribbon diagram of the rotavirus VP6 protein 9

Figure 2-1: The resultant VP6 consensus sequence 16

Figure 2-2: pET-28a(+) vector map 17

Figure 3-1: Optimisation of inducer concentration observed in whole cell lysates of BL21 and KRX cells 26

Figure 3-2: Effect of IPTG and L-rhamnose concentrations on expression of soluble versus insoluble VP6 in KRX cells 27

Figure 3-3: Effect of IPTG concentration on expression of VP6 in BL21 cells 28

Figure 3-4: Effect of post-induction temperature on over-expression VP6 in BL21 cells 31

Figure 3-5: Effect of post-induction temperature on over-expression of VP6 in KRX cells 32

Figure 3-6: Effect of induction growth time on over-expression of VP6 in BL21 cells 33

Figure 3-7: Effect of induction growth time on over-expression of VP6 in KRX cells 35

Figure 3-8: Affinity (HisTag) chromatography purification of VP6 using a sodium phosphate buffer and a gradient elution of 0.01 M to 0.3 M imidazole 37

Figure 3-9: Affinity (HisTag) chromatography purification of VP6 using a sodium phosphate buffer, 6 M urea, and a gradient elution of up to 0.3 M imidazole 38

Figure 3-10: Protein precipitation using ammonium sulphate. 40

Figure 3-11: Anion (DEAE Sepharose) exchange chromatography purification of VP6 using a MOPS buffer with a gradient elution of up to 0.3 M sodium chloride 42

Figure 3-12: Anion (DEAE Sepharose) exchange chromatography purification of VP6 using a sodium phosphate buffer and a gradient elution of up to 1 M sodium chloride. 43

Figure 3-13: Anion (DEAE Sepharose) exchange chromatography purification of VP6 using a sodium phosphate buffer and a gradient elution of up to 0.7 M sodium chloride 44

Figure 3-14: Anion (DEAE Sepharose) exchange chromatography purification of VP6 using a sodium phosphate buffer and a gradient elution of up to 0.1 M sodium chloride at pH 5.0. 46

Figure 3-15: Anion (DEAE Sepharose) exchange chromatography purification of VP6 using a sodium phosphate buffer and varying pH for elution 47

Figure 3-16: Anion (DEAE Sepharose) exchange chromatography purification of VP6 using a sodium phosphate buffer and sodium chloride elution using 0.2 M, 0.3 M, 0.5 M and 0.7 M concentrations 49

Figure 3-17: Anion (DEAE Sepharose) exchange chromatography purification of VP6 using a sodium phosphate buffer and a gradient elution of up to 0.2 M sodium chloride 50

Figure 3-18: Partial purification of VP6 using anion (DEAE Sepharose) exchange chromatography with a gradient elution of up to 0.2 M sodium chloride 52

Figure 3-19: Affinity (HisTag) chromatography purification of VP6 using a sodium phosphate buffer and a gradient elution from 0.01 M up to 0.2 M imidazole 54

Figure 3-20: Affinity (HisTag) chromatography purification of VP6 using a sodium phosphate buffer and a gradient elution from 0.01 M up to 0.1 M imidazole 55

Figure 3-21: Affinity (HisTag) chromatography purification of VP6 using a sodium phosphate buffer and a 15 column volumes gradient elution from 0.01 M up to 0.1 M imidazole 56

Figure 3-22: Anion (DEAE Sepharose) exchange chromatography partial purification of VP6 using a gradient elution of up to 0.2 M sodium chloride, trial 2 57

Figure 3-23: Affinity (HisTag) chromatography purification of VP6 using a sodium phosphate buffer and a 15 column volume gradient elution from 0.01 M up to 0.1 M imidazole, trial 2 . 59

Figure 3-24: Affinity (HisTag) chromatography purification of VP6 using a sodium phosphate buffer and a 20 column volumes gradient elution from 0.01 M up to 0.055 M imidazole 60

Figure 3-25: Buffer exchange using HiPrep desalting column 62

Figure 3-26: Absorbance spectrum of purified rotavirus VP6 63

Figure 3-27: Partial purification of VP6 using anion (DEAE Sepharose) exchange chromatography with a gradient elution of up to 0.3 M sodium chloride 64

Figure 3-28: Affinity (HisTag) chromatography purification of VP6 using a sodium phosphate buffer and a 20 column volumes gradient elution from 0.01 M up to 0.055 M imidazole, trial 2 66

Figure 3-29: Absorbance spectrum of purified rotavirus VP6 67

Figure 3-30: Native VP6 assessed by far-UV CD and Fluorescence 68

Figure 3-31: Thermal unfolding of VP6 monitored by far-UV CD and intrinsic fluorescence 70

Figure 3-32: Reversibility of thermally unfolded VP6 monitored by Far-UV circular dichroism and intrinsic fluorescence 72

Figure 3-33: Effect of urea and sodium chloride on the secondary and tertiary structure of VP6 74

Appendix A: SDS-PAGE analysis of VP6 96

Appendix B: Circular dichroism during thermal unfolding of VP6 97

Appendix C: Fluorescence thermal unfolding of VP6 excited at 280 nm 98

Appendix D: Globular diagram of rotavirus VP6 99

List of buffers and composition

Buffer A: 0.05 M sodium phosphate (dibasic) buffer, pH 7.04, containing 0.08 M sodium chloride, 0.01 M imidazole, and 0.02% (w/v) sodium azide.

Buffer B: 0.05 M sodium phosphate (dibasic) buffer, pH 7.04, containing 0.08 M sodium chloride, and 0.02% (w/v) sodium azide.

Buffer C: 0.03 M MOPS buffer, pH 7.04, containing, 0.02% (w/v) sodium azide.

Buffer D: 0.05 M sodium phosphate (dibasic) buffer, pH 7.04, containing 0.02 M sodium chloride, and 0.02% (w/v) sodium azide.

Buffer E: 0.02 M sodium phosphate (dibasic) buffer, pH 7.04, containing 0.02 M sodium chloride, 0.02% (w/v) sodium azide, and 0.02% (w/v) DTT.

Chapter 1: Introduction

Gastroenteritis is responsible for causing 2.1 million deaths in children every year globally (Parashar *et al.* 2006), and 683,100 deaths in 2011 (Lanata *et al*. 2013), even though there is a reduction in gastroenteritis related mortality, diarrhoea remains the second leading cause of death in children under the ages of five around the world (Walker *et al.* 2012). A number of agents have been identified as causing gastroenteritis namely, enteric adenovirus, calicivirus, norovirus and astrovirus, but the most commonly known virus associated with severe gastroenteritis in young children is rotavirus (RV) (Wilhelmi *et al.* 2003).

Rotaviruses are known to invade the intestine via the faecal-oral route (Ward *et al.* 1991), and are capable of causing long-term infection owing to their ability to survive on dry inanimate objects (Sattar *et al.* 1986). Of all the annual deaths occurring worldwide due to diarrhoea-related gastroenteritis in infants, RV is responsible for at least 453,000 (21.5%) of the deaths (Parashar *et al.* 2003; Tate *et al.* 2012). In developing countries the mortality rate in infants and young children was found to be higher than in developed countries, with deaths estimated to be about 500,000 every year (Cunliffe *et al.* 2002); 230,000 of these deaths occurring in Africa (Mwenda *et al.* 2010).

Rehydration with water or dextrose-saline (in severe water loss) is often required to prevent dehydration-related death (Atherly-John *et al.* 2002; Kirkwood *et al.* 2011). There are vaccines that are administered to reduce the severity of RV gastroenteritis (i.e. RotaTeq^{TM} and Rotarix$^{®}$). However virus-like proteins (VLP) or protein-based, non-replicative particles have been targeted as possible vaccine candidates with promising results and are more cost effective (Parez, 2008; Shoja *et al.* 2014).

1.1. Rotavirus structure and genome composition

Rotaviruses belong to the Reoviridae family and they consist of eleven double-stranded ribonucleic acid (dsRNA) enclosed within layers of proteins (Gorziglia *et al.* 1990). Rotaviruses are non-enveloped, triple-layered viruses with a wheel-like shape and spoke-like protrusions made up of VP4 on the outer surface, and with VP7 forming the smooth outer layer (Figure 1-1) (Prasad & Estes, 1997). VP4 is cleaved by trypsin into VP8 and VP5 during the maturation stage (Patton *et al.* 1997).

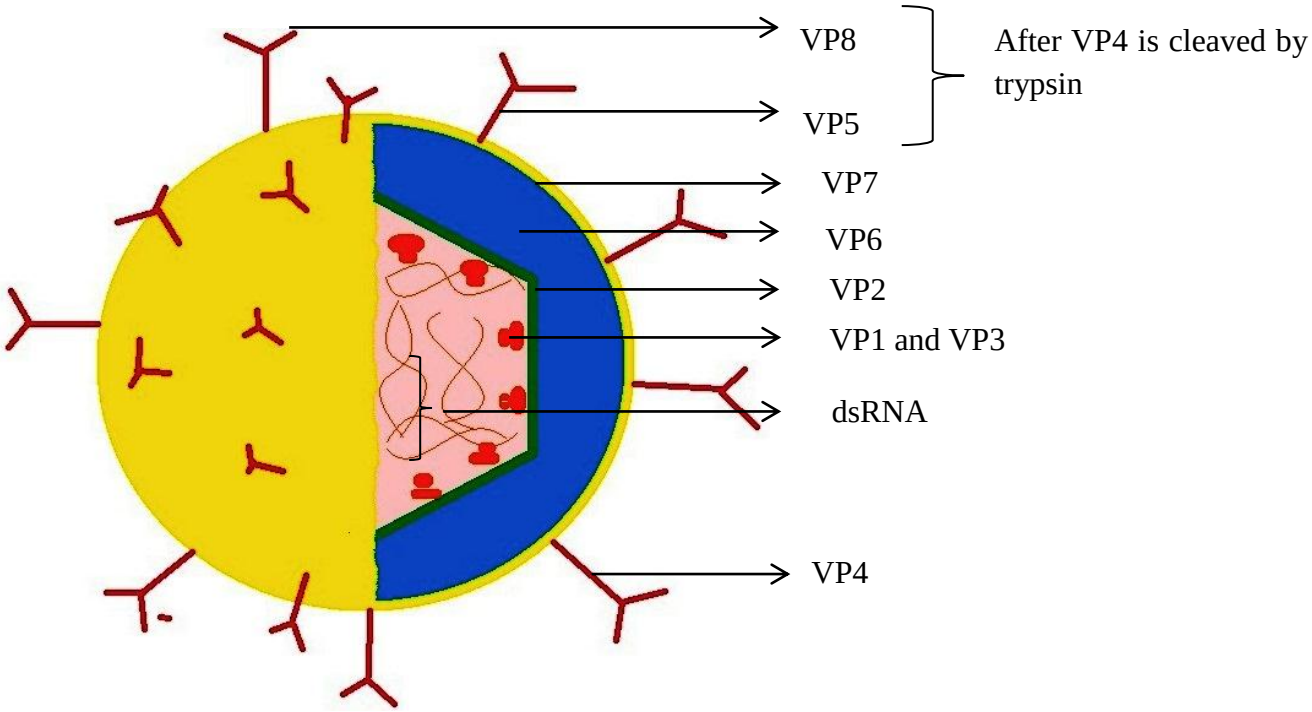

Figure 1-1: Rotavirus structure and composition
The figure represents the spherical structure of rotavirus showing VP4 (or VP8 and VP5 after cleavage by trypsin) forming the outer spikes, VP7 forming the smooth outer layer of the virus.VP6 dominates the middle layer of the virus, and VP2 acts as the inner layer that encloses VP1, VP3 and the dsRNA genome segments located in the core of the virus.

The second or intermediate layer is made up of VP6 which covers an inner layer made up of VP2, this layer encloses two enzymes (VP1 and VP3) and 11 dsRNA segments (Zeng *et al.* 1997) (Figure 1-1).

There are also non-structural proteins (NSPs) that are named from NSP1 to NSP5. These proteins are synthesized in infected cells and do not form part of the RV structure, but they assist in the replication and assembly of new RV virions (Crawford *et al.* 2001). Each of the 11 dsRNA segments encode either a VP or a NSP with the exception of segment number 11, which in some RV strains codes for two NSPs (NSP5 and NSP6) (Mascarenhas *et al.* 1997; Hu *et al.* 2012). Figure 1-2 depicts the migration pattern of the RV genome segments on a polyacrylamide gel along with the protein that each genome forms.

1.2. Rotavirus replication cycle

The RV capsid proteins help protect its viral genome, assist in host cell entry and initiate transcription of the viral genome (Jayaram *et al.* 2004). Rotavirus enters the cell via endocytosis (Sánchez-San *et al.* 2004; Gutiérrez. *et al.* 2010), and the outer layer is removed forming a double layered particle (DLP) which triggers endogenous transcriptase activity (Crawford *et al.* 2001) which enable the virus to release its capped transcripts through VP6 aqueous channels for translation (Lawton *et al.* 1997)[a]. The viral genome is translated into six structural proteins (VP1 to VP4, VP6, and VP7); and six non-structural proteins (NSP1 to NSP6). The proteins are necessary for the assembly of new viral particles (Patton & Spencer, 2000). The NSPs adapt and modify the cellular machinery by antagonising the interferon (IFN) activity; shutting down the host's cell translation; forming viroplasm inclusion bodies for viral replication and assembly; and assisting in the structural orientation the VPs (Fabbretti *et al.* 1999). The translated VP2 and VP6 form a double-layered RV particle which enters the rough endoplasmic reticulum (RER) acquiring VP4, VP7 and NSP4 that were also translated and assembled on the membrane of the RER. The newly formed viral particle undergoes intermediate membrane displacement by VP7, thus forming a triple-layered RV particle. The viral particle leaves the cell by exocytosis or cell lysis. Once the RV has exited the cell, trypsin cleaves VP4 into VP5 and VP8, forming a mature RV particle (Lawton *et al.* 1997)[b] that is capable of infecting other cells (Figure 1-3).

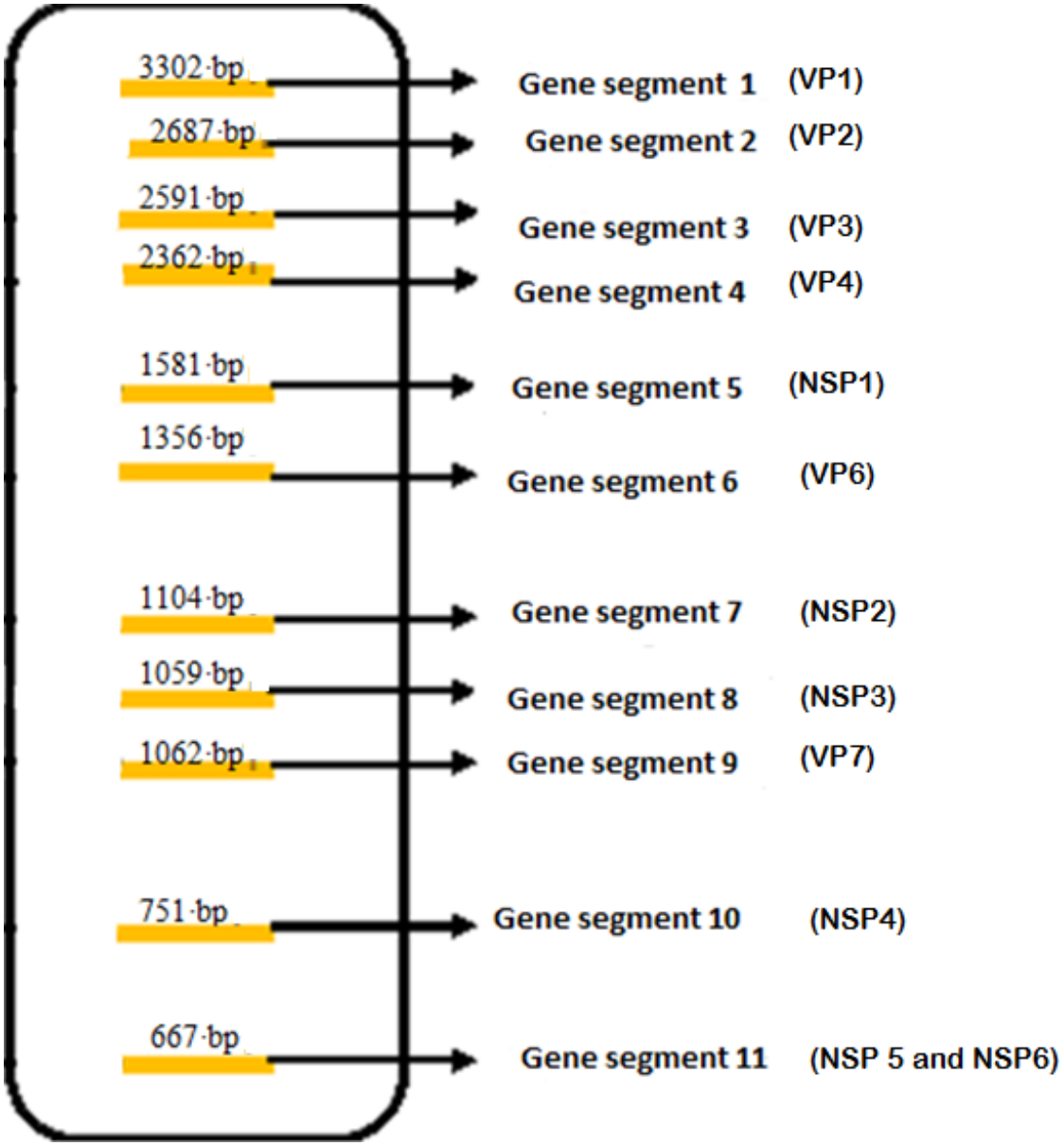

Figure 1-2: Electrophoresis gel migration pattern of 11 rotavirus dsRNA genome segments and the proteins that they form
Rotavirus gene segments are labelled 1 to 11 on the basis of their size with gene segment 1 having the highest number of base pairs and gene segment 11 with the least number of base pairs (Rixon *et al.* 1984).

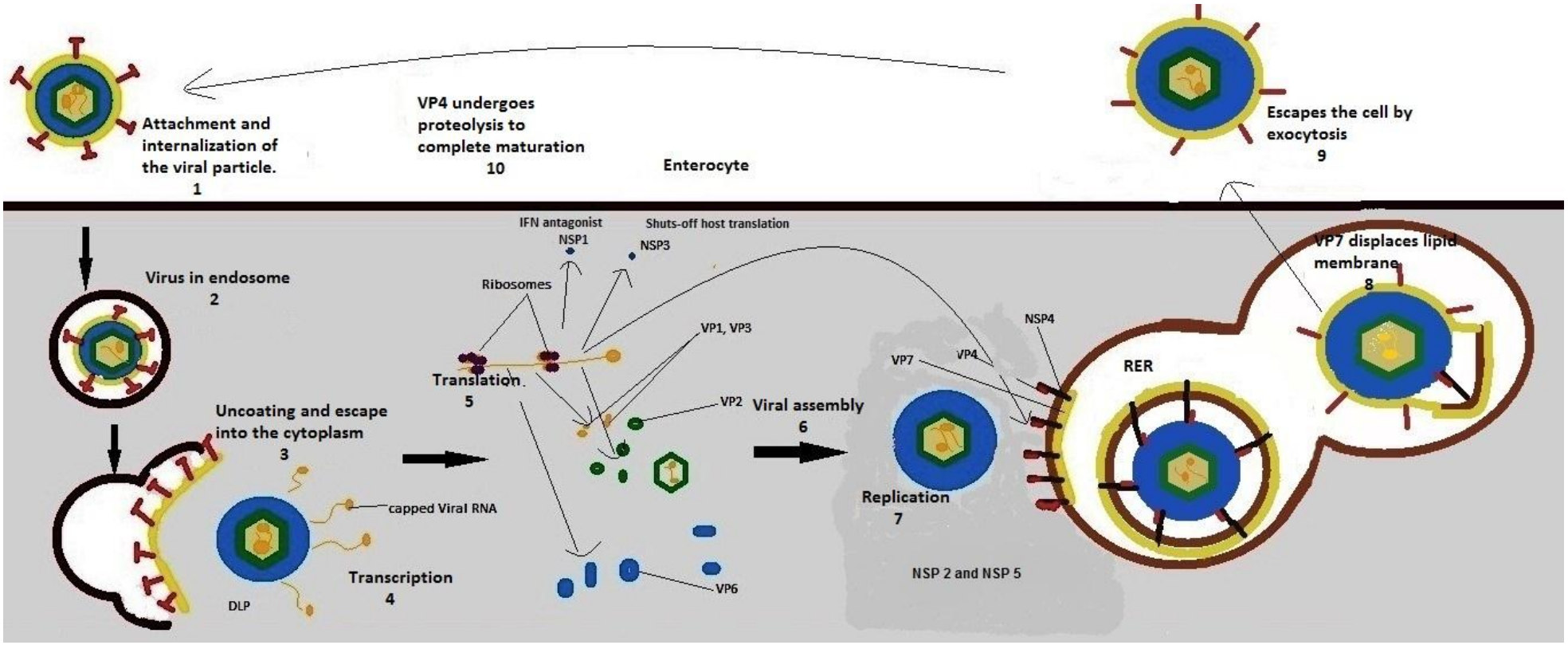

Figure 1-3: Rotavirus replication cycle

The figure is an author drawn image adapted from ViralZone-ExPASy, (2014) (https://viralzone.expasy.org). Rotavirus starts by attaching to the host's cell membrane (1), and is engulfed after interacting with membrane receptors (2). It escapes the endosome by shedding its outer layer and becoming a double layered particle (3). The now double layered particle starts to release viral genome transcripts from aqueous channels found on the now exposed VP6 layer (4). The RNA is translated forming VPs and NSPs necessary for assembling new virions (5). New double layered virions are formed from translated VPs with the assistance of NSP2 and NSP5 (7). The newly formed virions undergo lipid membrane displacement by VP7 (8) before escaping through the rough endoplasmic reticulum by exocytosis (9) (Trask *et al.* 2012). VP4 is cleaved by trypsin into VP5 and VP8 to complete the maturation of rotavirus (10).

1.3. Rotavirus capsid proteins and non-structural proteins

1.3.1. Outer layer proteins

The proteins that form the outer most layer of RV are VP7 and VP4 (Figure 1-1) (González *et al.* 1998). These two proteins help protect the virus and assist with host cell entry (Zárate *et al.* 2003; Trask *et al.* 2012). VP7 is a 37 kDa glycoprotein, and the VP7 layer is formed by 780 proteins (Nava *et al.* 2004; Coulson, 2012).

VP4 is an 88 kDa protein that forms 60 dimers of spiky protrusions on the RV's outer surface (González *et al.* 1998; Crawford *et al.* 2001). VP4 is cleaved into VP8 and VP5 by trypsin, an enzyme found in the digestive system of vertebrates (Espejo *et al.* 1981; Graham *et al.* 2003).

VP8 binds to mature enterocytes of the small intestine and initiates conformational changes that aid the interaction between VP5 and the host cell membrane to initiate phagocytosis of the virus into the cell (Graham *et al.* 2003; Settembre *et al.* 2011) (Figure 1-3).

1.3.2. Middle layer protein

The middle layer is dominated by 260 trimers of VP6 (Vieira *et al.* 2005). This protein has a major role in structural and functional organisation of RV as it is in direct contact with the outer layer (VP7) that is involved in cell entry; and the inner layer (VP2) that is involved in genomic RNA packaging. VP6 becomes exposed after VP4 and VP7 are removed during cell entry (Figure 1-3). As a result the former triple-layered virus becomes a double-layered virus (Lawton *et al.* 1997; Tihova *et al.* 2001). This transition enables the virus to be transcriptionally active, allowing dsRNA strands to pass from the viral core through VP2 layer and then out through the VP6 layer via a system of aqueous channels that penetrate VP6 and VP2 (Jayaram *et al.* 2004).

1.3.3. Inner core proteins

The inner layer of RV is an icosahedral barrier formed by 60 dimers (120 molecules) of VP2 (González *et al.* 1998). This layer encloses the viral dsRNA genome segments, polymerase enzymes (VP1) and guanyltransferase methylases (VP3) (Crawford *et al.* 2001) (Figure 1-1). VP2 interacts with VP6 through aqueous channels that aid in transporting metabolites from the outside to the inside of the virus, and releasing dsRNA during replication (Zeng *et al.* 1998).

1.3.4. Non-structural proteins

The NSPs carry out functions during the viral replication cycle and morphogenesis (Crawford *et al.* 2001). Non-structural protein 2 is a 35 kDa multimeric protein with nucleoside triphosphatase and helix-destabilizing activities (Taraporewala *et al.* 2006). It's role is to unwind the RV dsRNA (Silvestri *et al.* 2004). Non-structural protein 5 is a 12 kDa protein and was reported to interact with NSP2, VP1 and VP2 during viral replication and assembly (Vitour *et al.* 2004). Non-structural protein 2 and NSP5 are involved in the formation of a viroplasm necessary for viral replication and assembly inside the hosts' intestinal cells (González *et al.* 1998). Non-structural protein 1 and NSP3 are released into the cytoplasm after translation, where they assist in ensuring successful cell invasion and translation by acting as IFN antagonists (role of NSP1); and shutting off host cell translation (role of NSP3) (Trask *et al.* 2012). NSP4 is a 20 kDa protein that is encoded by gene segment 10, and has three hydrophobic domains named H1 to H3 (Hu *et al.* 2012). The H3 domain is considered to affect the calcium homeostasis by increasing intracellular calcium accompanied by release of chloride ions from the cells (Hyser *et al.* 2010). NSP4 also disrupts plasma membrane integrity which inhibits sodium absorption, thus, increasing sodium and chloride ions in the lumen and inducing diarrhoea (Ousingsawat *et al.* 2011).

1.4. Rotavirus serotype and subgroup classification

Rotaviruses are classified into G-serotypes based on the sequence of the glycoprotein VP7, and also into P-serotypes based on the sequence of the protease-sensitive protein VP4 (Georges-Courbot *et al.* 1988). Group A rotaviruses (RVA) have at least 27 G-serotypes (G1 to G27) and 37 P-serotypes (P1 to P37) (Matthijnssens *et al.* 2011; Rotavirus Classification Working Group, 2013). The most common G and P-serotype combinations that are responsible for many RV infections in children globally are G1P1A[8], G2P1B[4], G3P1A[8], G4P1A[8]; serotypes G9P1A[8] and G12P1A[8] were later detected in high frequencies (Santos & Hoshino, 2005; Iturriza-Gomara *et al.* 2011). Developing countries in Africa, Asia and South America showed high frequencies of other genotypes including G5, G6 and G8 (Kang *et al.* 2013, Luchs & Timenetsky, 2014).

Rotaviruses are also classified into seven antigenically distinct groups (Group A to G) (Riepenhoff-Talty *et al.* 1996; Ward & McNeal, 2010). Group A, B, and C are infectious to both humans and animals, with group A being the most globally prevalent in humans (Geyer *et al.* 1996, Estes, 2001). There are also four subgroups of RVs namely, SGI, SGII, SGI/II, and SG non I/II which depends on the presence of I and II antigens (Estes & Cohen, 1989; Saif & Jiang, 1994). These group-specific and subgroup-specific sites for antigenic determination are founded on the type of immune reaction against VP6 (Tang *et al.* 1997).

1.5. Structure of the VP6 protein

The VP6 protein structure is organized into two distinct domains (Figure 1-4). The domains are represented as S and H, the S domain is comprised of β-sheets and the H domain contains eight α-helices which are formed from the first 150 amino acids of the N-terminus and 335-397 residues of the C-terminus (Mathieu *et al.* 2001).

The amino acid sequence of RV VP6 is highly conserved among strains belonging to the same RV group, thus making VP6 a perfect candidate for determining RV group specificity and it is also known to be the most immunogenic protein of all the RV proteins (Estes & Cohen, 1989). Administering RV VP6 in rotavirus-infected mice as the only viral antigen was reported to have induced a protective immune response in the mice irrespective of the strain of the virus (Choi *et al.* 2000; Madore *et al.* 1999; Esteban *et al.* 2013). This indicates that vaccines that include VP6 antigen derived from RVA will help protect against infection by any RVA strain (Choi *et al.* 2002).

When the RV's outer capsid layer is removed during cell entry (Figure 1-3), VP6 becomes exposed (Estes & Kapikian, 2007) explaining why there are antibodies (Abs) that are generated against VP6 in infected mice (Ward & McNeal, 2010). Since VP6 is important for RV replication, immunity induced against VP6 might interfere with the replication cycle of RV, thus making VP6 an appropriate vaccine candidate (Bertolotti-Ciarlet *et al.* 2003). Studies by Corthesy *et al.* (2006); Garaicoechea *et al.* (2008) and Aiyegbo *et al.* (2013) also proved that the anti-replicative ability of VP6 antibodies against RV and approved protein-based vaccines are important as part of a safe and cost effective vaccine candidate in developing countries

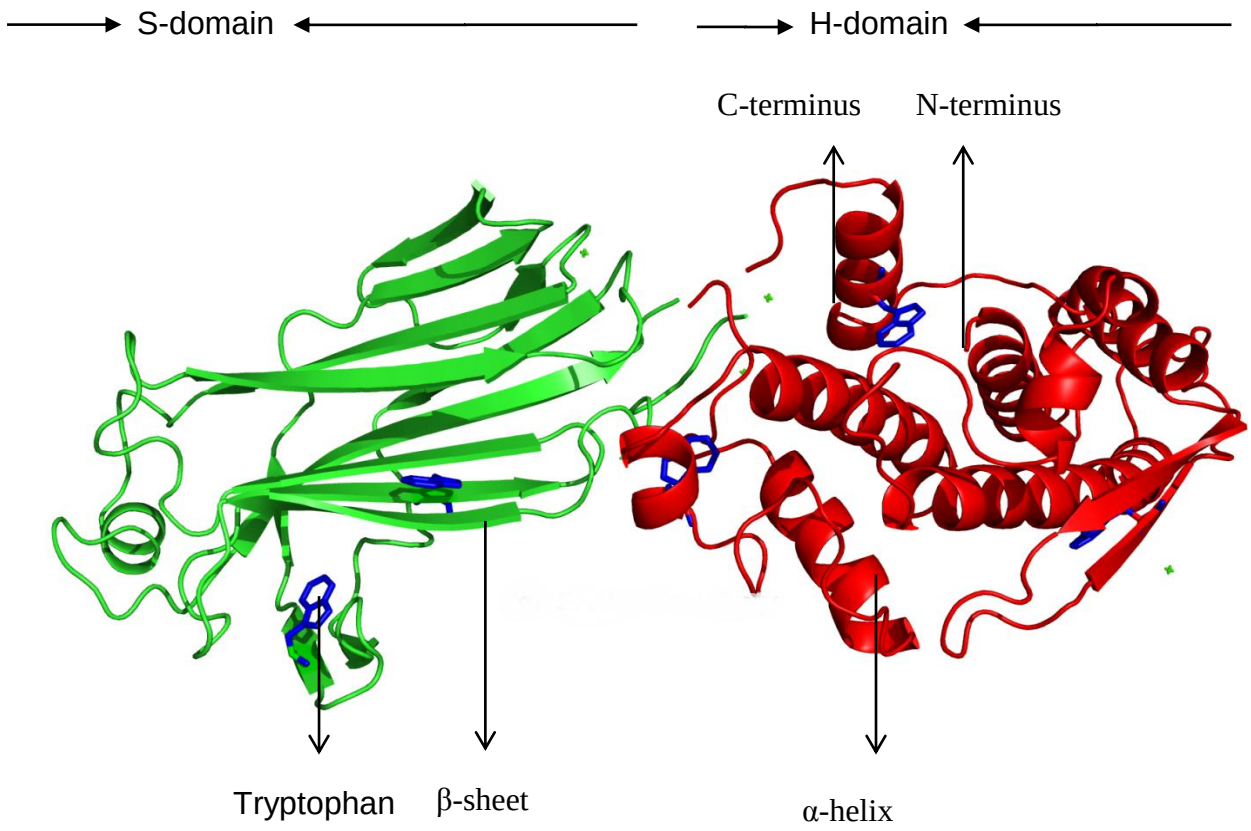

Figure 1-4: Ribbon diagram of the rotavirus VP6 protein
The 3-D ribbon structure of a rotavirus VP6 monomer (Mathieu *et al.* 2001) was generated as part of the current study. The green region (S-domain) represents the beta–sheets, and the red region (H-domain) comprises mainly of alpha-helices. VP6 is comprised of five tryptophan residues (blue) (Mathieu *et al.* 2001). The Image was generated using PyMol [Delano Scientific, (2009)], from rotavirus VP6, PDB code: 1QHD.

1.6. Rotavirus vaccines

Current RV vaccines include Rotashield® (Wyeth–Lederle Vaccines, now a part of Pfizer), Rotateq® (Merck) and Rotarix (GlaxoSmithKline). All three of the vaccines have been approved by the food and drug administration (FDA) (Linhares *et al.* 2008; Payne *et al.* 2010). Rotashield was suspended from use in USA since 1999, this was after it was thought to cause intussusception in vaccinated individuals (Program, 2001). Rotarix® is "a live human-attenuated RV vaccine" (De Vos *et al.* 2004), and RotaTeq™ is a recombinant bovine-human vaccine (Heaton *et al.* 2005). Both of these vaccines have shown to be effective in developed countries (Ruiz-Palacios *et al.* 2006, Vesikari *et al.* 2006; Snelling *et al.* 2011). However, the immunogenicity and effectiveness of these vaccines was shown to be lower in certain low-income countries of Africa (Cunliffe *et al.*2002; Sow *et al.* 2012); Asia (Zaman *et al.* 2010) and Central America (Patel *et al.* 2010). The reason for this is based on the difference in regional genotypes of the RV strains and serotypes that are different from the vaccine strains (Kirkwood *et al.* 2011; Bredell *et al.* 2016). This leaves not only a great demand to develop a cheaper RV vaccine candidate but also a demand for a vaccine that can protect against different RV strains, and a protein-based vaccine can meet those demands (Maranga *et al.* 2002, Palomares & Ramirez, 2009).

An efficient protein-based vaccine candidate has to have conserved epitopes, allowing the vaccine to be effective against different RVA strains (Parbhoo *et al.* 2016). The challenge is that there are reports of continuous changes in RV strains that affect humans (Collins *et al.* 2015), these changes arise from inert-species transmission and RV genome reassortment (Nyaga *et al.* 2015).

As indicated above, VP4 and VP7 form part of the outer protein layer for RV and have been thought to provide protective immunity due to the presence of neutralizing antibodies formed in the host after natural RV infection (Offit & Blavat, 1986; and Desselberger & Huppertz, 2011). However, these antibodies are not present after vaccination using attenuated viruses (Lappalainen *et al.* 2015), which renders the vaccine useless for raising immunity against VP4 and VP7 epitopes (Bertolotti-Ciarlet *et al.* 2003; Aiyegbo *et al.* 2013).

On the other hand, VP6 is found to be the best marker for RV vaccination as it generates serum immunoglobulin A (IgA) antibodies against VP6, particularly against

the conserved epitopes (Tang *et al.* 1997) this shows that a VP6-based vaccine will enable the vaccine to be effective against changing viral serotypes.

1.7. Expression and purification of recombinant VP6 protein

There are various expression systems used in protein production, i.e. yeast, fungi, insect, plant, animal, and bacterial cells that have been explored for production of proteins (Rosa, 1979; Dunn *et al.* 1983; Jonasson *et al.* 2002; Villaverde & Carrio, 2003).

Mason & Arntzen, (1995) and Johnson *et al.* (1997) reported plants to be a novel way of expressing "inexpensive" protein-based vaccine subunits. Engineered transgenic plants can express foreign proteins through integration of a foreign gene into the plant chromosome, which results in low protein yields (Mason & Arntzen, 1995).

Insect cell/baculovirus expression systems have been used for RV protein development which allows for high outputs, does not contain contaminants from mammalian sources and the baculovirus expression vectors are flexible and easy to handle (Maranga *et al.* 2002). However, it was later observed that the need for expression of recombinant proteins using insect cells poses challenges for vaccine bioprocessing and bioanalytics (Palomares & Ramírez, 2009). This was because large insect cells produce large tube structures that are difficult to isolate during size exclusion chromatography, and giving the possibility that other proteins are isolated along with the protein of interest, thus, contaminating a possible vaccine candidate. A study by Erk *et al.* (2003) found the presence of protease activity in the samples that were purified from a baculovirus-insect cell expression system, proving that there was incomplete purification. VP6 can take up different conformational structures including trimerization when exposed to different buffer pH or ionic strength (Estes *et al.* 1987; Lepault *et al.* 2001), formation of VLPs were observed when expression performed using plants, or during dual expression with VP2 using insect-cell expression systems (O'Brien *et al.* 2000).

Escherichia coli cells are considered ideal for protein over-expression because they are low cost, and show rapid growth with high expression rate (Tabor & Richardson, 1985; Amerein *et al.* 1995; Li *et al.* 2014). One of the important features of a bacterial expression system is the T7 RNA polymerase gene that is specific for a

conserved promoter region (Rosa, 1979). Inducers such as isopropyl β-D-1-thiogalactopyranoside (IPTG) and *L*-rhamnose are required to initiate protein expression by enabling transcription to occur. Isopropyl β-D-1-thiogalactopyranoside causes the repressor to be released from the promoter sequence allowing transcription of genes from the *lac* operon to occur (Dunn *et al*. 1983). *L*-rhamnose induces the expression of the T7 promoter gene, which in-turn transcribes the gene of interest (Hartnett *et al*. 2006). Sørensen & Mortensen, (2005) reported that 80% of the proteins used for three-dimensional structures on the protein data bank (PDB) in 2003 were expressed in *E.coli* cells. *Escherichia coli* cells transformed with pET plasmid were used in more than 90% of PDB proteins. This makes the combination of pET plasmid with *E.coli* cells the most popular protein expression system.

Escherichia coli cells have also been reported to improve expression and purification of high amounts of recombinant proteins (Studier, 2005; Lobstein *et al*. 2012; Sethia *et al*. 2014), even though bacterial expression systems are reported to undergo irregular or incomplete folding processes that tend to render the protein to be presented as insoluble aggregates that are referred to as inclusion bodies (Hoffmann & Rinas, 2000; Schweder *et al.* 2002; Villaverde & Carrió, 2003; Fanhert *et al.* 2004). Improvement in expression of soluble proteins has been reported to be inconsistent because of the different protein species being expressed, the bacterial strain used or the expression system used (Thomas & Baneyx, 1996; Thomas & Baneyx, 1997). Expressing soluble proteins is ideal for easy and efficient purification because there is no requirement for pre-purification techniques.

A study by Li *et al.* (2014) showed successful, separate expression of two RV capsid proteins (VP2 and VP6) in *E.coli* expression system. According to Li *et al.* (2014) the cells were incubated at 20°C for 6 h after inducing the cells with an unspecified concentration of IPTG. The low growth temperature is ideal for reducing stress within the expression system, and preventing aggregation of the expressed proteins (Lilie *et al.* 1998). The brief harvest time was stated to be important in reducing the presence of dead cells, thus, reducing the release of proteases from the dead cells (Chakrabarti *et al.* 2016).

Chromatography was developed as a technique used to purify macromolecules following their interaction with an immobilised substrate (Cuatrecasas *et al.* 1968; Gerberding & Byers, 1998; Coskun, 2016). The commonly used protein purification

techniques are ion-exchange chromatography which binds molecules based on their charge, and can be selectively eluted off the charged resin by changes in pH or an increase in either sodium or chloride ions (Kopaciewicz *et al*. 1983; Jungbauer & Hahn, 2009). Another purification technique is affinity chromatography which binds molecules based on the type of immobile phase, whereby metals have an affinity to the imidazole ring of amino acids, and antibodies have affinity to a protein (antigen) (Magdeldin & Moser, 2012). There is also size exclusion chromatography where the biological molecules are separated by size when passed through a Sepharose column (Barth *et al.* 1996).

Over-expressed target proteins from bacterial cell expression contain other bacterial cellular proteins and sometimes preparative purification measures are required such as precipitation with ammonium sulphate to salt-out the target protein before loading the protein sample on a column (Oldfield *et al*. 1990; Jiang *et al*. 2004). Salting-in proteins is when the increase in salt in a protein solution increases the solubility of the proteins, further increase in salt may cause the proteins to precipitate due the reduced interaction of the water molecules to the protein, and this is referred to as salting-out (Green & Hughes, 1955; Wingfield, 2001).

Uhlén *et al.* (1992) reported that over-expressed target proteins are best expressed linked to a fused affinity tag because it helps in purifying the target protein after expression, and fusion tags do not affect the biological or biochemical activity of the expressed protein. Studies that expressed their target proteins along with a HisTag usually use a denaturant to ensure that the tag is exposed.

A study by Choi *et al.* (2002) employed a method by Jarrett and Foster which involved cloning the VP6 gene into pMAL/c2X plasmid and using it to transform *E.coli* cells which were thereafter lysed and centrifuged to separate the insoluble proteins in the pellet from the soluble fraction in the supernatant. The proteins were denatured using 8 M urea to unfold proteins that have been misfolded and aggregated during expression, the proteins were refolded before conducting affinity chromatography. Badillo-Godinez *et al.* (2015) successfully purified VP6 using affinity chromatography (Nickel resin) with chemical denaturants to assure the affinity tag was not folded into the protein structure.

1.8. Aims and objectives

The principle aims of this study were to optimise the over-expression and purification of soluble RV VP6, and to then characterise the expressed VP6 using various spectroscopic techniques. Achieving these aims required addressing the following objectives:

- To transform the KRX and BL21 bacterial expression cells with recombinant VP6-pET-28a(+) plasmid.
- To compare the two bacterial expression systems in terms of their ability to over-express soluble VP6 when induced with different inducer concentrations, post-induction time and temperature.
- To purify VP6 using liquid chromatography techniques.
- To use spectroscopic techniques to determine protein concentration, native structure and structural changes of VP6 in the presence of urea, high sodium chloride concentrations and under varying temperatures.

Chapter 2: Experimental procedure

2.1. Materials

The VP6 gene was synthesised, then cloned at the *Nde* I and *Bam*H I restriction sites of the pET-28a(+) plasmid by Genscript® (China). Kanamycin and IPTG were purchased from Separations (Johannesburg, South Africa). The BL21 (DE3) cells and KRX *E.coli* cells (Promega) were purchased from Anatech (Johannesburg, South Africa). The SDS-PAGE molecular weight marker (MWM) was purchased from Thermo Fisher Scientific (United States of America). The HisTrap and HiPrep nickel-Sephacryl prepacked columns, the DEAE-Sepharose beads and imidazole were purchased from Sigma-Aldrich (United States of America). All other chemicals were of analytical grade.

2.2. Bioinformatics

The VP6 gene used for this study was selected by searching the National Center for Biotechnology Information (NCBI) database (https://www.ncbi.nlm.nih.gov/) for full length (397 amino acids) RVA VP6 peptide sequences. A total of 130 full length peptide sequences were randomly selected from different countries reported from 2005 to 2010. The obtained VP6 peptide sequences were used to generate a single consensus VP6 peptide strand (Figure 2-1) by using CLC genomics workbench v3.6.1 software (CLC Bio USA, Cambridge, MA).

The consensus peptide sequence was reverse translate into a gene sequence using ExPASy, reverse translation tool (SIB Bioinformatics Resource Portal) (https://www.expasy.org/resources/search).

The VP6 gene sequence was then sent to GenScript for synthesis and cloning into a pET-28a(+) plasmid cloned at the *Nde* I and *Bam*H I restriction sites. The plasmid carried HisTag sites which are comprised of nucleotides sequences that code for 6 histidine amino acids. One of the HisTag site was located on the N-terminal (incorporated by the *Nde* I restriction enzyme), and the other was located on the C-terminal (incorporated by cleaving using the *Bam*H I restriction enzyme) (Figure 2-2)

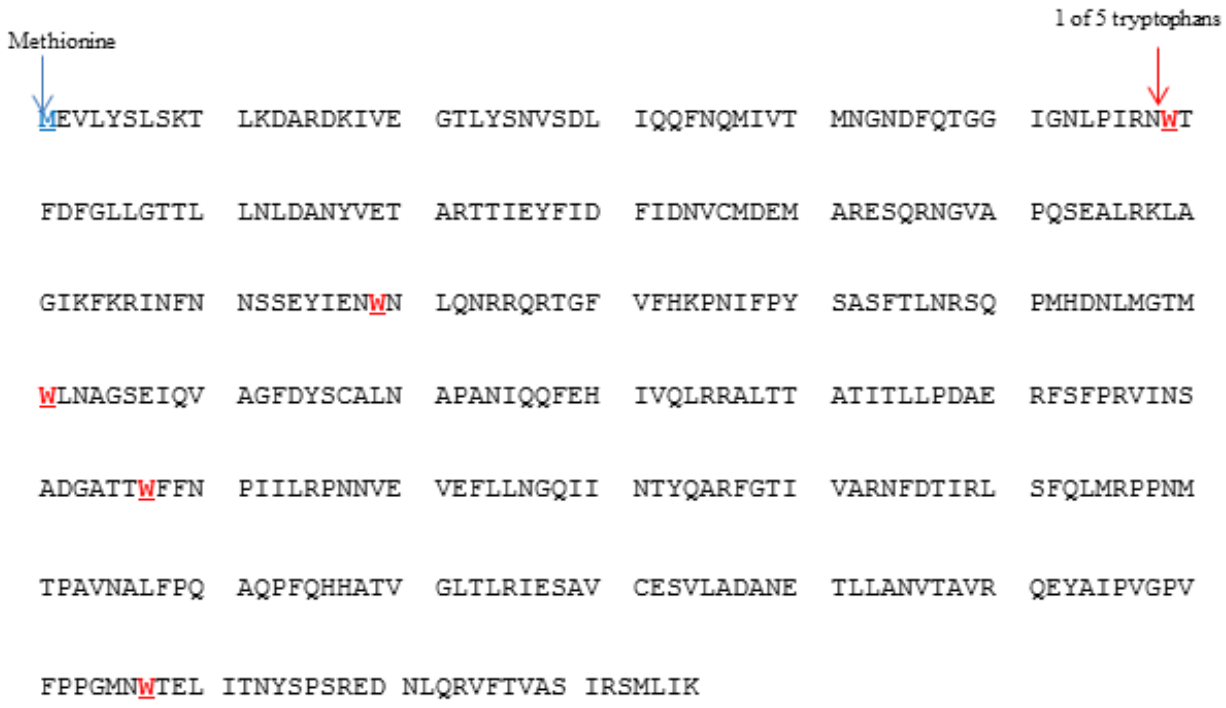

Figure 2-1: The resultant VP6 consensus sequence
The resultant consensus protein sequence was generated from 130 full length RVA VP6 peptide sequences. The five tryptophan residues are underlined and highlighted in red. The methionine (underlined and highlighted in blue), signifies the start/amino terminal of VP6. The sequence was derived using CLC genomics workbench v3.6.1 software (CLC Bio USA, Cambridge, MA).

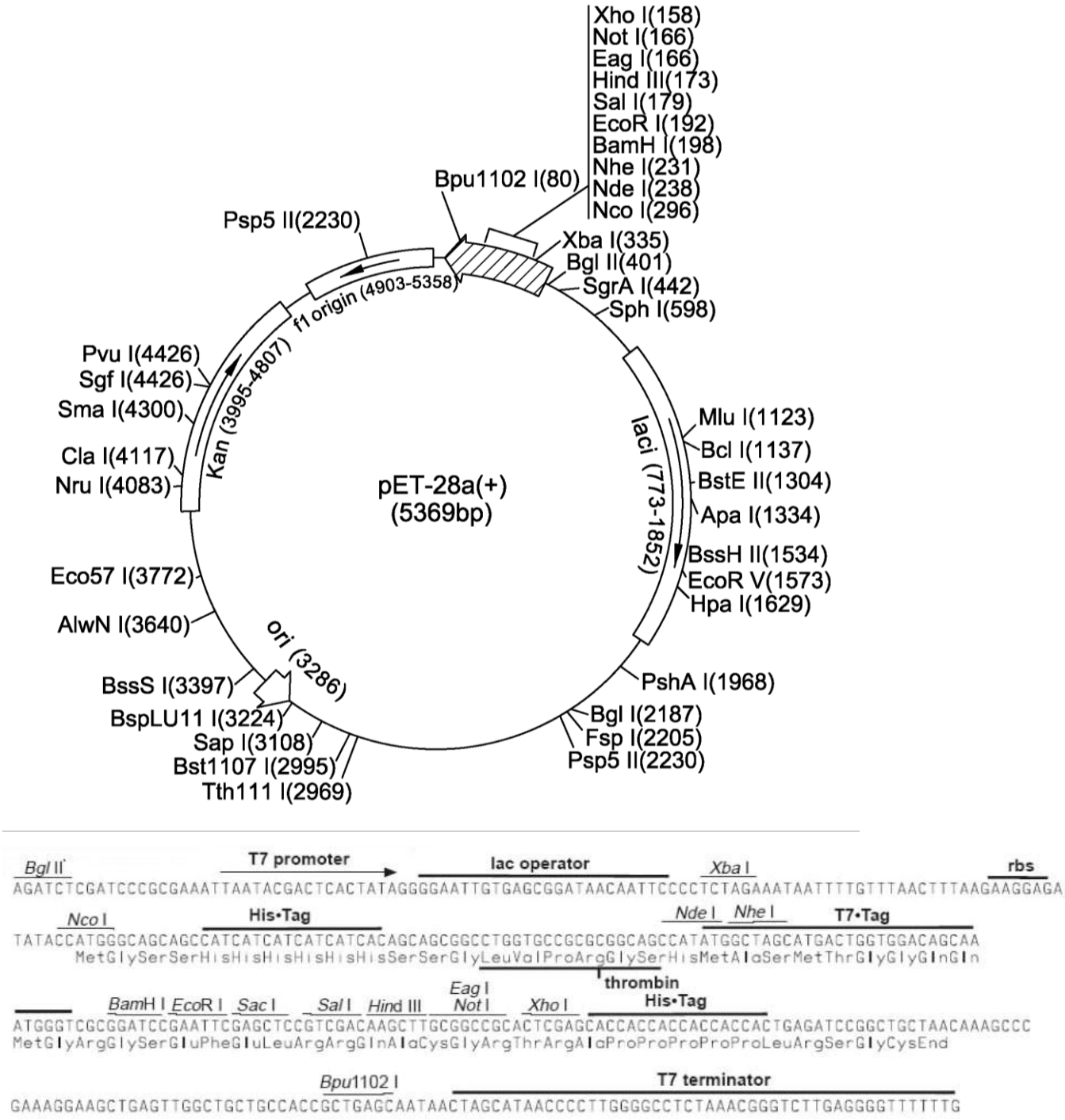

Figure 2-2: pET-28a(+) vector map

The image was adapted from pET-28a-c(+) Vectors technical specification sheet (Novagen, product: TB074), Merck. The restriction sites (*Nde* I and the *Bam*H I sites) are located within the multiple cloning site (MCS) where the VP6 gene was inserted. “Ori” represents the origin of replication; “Kan” represents the kanamycin resistant gene. The plasmid has been engineered to have two histidine tags, one situated on the N-terminus and the other on the C-terminus.

2.3. Cell transformation and over-expression of VP6

The recombinant plasmid [VP6-pET-28a(+)] was introduced into the competent *E.coli* (BL21 and KRX strain) cells in a process called transformation (Kruger & Stingl, 2011). The competent cells were thawed on ice along with an aliquot of the plasmid containing the VP6 coding insert. Then, 2 µl of recombinant plasmid was added to a 100 µl of KRX and BL21 (DE3) competent cell vial, the reaction mixture was then gently swirled before being incubated on ice for 30 min.

The cells were then heat shocked at 42°C for 45 s, then quickly incubated back on ice for 2 min. Then SOC media, preheated at 42°C, was added to the mixture and, incubated for 60 min at 37°C, before the cells were plated on an LB-agar containing 0.05 mg/ml of kanamycin. The agar-plates were incubated at 37°C for 20 h. A single colony from successfully transformed cells was added to a fresh 25 ml LB broth supplemented with 0.05 mg/ml kanamycin. The cells were grown at 37°C for 20 h, then added to a fresh LB broth that was supplemented with 0.05 mg/ml kanamycin with a dilution of 1:50. The cells were grown at 37°C until the OD_{600} reached an absorbance of approximately 0.6.

To test for the most optimum conditions for expressing soluble VP6, two *E.coli* cell strains (BL21 and KRX) were induced with different IPTG concentrations (0.0001 M; 0.0005 M and 0.001 M). The KRX cells were also induced with either 0.05% or 0.1% (w/v) of *L*-rhamnose. The IPTG functions as allolactose by binding to the *lac* repressor, changing its structure and preventing it from binding to the promoter region, and allowing the highly selective RNA polymerase to transcribe the T7 promoter (Studier & Moffat, 1986; Narita & Tokuda, 2009).

KRX cells have a copy of T7 RNA polymerase gene driven by a rhamnose promoter whose expression is induced by *L*-rhamnose (Hartnett *et al.* 2006), thus all expression trials with KRX cells were tested with the addition of *L*-rhamnose for induction. The IPTG and *L*-rhamnose concentrations used in this study were selected on basis of suitable inducer concentrations for expressing soluble proteins from the technical bulletin, Single Step (KRX) Competent Cells instruction manual (www.promega.com/protocols).

Two separate flasks were used when performing experiments for time-dependant experiments of 6 h and 16 h analysis, and when performing temperature dependent experiments of 25°C or 37°C.

After expression the cells were harvested via centrifugation at 5000 rpm, at 4°C for 20 min, the cells where then resuspended in one of the different buffers (the specific buffers are mentioned in the results text). The resuspended cells were then sonicated on ice for 90 s at amplitude 35 using an ultrasonic liquid processor Q700 (QSonica, 53 Church Hill Rd. Newtown, CT, USA). The sonicated cells were then centrifuged at 13 000 rpm, at 4°C for 20 min. Samples of the supernatant and pellet (re-solubilised first) were then electrophoresed through a 12% SDS-PAGE gel.

2.4. SDS-PAGE

The expressed proteins and the post-purification fractions were assessed by SDS-PAGE with a discontinuous buffer system, prepared as described by Laemli, (1970). The resolving gel was a 12% acrylamide/bis-acrylamide gel [0.38 M Tris/HCl, pH 8.8, 0.1% (w/v) SDS, 0.02% (w/v) ammonium persulphate and 0.09% (v/v) TEMED], and the stacking gel consisted of 4% polyacrylamide [0.13 Tris/HCl, pH 6.8, 0.1% (w/v) SDS, 0.06% (w/v) APS and 0.25% (v/v) TEMED]. Before the protein samples were loaded onto the gel wells they were mixed at a ratio of 1:1 with a sample buffer [0.0625 M Tris-HCl buffer, pH 6.8, 10% (v/v) glycerol, 2% (w/v) SDS, 5% (v/v) β-mercaptoethanol and 0.05% (v/v) bromophenol blue], and then boiled for 5 min. The samples were loaded and electrophoresed for an hour at 160 Volts using a Bio-Rad Mini-PROTEAN Tetra cell. The electrode buffer contained 0.3% (w/v) Tris/HCL, 1.88% (w/v) glycine and 0.1% (w/v) SDS. The unstained molecular weight marker was from Thermo Fisher Scientific (Massachusetts, USA) contained a mixture of proteins sizes ranging from 14 kDa to 116 kDa. Equal volumes (10 µl) of protein samples of were loaded onto the gel. After electrophoresis the gels were stained in 0.2% (w/v) Coomassie Blue R250 dissolved in 10% (v/v) acetic acid, and 18% (v/v) methanol, and destained in a 10% (v/v) ethanol and 7% (v/v) acetic acid solution. Protein samples containing VP6 were electrophoresed against a molecular weight marker with the 45 kDa marker used as a qualitative measure for the presence of VP6, this is because the VP6 has a theorectical size of 46.58 kDa when expressed with 12 histidine residues.

2.5. Ammonium sulphate protein precipitation.

Ammonium sulphate (AS) precipitation is an ideal technique used in the preparation of proteins prior to purification (Polson *et al.* 2003 Jiang *et al.* 2004). The soluble protein fractions were aspirated and aliquoted into four tubes that contained different AS percentage saturation of 10 (900 µl of protein and 100 µl of AS); 12% (880 µl of protein and 120 µl of AS); 16% (840 µl of protein and 160 µl of AS) and 20% (800 µl of protein and 200 µl of AS). The four tubes were mixed gently, incubated for 20 min, and then centrifuged at 13 000 rpm. Supernatants from the four tubes were removed to four different tubes and the precipitated proteins were re-solubilised in 500 µl of Buffer B. Both the supernatants and the re-solubilised pelleted fractions were electrophoresed on an SDS-PAGE gel.

2.6. Protein purification

The purification techniques used in the current study were ion anion exchange chromatography and affinity chromatography, performed on a Bio-Rad NGC Chromatography System.

2.6.1. HisTag affinity chromatography

Affinity chromatography is based on purifying biomolecules from one another based on the fact that they possess inherent recognition sites that can bind to a natural or artificial molecule bound to a fixed column. In the current study the affinity chromatography used was a HisTag affinity chromatography.

The HisTag has an affinity for metal ions (i.e. nickel) to which it selectively binds during purification, this occurs because of the electron donor groups on the histidine imidazole ring that form bonds with metal (Ni2+) (Bornhorst & Falke, 2000)

The supernatant obtained from cell lysate after centrifugation was applied to a HisTrap column (the volume of the columns used is stated in the results text) that was equilibrated with Buffer A. The column was washed with 4 × column volumes (CV) of Buffer A, followed by a 10 × CV linear elution gradient of mixing Buffer A with the same buffer containing a higher imidazole concentration (specific imidazole concentrations are stated in the results text), the fractions were collected in volumes of 4 ml.

2.6.2. Ion exchange chromatography

Ion exchange chromatography is based on attraction between a charged fixed column matrix that is commonly made up of polysaccharides such as Sepharose containing a charged species (Jungbauer & Hahn, 2009). In the case of protein purification using ion exchange chromatography the protein's charge is affected by its the buffer pH. The buffer pH manipulates the charge of the protein considering the proteins pI, if the protein is in a buffer with a pH below its pI the protein is protonated and becomes positively charged, if the buffer pH is above the protein's pI then deprotonation occurs giving the protein a net negative charge. Positively charged proteins bind to negatively charged Sepharose beads, and vice versa.

Protein supernatant were obtained as described in section 2.3 above, the cells were resuspended in Buffer B before lysis. The resuspended cells were lysed then centrifuged for 20 min as described in section 2.3 above. The supernatant was loaded on a 35 ml DEAE column that was pre-equilibrated and washed with Buffer B. A 10 × CV elution gradient of Buffer B against Buffer B containing a higher sodium chloride concentration (specific sodium chloride concentrations are stated in the results text) was used for elution. In ion exchange chromatography the fractions were collected in volumes of 8 ml

2.7 Absorbance spectroscopy

Absorbance of VP6 was measured from 340 nm to 220 nm, before the corrected absorbance at 280 nm was used to determine the protein concentration using a Chirascan plus instrument (PhotoPhysics, Leatherhead, UK). The Beer-Lambert Law ($A = c.\varepsilon.l$) was used to calculate the protein concentration from the corrected absorbance (A_{340} subtracted from A_{280}) reading, where A is the absorbance determined, ε is the extinction coefficient, which is a constant, "c" is the concentration of the solution containing absorbing molecule, and "l" is the cuvette path length which was 1 cm unless otherwise specified. Before every absorbance reading a background correction was performed using the buffer in which the protein was suspended. Absorbance was read at 1 nm step and performed in triplicates, then produced an average spectrum. The extinction coefficient of RV VP6 was calculated to be 42 525 $M^{-1}.cm^{-1}$ using ExPASy ProtParam tool (Gasteiger *et al.* 2005). Protein concentration obtained after purification varied in some

characterisation experiments, concentration for each experiment is stated in the results text.

2.8. Fluorescence

Fluorescence spectrophotometry is the emission of light from a molecule that has been excited to a higher electronic state after it has absorbed light. Light absorbance by a molecule is specific to a particular wavelength of light based on the molecule's electron properties. The excited molecule only has a short excited state or lifetime, it will then return to ground state and emit light. The light emitted usually has a lower energy and a longer wavelength compared to the light absorbed by the molecule (Ward *et al.* 1991).

Phenylalanine, tyrosine and tryptophan contain 5 or 6 membered aromatic rings and are intrinsic fluorophores in proteins. Tyrosine and tryptophan are excited by wavelengths of 280 nm and 295 nm, respectively.

In the current study intrinsic fluorescence was used to identify the local tertiary environment around the fluorophores of VP6 when excited at 280 nm and 295 nm. A background correction was performed before any fluorescence reading was carried out using an empty 10 mm pathlength quartz cuvette that was used to hold the protein sample. Fluorescence emission spectra were recorded in the range of 500 nm to 280 nm at 20°C in triplicates which were used to produce an average spectrum. Excitation and emission slit widths were both set at 5 nm. A pathlength of 1 cm was used for all intrinsic fluorescence experiments.

2.9 Circular dichroism

Circular dichroism (CD) refers to the differential absorption of left and right circularly polarized light (Atkins & de Paula, 2005). A circular dichroism spectrum is influenced by the aromatic amino acid residues; the twists of the β sheets, and the lengths of the α-helices (Johnson, 1999), making it ideal for assessing the secondary structure of a protein. Far UV CD uses a range of wavelengths from 250 nm to 190 nm for peptide bond absorbance in determining the secondary structural content of a protein. A background correction was performed before any far-UV CD reading was carried out using an empty quartz cuvette that was used to hold the protein sample.

Far-UV CD spectra ranged were recorded at 20°C in triplicates which were used to produce an average spectrum. A 1 mm path length quartz cuvette was used during far-UV CD with the bandwidth set to 1 nm.

2.10. Thermal unfolding.

Thermal unfolding was measured by exposing VP6 to increasing temperatures from 20°C to 90°C. Heat denaturation of VP6's secondary structure was assessed by monitoring the far-UV CD using specifications stated in section 2.9. Ellipticity was measured at 1 nm step per temperature increase using 0.5 nm bandwidth.
Heat denaturation of VP6's tertiary structure was assessed by monitoring fluorescence emission at 1 nm step per temperature increase.

All protein characterisation experiments were performed using a Chirascan Plus instrument (PhotoPhysics, Leatherhead, UK).

2.11. Software and equations used for structural analysis, sequence analysis and data fitting

2.11.1. Calibration curve

The molecular weight of VP6 was analysed according to the migration distance on SDS-PAGE gel with reference to the molecular weight standards. The size of VP6 was extrapolated from a calibration curve constructed using the size and migration of the molecular weight standards. The size of the protein standards were represented as log values. An example of a calibration curve represented in the results section is shown in Appendix A.

2.11.2 Mean residue ellipticity

The circular dichroism ellipticity values (except for those used to monitor thermal unfolding experiment) were represented as mean residue ellipticity [θ] calculated from equation:

$$[\theta] = 100\ (\theta \text{ or mdeg})/\ (c \times n \times l).$$

Where "c" is the molar concentration of the protein in mM, "n" is the number of amino acid residues in the polypeptide chain and "l" is the pathlength in cm.

2.11.3 Software

Protein illustrations were generated through PyMol version 1.7 [Delano Scientific, (2009)].

Images and life cycles were generated using Microsoft Office PowerPoint (2010).

VP6 protein sequence was obtained from CLC genomics workbench version 3.6.1 software (CLC Bio USA, Cambridge, MA).

Linear and non-linear graphs were fitted using Microsoft Office Excel (2010).

Absorbance, circular dichroism and fluorescence data was acquired using Chirascan version 4.4.0 software.

Chapter 3: Results

3.1. Protein over-expression

The recombinant pET-28a(+) plasmid with the RV VP6 gene insert was used to transform *E.coli* (BL21 and KRX strain) cells. Expression trials were performed to determine the optimum conditions for over-expressing soluble rotavirus VP6 in both lines. The expression conditions that were tested include: inducer concentration (IPTG in both cell lines and *L*-rhamnose in the KRX cells); post-induction growth temperature and post-induction growth time.

3.1.1. Optimizing inducer concentration

Total over-expression of VP6 inside both cell lines was tested, with the cells exposed to varying inducer concentrations described in section 2.3, and incubated at a post-induction temperature of 25°C for 6 h. The cell cultures were harvested and then sonicated using the methods explained in section 2.3.

3.1.1.1. KRX cells

The IPTG concentration was used at 0.0001 M and 0.0005 M with no observable difference in expression of VP6 when comparing proteins present in the whole cell lysates, but it was observed that no VP6 was expressed when *L*-rhamnose was omitted from the bacterial growth culture (Figure 3-1).

The whole cell lysates were centrifuged to separate the soluble proteins from insoluble proteins. It was observed that KRX cells expressed more soluble VP6 (see supernatant content in Figure 3-2), than the BL21 cells (see supernatant content in Figure 3-3). The KRX cells also showed no variation in over-expression of VP6 when induced with either 0.05% or 0.1% *L*-rhamnose with any combination of IPTG concentration of either 0 M or 0.0005 M IPTG.

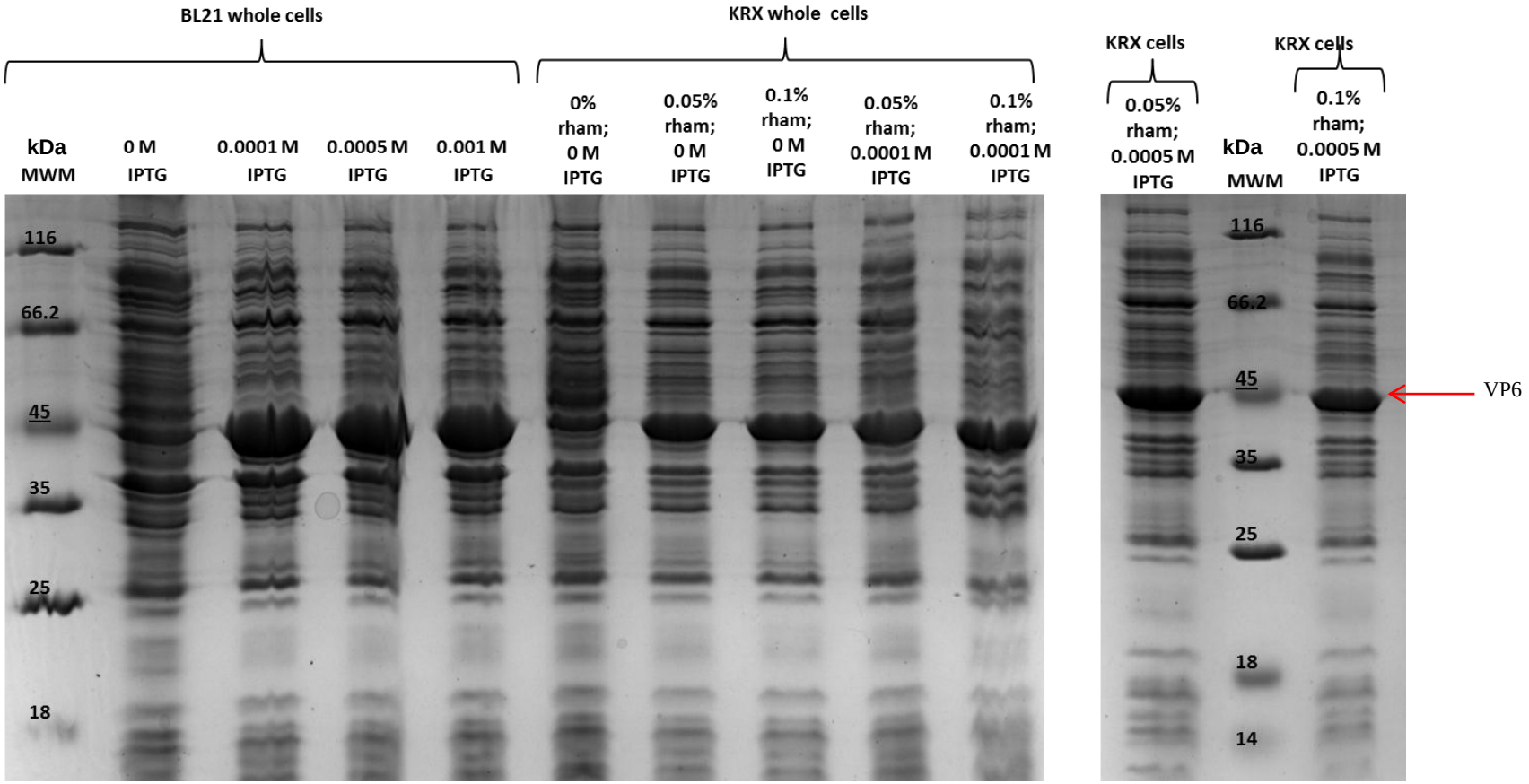

Figure 3-1: Optimisation of inducer concentration observed in whole cell lysates of BL21 and KRX cells
The effect of IPTG and *L*-rhamnose which represented by "rham" in were used to over-express VP6 in *E.coli* BL21 (DE3) and KRX cells. The SDS-PAGE lanes are labelled by the inducer concentration used. All cells with their respective IPTG and *L*-rhamnose concentrations were grown at 25°C for 6 h after induction. Molecular weight marker represented as "MWM" is represented in kDa. The 45 kDa mark is used to mark migration of VP6 that has a molecular weight of 50.12 kDa as determined using a calibration curve and data from this gel image (example of the calibration curve is depicted in Appendix A).

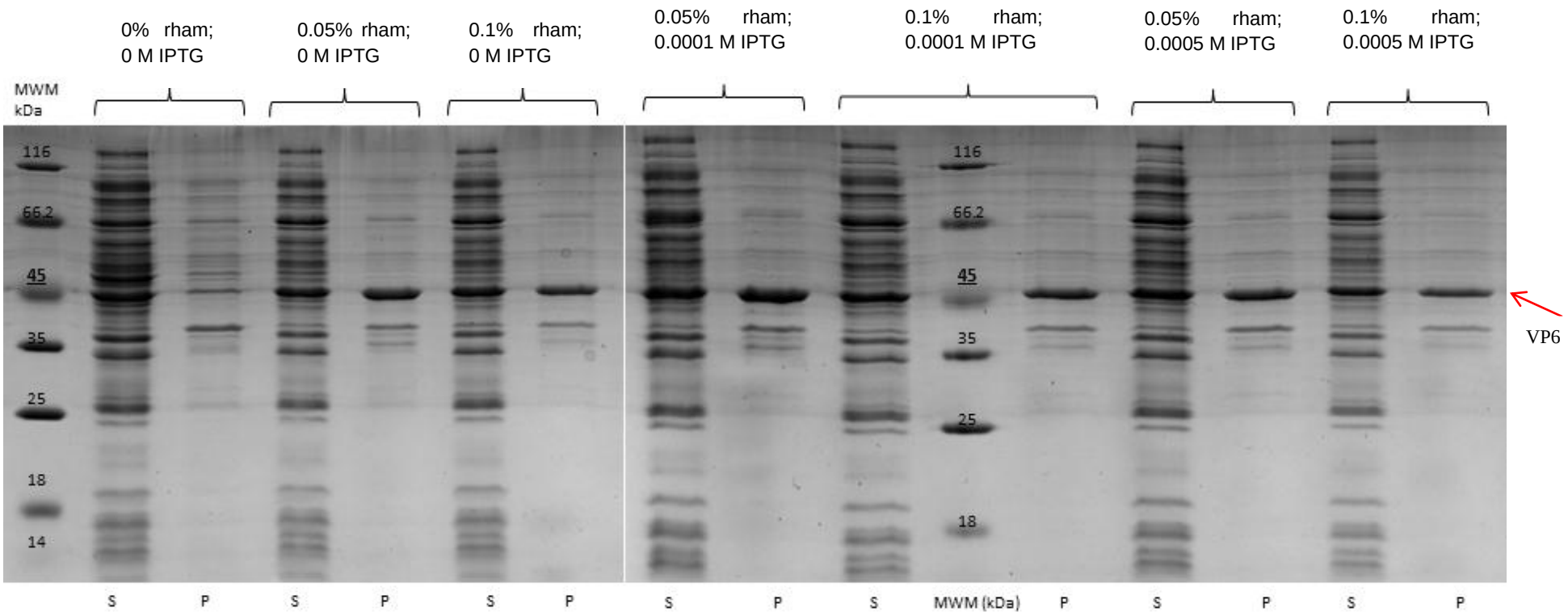

Figure 3-2: Effect of IPTG and L-rhamnose concentrations on expression of soluble versus insoluble VP6 in KRX cells
IPTG concentrations of 0; 0.0001; or 0.0005 M were assessed along with *L*-rhamnose represented by "rham" concentrations of 0; 0.05 or 0.1% (w/v). "S" represents the soluble proteins obtained from the supernatant and "P" represents the pelleted proteins precipitated the re-solubilised from the cell lysate. "MWM" represents the molecular weight marker in kDa. The 45 kDa marker is used to mark migration of VP6 which has a molecular weight of 50.12 kDa as determined using a calibration curve and data from this SDS-PAGE gel (example of a calibration curve is depicted in Appendix A).

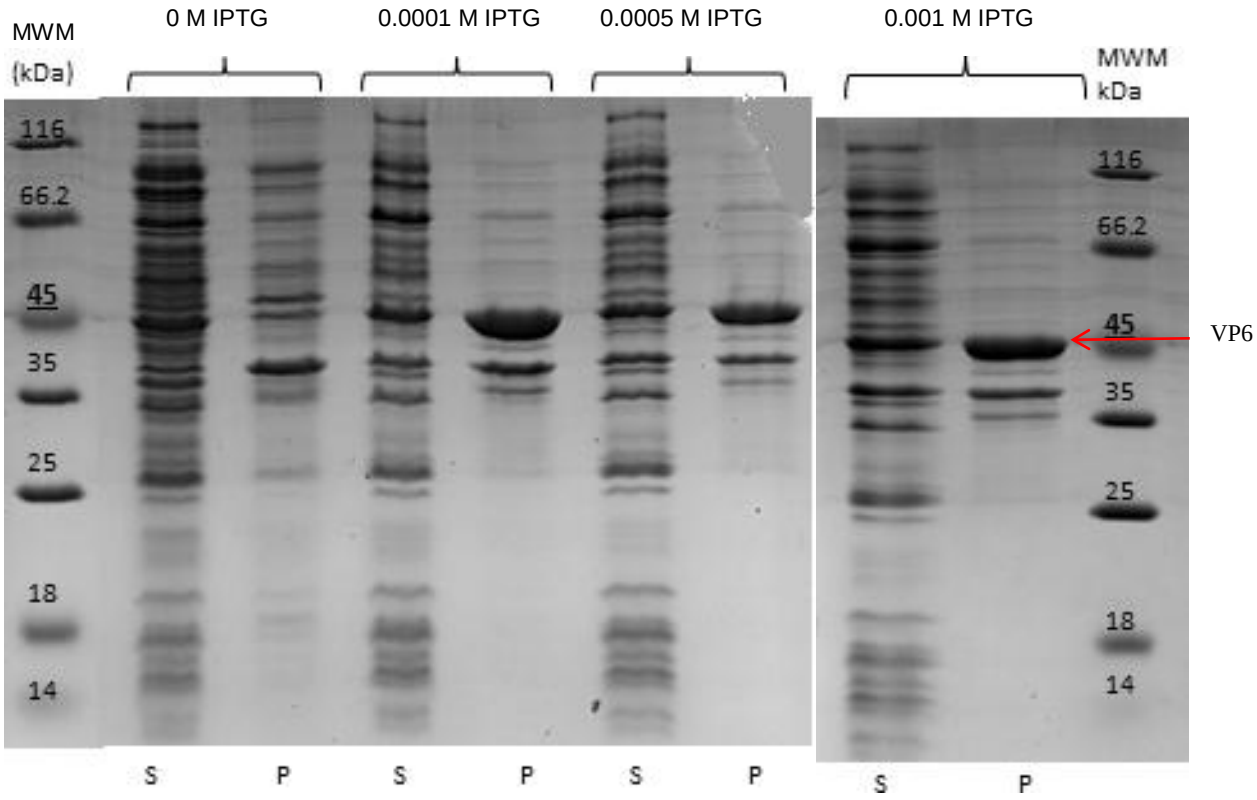

Figure 3-3: Effect of IPTG concentration on expression of VP6 in BL21 cells
IPTG concentrations of "0 M"; "0.0001 M"; "0.0005 M" and "0.001 M" are shown on the SDS-PAGE gel lanes. "S" represents the soluble proteins obtained from the supernatant and "P" represents the pelleted proteins precipitated then re-solubilized from the cell lysate. "MWM" represents the molecular weight marker in kDa. The 45 kDa marker is used to mark migration of VP6 which has a molecular weight of 52.48 kDa as determined using a calibration curve and data from this SDS-PAGE gel (example of the calibration curve is depicted in Appendix A)

The high molecular weight of VP6 was due to the presence of the added 12 histidine residues along with extra amino acids from the plasmid. There was no expression of VP6 in KRX cells when *L*-rhamnose was omitted from the cells culture during induction with IPTG. This shows the crucial role of *L*-rhamnose in protein over-expression using KRX cells.

3.1.1.2. BL21 cells

Over-expression of VP6 was observed to be equal in BL21 (DE3) cells compared to the KRX cells when induced with either 0.0001 M or 0.0005 M IPTG (Figure 3-1), but separation of supernatant from pelleted proteins in BL21 cells showed that more of the VP6 was expressed as insoluble aggregates (present in the "P" lanes, Figure 3-3). There was no change in the amount of expressed VP6 in BL21 cells when IPTG concentration was increased (Figure 3-3).

3.1.2 Optimisation of post-induction incubation temperature

Protein expression is dependant not only on inducer concentration but also on the growth temperature. This determines the rate of cell growth and the protein over-expression. Post-induction temperatures of 25°C and 37°C were tested on their effect on over-expression of soluble VP6 in BL21 and the KRX cells. The induction time was kept constant at 6 h along with an IPTG concentration of 0.001 M for BL21 cells, and 0.0005 M and 0.1% (w/v) *L*-rhamnose for KRX cells.

3.1.2.1. BL21 cells

Expressing VP6 in BL21 cells at 37°C (Figure 3-4), produced a higher yield of VP6, but most of the protein was located in the pellet fractions and is, hence, insoluble. VP6 expressed at 25°C was expressed equally in both the supernatant and the pellet. This was because bacteria grow optimally at temperatures of ±37°C. High expression levels of recombinant protein often result in its aggregation and accumulation in inclusion bodies (Lilie *et al.* 1998). Decreasing bacterial culture temperature reduces the growth rate of cells and the expression of proteins, and this also reduces the rate at which proteins aggregate and form inclusion bodies (Georgiou & Valax, 1996).

3.1.2.2. KRX cells

KRX cells were grown at 37°C, induced at a reduced temperature of 25°C. But the cell culture that was used for expression of VP6 at 37°C was maintained at that temperature even after induction.

There were no differences in the expressed soluble VP6 from the KRX cells incubated at 25°C and those incubated at 37°C (Figure 3-5), indicating that variation in the induction temperature had no effect on expression of soluble VP6 in KRX cells.

The ideal post-induction temperature for expressing soluble VP6 chosen for the study was 25°C, as the use of low post-induction temperature for bacterial expression systems was recommended by Xue *et al.* (2015).

3.1.3 Assessment of optimum induction growth time for protein over-expression

The induction duration was tested to establish any difference in amount of expressed soluble VP6 over induction time of 6 h versus 16 h and above. Inducing for a longer period of time (i.e. 16 h) may help increase the number of cells in the growth culture and, hence, the amount of protein. However, inducing for a longer period of time implies that there will be a gradual increase in the presence of dead cells, which in turn release proteases (Chakrabarti *et al.* 2016). Both the 6 h and the 16 h post-induction trial was tested to observe the most appropriate induction required for expressing high amounts of soluble VP6.

3.1.3.1. BL21 cells

There was no difference in the amount of soluble VP6 from both the 6 h and the 16 h induction growth times (Figure 3-6), meaning either induction time may be used to express soluble VP6 in BL21 cells.

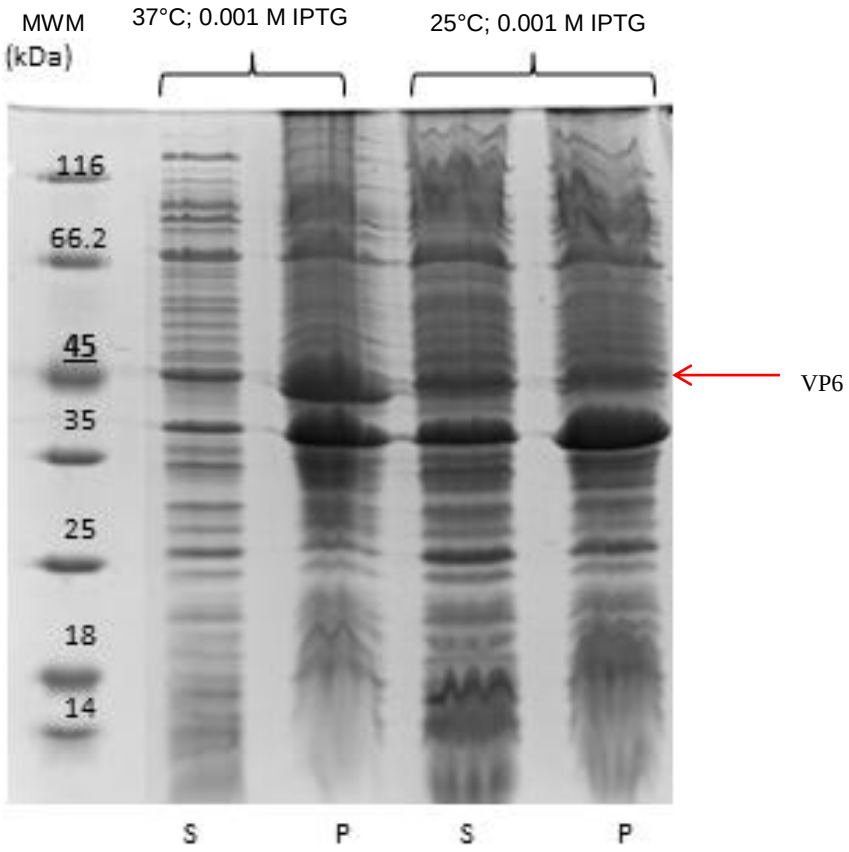

Figure 3-4: Effect of post-induction temperature on over-expression VP6 in BL21 cells
Temperatures of "37°C" and "25°C" were used to incubate the induced BL21 cells. "S" represents the soluble proteins obtained from the supernatant and "P" represents the pelleted proteins precipitated from the cell lysate. The cells were induced with 0.001 M IPTG for 6 h. "MWM" represents the molecular weight marker in kDa. The 45 kDa marker was used to mark the migration of VP6 which has a molecular weight of 48.98 kDa as determined using a calibration curve constructed from this SDS-PAGE gel (an example of a calibration curve is depicted in Appendix A).

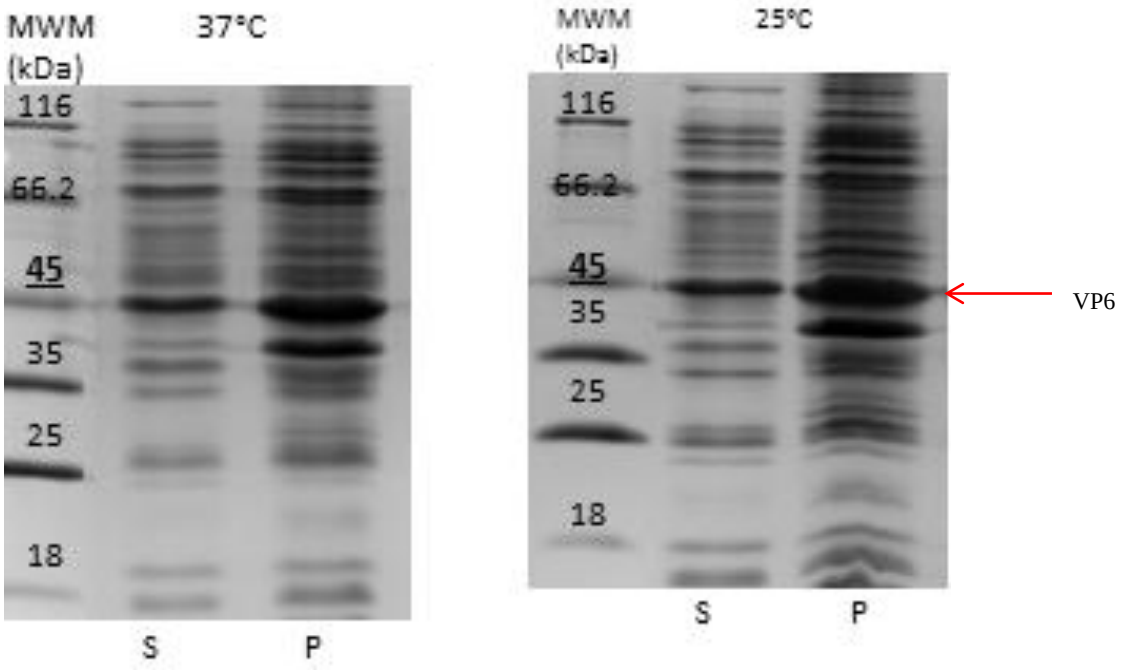

Figure 3-5: Effect of post-induction temperature on over-expression of VP6 in KRX cells

Temperatures of "37°C" and "25°C" were used to incubate induced KRX cells. "S" represents the soluble proteins obtained from the supernatant and "P" represents the pelleted proteins precipitated from the cell lysate. The cells were induced with 0.0005 M IPTG and 0.1% (w/v) *L*-rhamnose for 6 h. "MWM" represents the molecular weight marker in kDa. The 45 kDa marker was used to mark migration of VP6 which has a molecular weight of 52.48 kDa as determined using a calibration curve and data from this SDS-PAGE gel (example of a calibration curve is depicted in Appendix A).

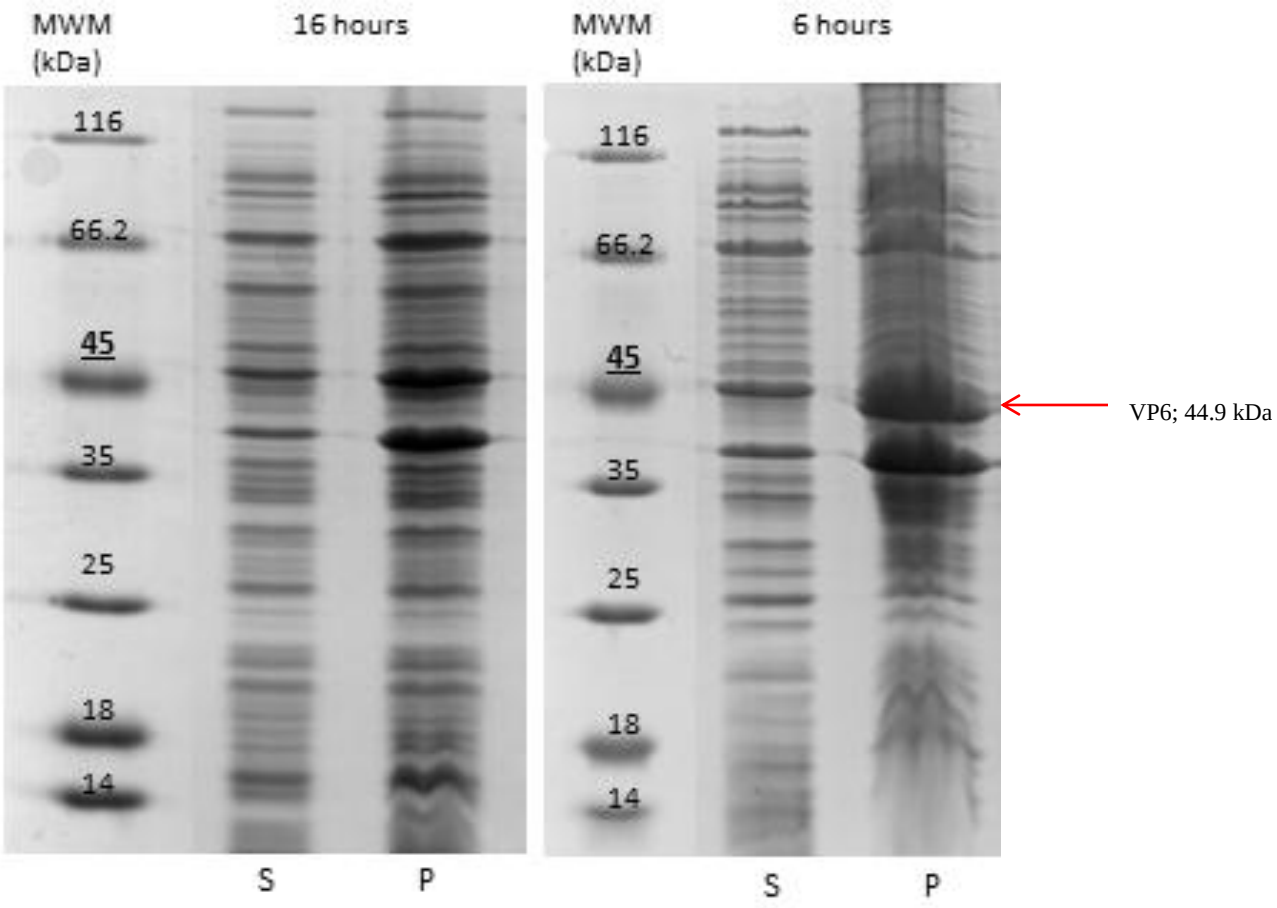

Figure 3-6: Effect of induction growth time on over-expression of VP6 in BL21 cells
Induction growth times of "16 h" and "6 h" were used in the expression of VP6 in induced BL21 cells. "S" represents the soluble proteins obtained from the supernatant and "P" represents the pelleted proteins precipitated from the cell lysate. The cells were induced with 0.001 M IPTG and incubated at 25°C after induction. "MWM" represents the molecular weight marker in kDa. The 45 kDa marker is used to mark migration of VP6 which has a molecular weight of 50.12 kDa as determined using a calibration curve and data from this SDS-PAGE gel (example of the calibration curve is depicted in Appendix A).

3.1.3.2. KRX cells

The 16 h induction time for KRX expression shows that there was a greater yield of proteins indicated by the dark bands on the SDS-PAGE from both the supernatant and pellet lanes (Figure 3-7); this was a result from a higher cell growth in the culture.

A 6 h induction time was preferred for this study because the lower the induction growth time the lower the cell death, hence less proteases present (Chakrabarti *et al.* 2016). The conditions used for BL21 cell growth and VP6 over-expression also resulted in increased expression of a protein species other than VP6 (Figures 3-3, 3-4 and 3-6), this protein had a theoretical molecular weight of 41 kDa (determined using a calibration curve). The 41 kDa protein was also over-expressed in the KRX cells, but it was consistently found in the pellet fraction (Figure 3-2 and 3-5).

BL21 cells yielded more VP6 overall, but the difference was observed in the yield of soluble VP6 which was higher in KRX cells. The KRX cells also produce less of the 41 kDa protein in the supernatant, this simplifies purification.

IPTG concentrations of 0.0001 M and 0.0005 M; *L*-rhamnose concentrations of 0.05% and 0.1%; induction temperatures of 25°C and 37°C, and induction time of 6 h and 16 h did not have an impact on the expression of soluble VP6 in KRX cells. The conditions that were preferred for the current study are an IPTG concentration of 0.0001 M; an *L*-rhamnose concentration of 0.05%, a post-induction temperature of 25°C, and an induction time of 6 h were. These conditions were chosen because they are cost effective and are less time-consuming.

3.2. Protein purification

Over-expressed VP6 was purified using different liquid chromatography purification techniques, namely ion (cation and anion) exchange chromatography, and affinity chromatography.

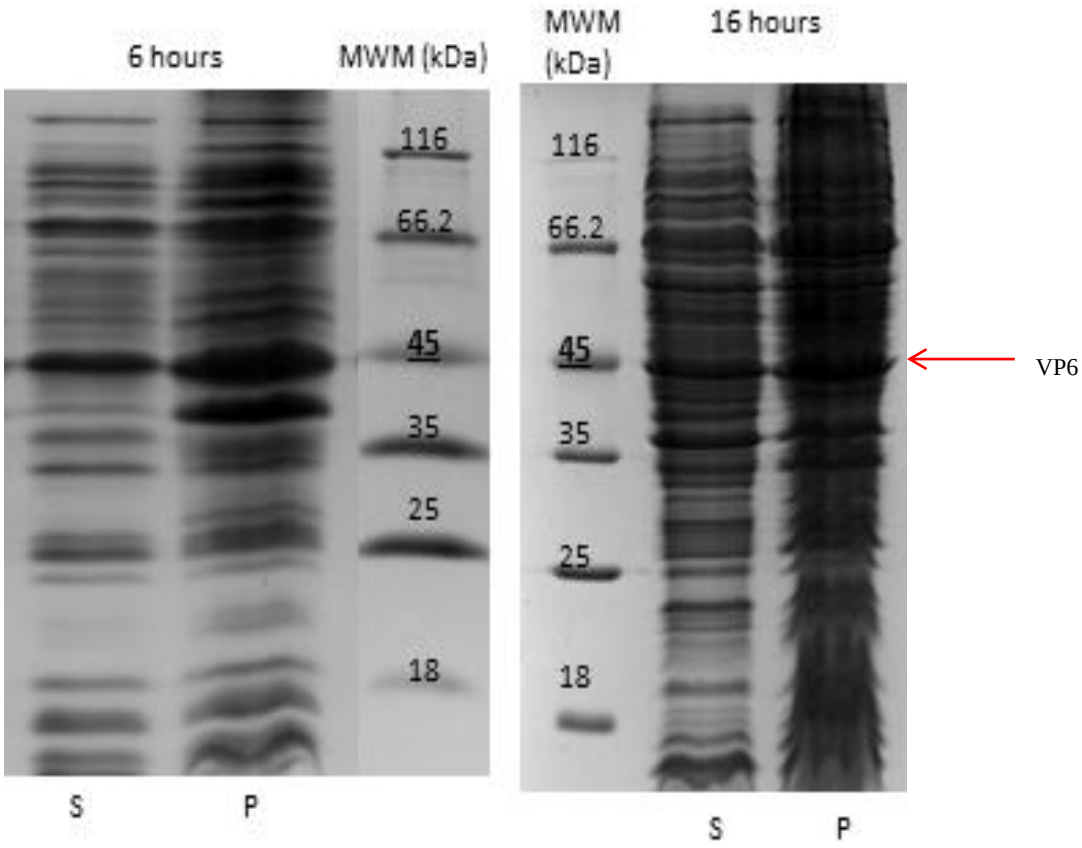

Figure 3-7: Effect of induction growth time on over-expression of VP6 in KRX cells
Induction growth times of "16 h" and "6 h" were used in the expression of VP6 in induced KRX cells. "S" represents the soluble proteins obtained from the supernatant and "P" represents the pelleted proteins precipitated from the cell lysate. The cells were induced with 0.0005 M IPTG, 0.1% (w/v) *L*-rhamnose and incubated at 25°C after induction. "MWM" represents the molecular weight marker in kDa. The 45 kDa marker is used to mark migration of VP6 which has a molecular weight of 47.86 kDa as determined using a calibration curve and data from this SDS-PAGE gel (example of a calibration curve is depicted in Appendix A).

3.2.1 Nickel affinity (HisTag) chromatography

VP6 was expressed using optimised conditions from section 3.1, then resuspended in Buffer A using procedure explained in section 2.3. The protein supernatant was collected and loaded on a 5 ml HisTrap resin from GE Healthcare (Little Chalfont, United Kingdom) that was equilibrated with Buffer A. The column was then washed with Buffer A, and eluted off the column using an elution gradient of Buffer A against Buffer A containing 0.3 M imidazole. The SDS-PAGE shows that VP6 did not bind to the HisTrap resin under these conditions and was completely washed off the column during a wash with Buffer A (Figure 3-8).

Bugli *et al.* (2014) used small ubiquitin-like modifier (SUMO) along with HisTag on VP6 to increase solubility of the target protein. Badillo-Godinez *et al*. (2015) added 8 M urea to the whole cell lysate in order to produce soluble proteins that can bind the nickel resin. The presence of a denaturant helps unfold the protein, thus, exposing the HisTag expressed with the protein, allowing it to bind to the nickel Sepharose resin.

An affinity chromatography using HisTrap resin was performed with the addition of 6 M urea to Buffer A was performed. An elution gradient spanning 0.01 M to 0.3 M imidazole was used to elute VP6 off the column. VP6 was successfully bound to the column and was eluted in collected fractions (Figure 3-9). VP6 was also present in the wash fraction, but that could have been a result of having exceeded the binding capacity of the resin.

VP6 was eluted approximately at 31% of the elution gradient; and was still not completely purified of other cellular proteins. Studies from Oldfield *et al.* (1990) and Li *et al.* (2014) described the use of ammonium sulphate precipitation to precipitate-out the protein of interest, thus reducing the amount of cellular proteins that compete with the target protein for binding on the column.

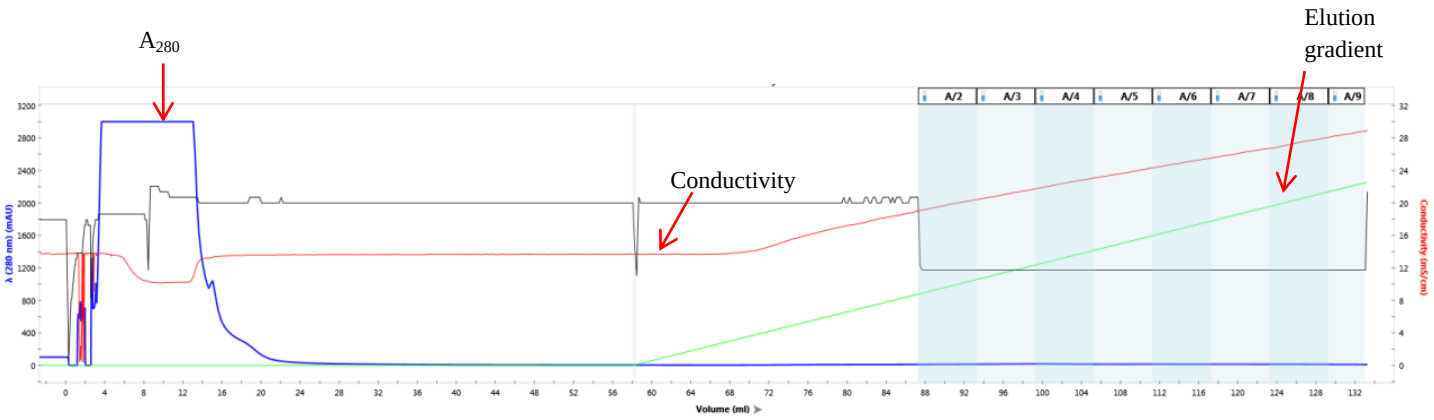

A.

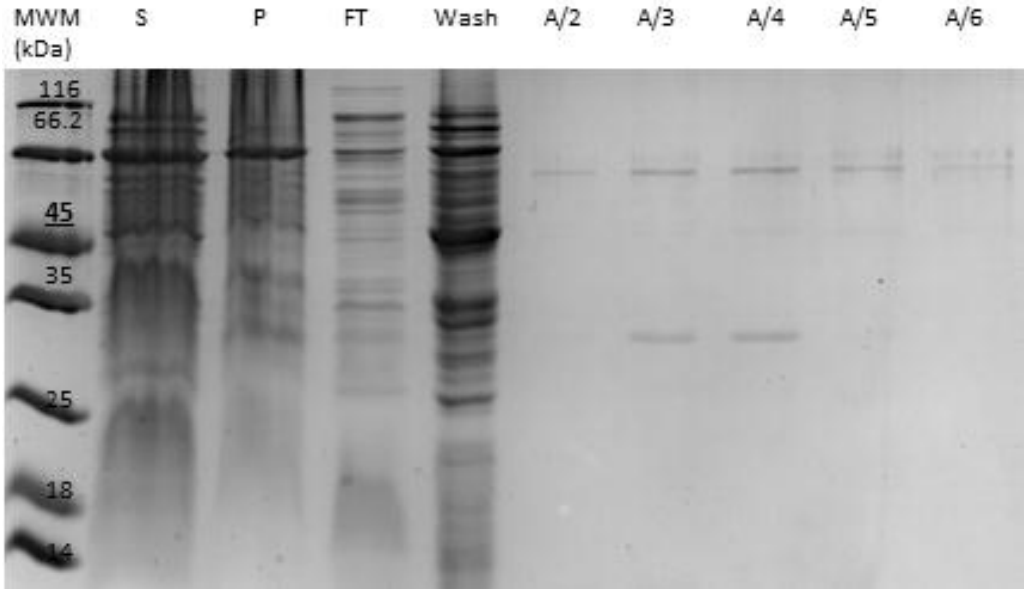

B.

Figure 3-8: Affinity (HisTag) chromatography purification of VP6 using a sodium phosphate buffer and a gradient elution of 0.01 M to 0.3 M imidazole

A. The elution chromatographic profile illustrating the absorbance at 280 nm (blue line), conductivity (red line) and elution gradient (green line). B. SDS-PAGE gel indicating the lane for the "MWM" which represents the molecular weight marker in kDa. The lane marked "S" represents the soluble proteins obtained from the supernatant of the cell lysate loaded on the column. "P" represents the pelleted proteins precipitated from the cell lysate. The lane labelled "FT" represents the flow-through protein sample that did not bind, but passed through the column during sample loading. The lane marked "Wash" represents the proteins from the column wash, where loading buffer was allowed to pass through the column to remove any unbound proteins. Lanes marked with "A/2" to "A/6" are protein fractions that were collected during the elution gradient from 0.01 M up to 0.3 M imidazole concentration.

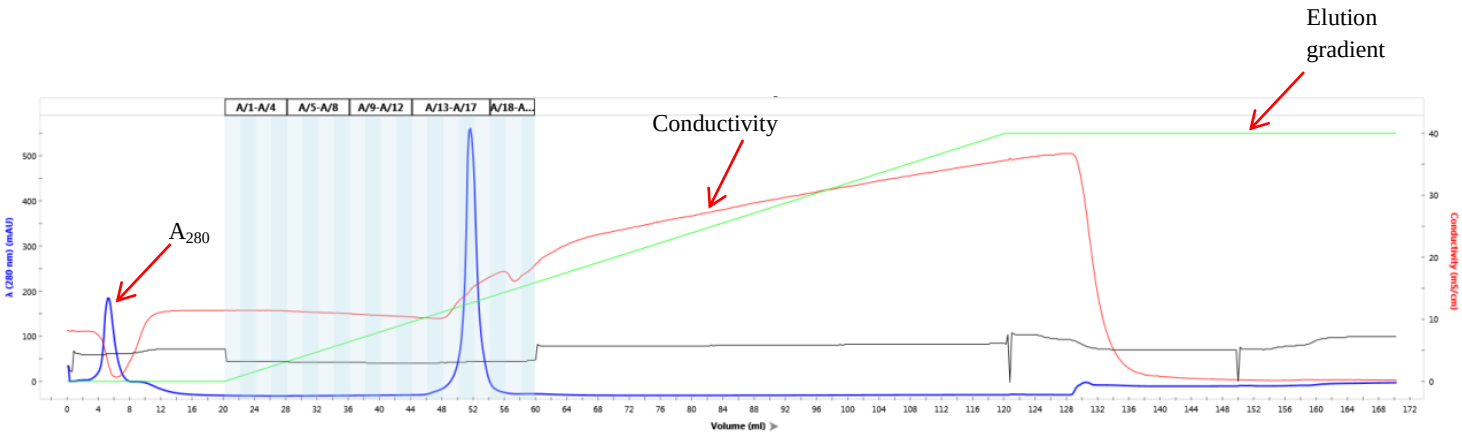

A.

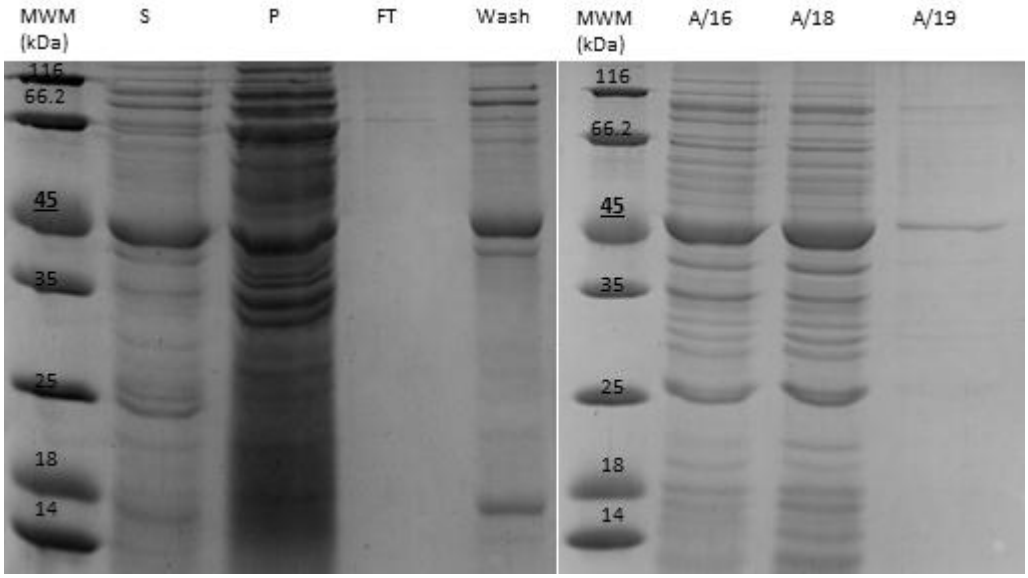

B.

Figure 3-9: Affinity (HisTag) chromatography purification of VP6 using a sodium phosphate buffer, 6 M urea, and a gradient elution of up to 0.3 M imidazole

A. The elution chromatographic profile illustrating the absorbance at 280 nm (blue line), conductivity (red line) and elution gradient (green line). B. SDS-PAGE gel indicating the lane for the "MWM" which represents the molecular weight marker in kDa. The lane marked "S" represents the soluble proteins obtained from the supernatant of the cell lysate loaded onto the column. "P" represents the pelleted proteins precipitated from the cell lysate. The lane labelled "FT" represents the flow-through protein sample that did not bind, but passed through the column during sample loading. The lane marked "Wash" represents the proteins from the column wash fraction, where loading buffer was allowed to pass through the column to remove any unbound proteins. Lanes marked with "A/16"; "A/18" and "A/19" are protein fractions that were collected during the elution gradient set from 0.01 M up to 0.3 M imidazole concentration.

3.2.2 Salting out

Ammonium sulphate is widely used as a preparative method to concentrate and selectively separate target proteins from other protein species. Protein samples are pre-treated before purification in order to help purification reach a higher purity level after performing purification (Mini *et al.* 2016). Oldfield *et al.* (1990) made use of 20% AS to precipitate bluetongue VP7 which is a structurally similar protein to RV VP6. VP7 was dialysed against a 0.01 M Tris-HCl buffer, at pH 7.5, and then loaded the protein onto a DEAE Sephacel column. The proteins were successfully precipitated in large yields and excluded most of the other host cellular proteins (Oldfield *et al.* 1990).

To carry out the salting-out procedure VP6 was expressed in KRX cells, and supernatant was obtained procedures stated in section 2.3. The supernatant was treated as described in section 2.5. it was found that precipitation using AS was non-selective, and failed to separate VP6 from other bacterial cellular proteins (Figure 3-10), and increasing the AS concentration would only precipitate the other bacterial protein species along with VP6.

Salting-out proteins can affect results on proteomic studies these include affecting their interaction and modification, influencing behaviour during purification and conformation during structural characterisation (Fountoulakis, 2001). Jiang *et al.* (2004) also reported that target proteins are not completely recovered after salting out.

3.2.3 Anion exchange chromatography

Vicente *et al.* (2008) used a weak anion exchange matrix (i.e. DEAE), and also reported that this purification procedure was essential in purifying RV proteins as it requires a nearly neutral pH (pH 7.4) which is less aggressive when considering developing a vaccine and important in preserving the stability of the protein.

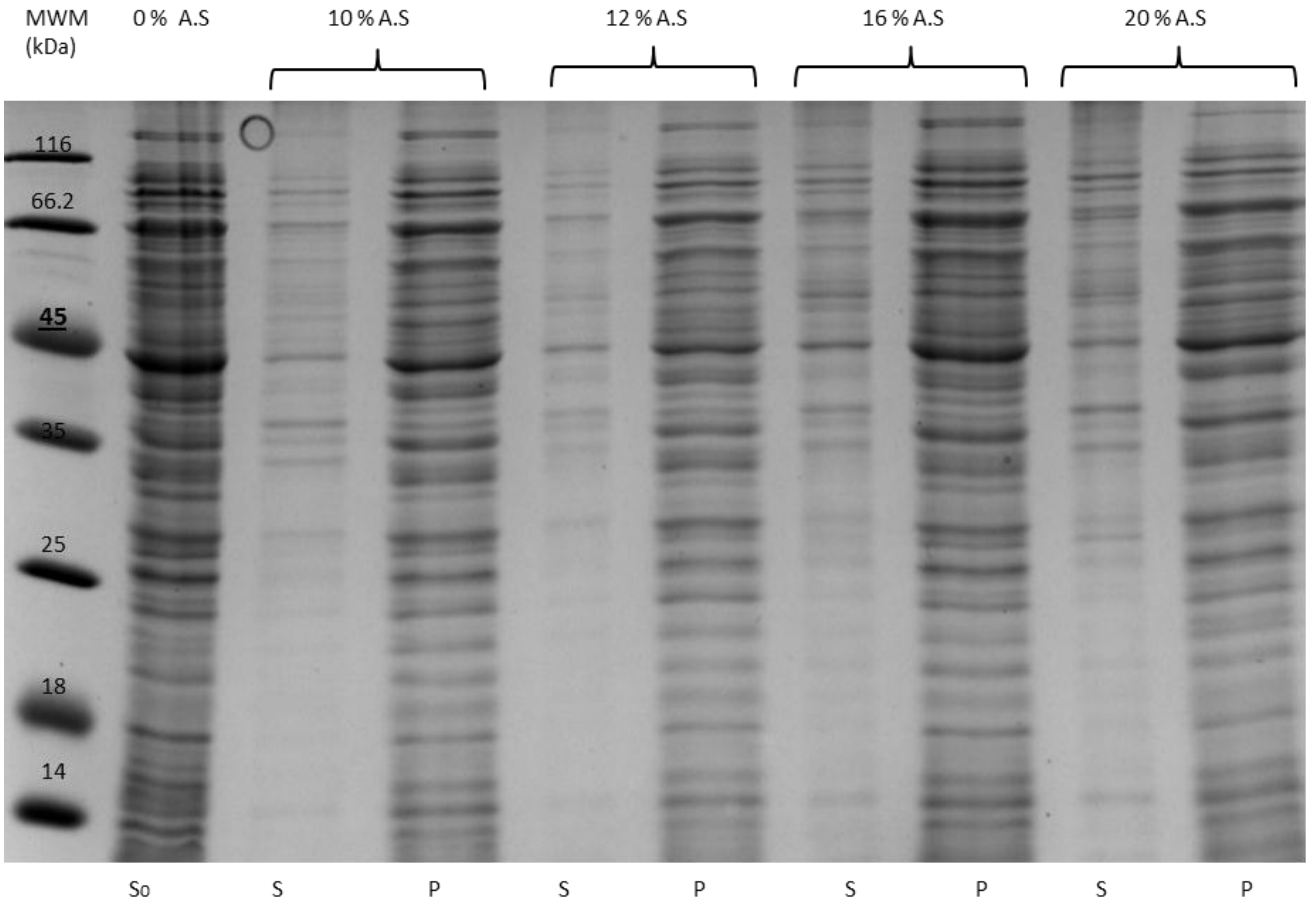

Figure 3-10: Protein precipitation using ammonium sulphate.
AS represents the ammonium sulphate used in different concentrations to precipitate the protein sample. "S_0" presents the initial supernatant with no AS. "S" represents the supernatant obtained from addition of AS followed by centrifugation; and "P" represents the precipitated proteins collected from the pelleted protein sample after the addition of AS and centrifugation. The protein sample aliquots were exposed to different AS concentrations from 0% up to 20%. "MWM" represents the molecular weight marker in kDa. The 45 kDa marker is used to mark migration of VP6.

Purification of VP6 was performed on a DEAE resin, the column was equilibrated and washed with Buffer C. An elution gradient was from 0 M to 0.3 M sodium chloride was used to elute VP6 off the column. Most of the VP6 failed to bind to the resin (Figure 3-11), while the small amounts of the protein that did bind were found to be present at different elution gradient percentages. This indicates that VP6 was present in different conformation, thus, displaying instability.

Sodium phosphate is the most commonly used buffer in anion exchange purifications (Choi *et al.* 1999). Buffer B was used to resuspend the pelleted cells before sonication and centrifugation. The supernatant was loaded on a DEAE column pre-washed with Buffer B. The bound proteins were eluted off the column using an elution gradient between Buffer B against a 1 M sodium chloride Buffer B. VP6 was successfully bonded to the DEAE resin, and absence of VP6 in the column wash fraction indicated that it was bound to the column (Figure 3-12). VP6 was eluted early in the gradient, and it was not isolated from other cellular proteins.

The protein sample was suspended in Buffer B before being loaded onto a DEAE column that was pre-equilibrated with Buffer B. The column was washed and an elution gradient between Buffer B against Buffer containing 0.7 M sodium chloride was used. The gradient length was shortened to better isolate VP6 from other cellular proteins. Fractions were collected as the absorbance started to increase by two units (Figure 3-13 A.). There were no presence of VP6 in the regeneration fraction indicating that an elution gradient of up to 0.7 M sodium chloride was sufficient in eluting VP6 off the column. A reduction in the elution gradient from 1 M to 0.7 M helped separate the eluted VP6 from many of the cellular proteins, and elution of VP6 at an early stage in the elution gradient indicates that the elution gradient could be further reduced to increase the purity of VP6.

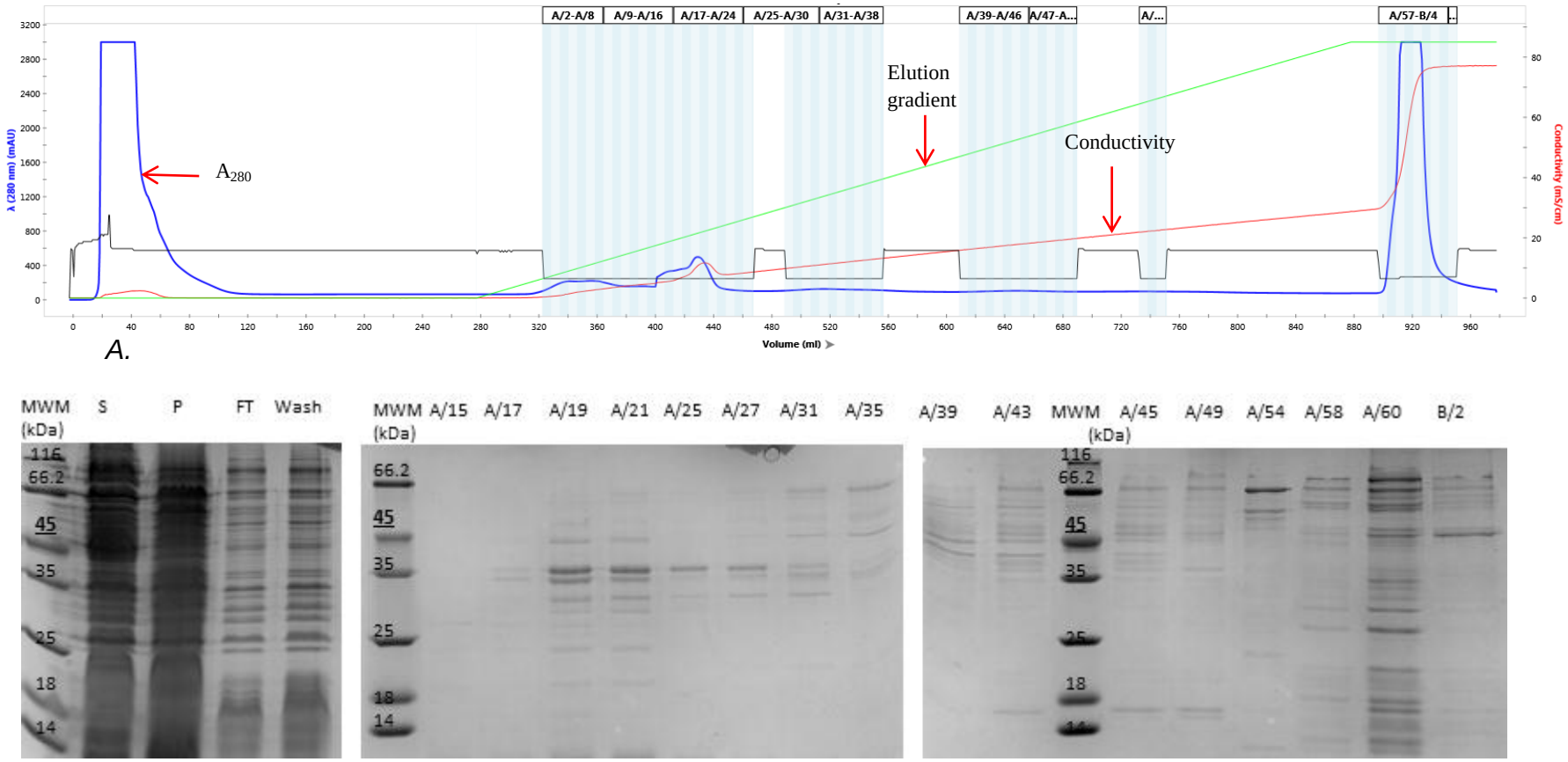

Figure 3-11: Anion (DEAE Sepharose) exchange chromatography purification of VP6 using a MOPS buffer with a gradient elution of up to 0.3 M sodium chloride

A. The elution chromatographic profile illustrated the absorbance at 280 nm (blue line), conductivity (red line) and elution gradient (green line). B. SDS-PAGE gel indicates the lane for the "MWM" which represents the molecular weight marker in kDa. The lane marked "S" represents the soluble proteins obtained from the supernatant of the cell lysate loaded onto the column. "P" represents the pelleted proteins precipitated from the cell lysate. The lane labelled "FT" represents the flow-through protein sample that passed through the column during sample loading. The lane marked "Wash" represents the proteins washed from column during the wash step. Selected fractions between "A/15" to "A/60", and "B/2" represent fractions that were collected during the elution gradient from 0 M up to 0.3 M sodium chloride.

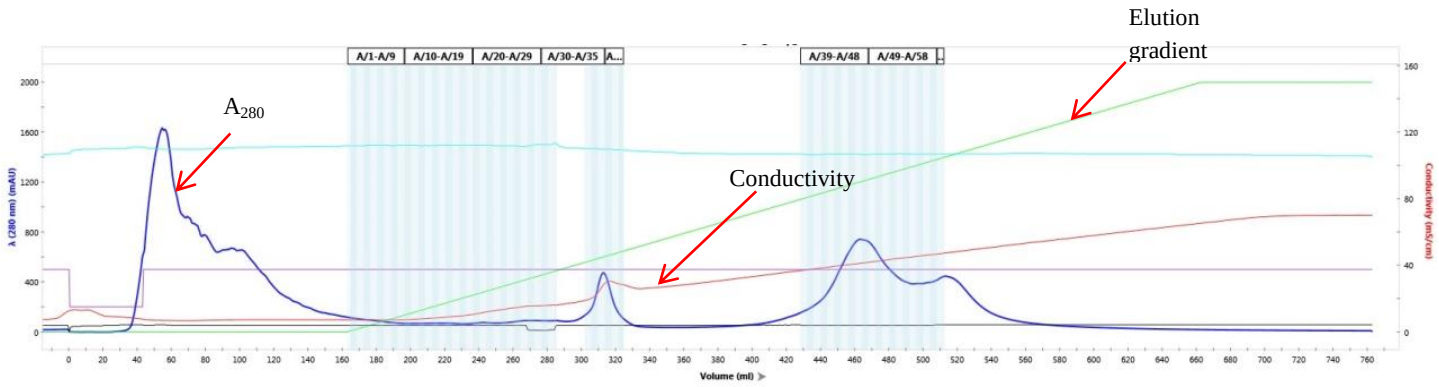

A.

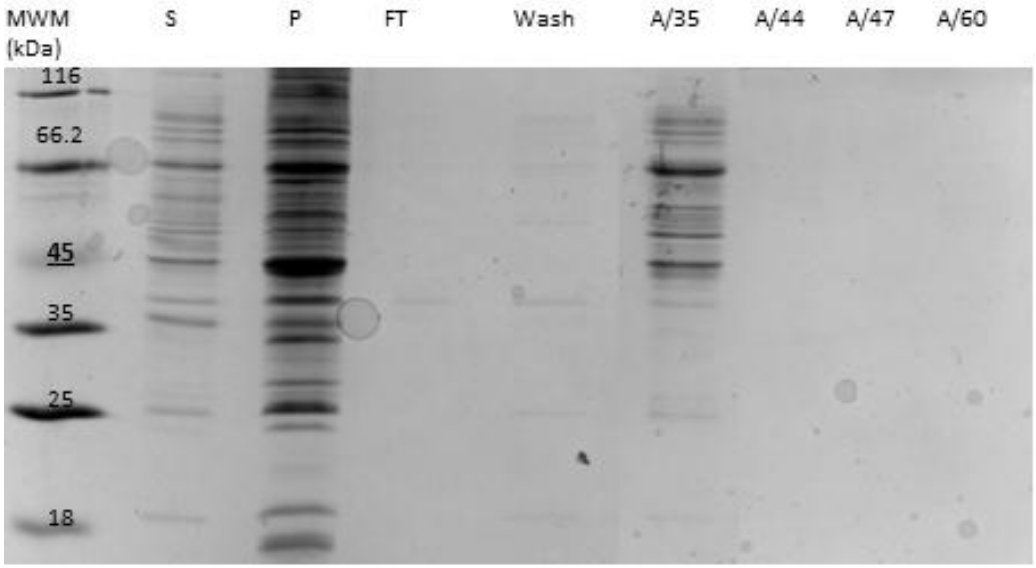

B.

Figure 3-12: Anion (DEAE Sepharose) exchange chromatography purification of VP6 using a sodium phosphate buffer and a gradient elution of up to 1 M sodium chloride.
A. The elution chromatographic profile illustrates the absorbance at 280 nm (blue line), conductivity (red line) and elution gradient (green line). B. SDS-PAGE gel indicates the "MWM" lane which represents the molecular weight marker in kDa. The lane marked "S" represents the soluble proteins obtained from the supernatant of the cell lysate loaded on the column. "P" represents the pelleted proteins precipitated from the cell lysate. The lane labelled "FT" represents the flow-through protein sample that did not bind, but passed through the column during sample loading. The lane marked "Wash" represents the proteins washed from column during the wash step. Selected fractions between "A/35" to "A/60" represent fractions that were collected during the elution gradient from 0 M up to 1 M sodium chloride.

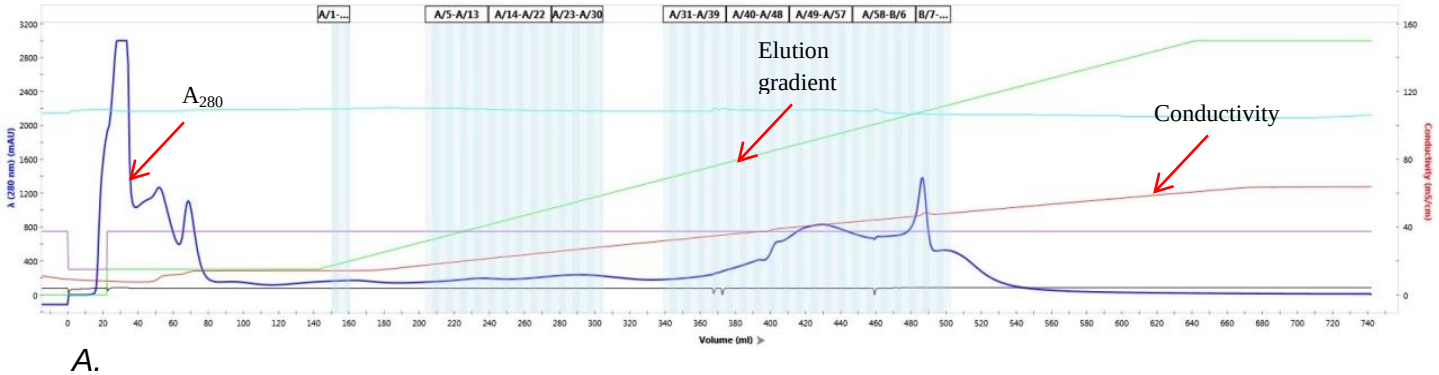

A.

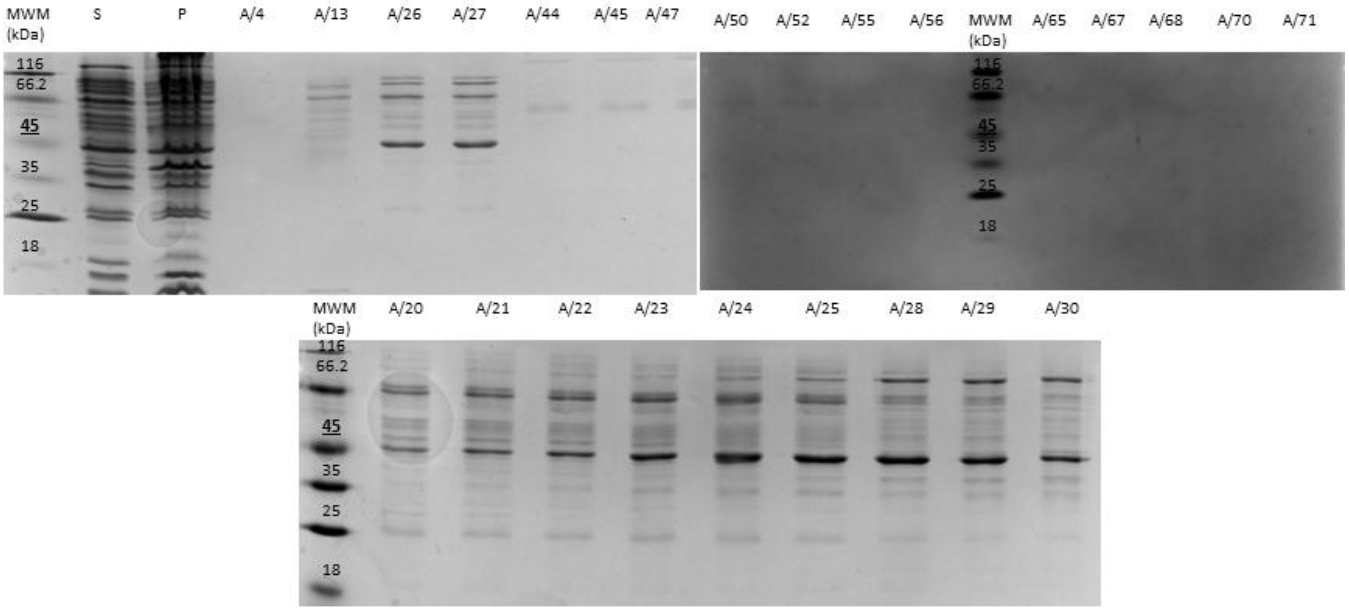

B.

Figure 3-13: Anion (DEAE Sepharose) exchange chromatography purification of VP6 using a sodium phosphate buffer and a gradient elution of up to 0.7 M sodium chloride

A. The elution chromatographic profile illustrates the absorbance at 280 nm (blue line), conductivity (red line) and elution gradient (green line). B. SDS-PAGE gel indicating the lane "MWM" represents the molecular weight marker in kDa. The lane marked "S" represents the soluble proteins obtained from the supernatant of the cell lysate loaded on the column. "P" represents the pelleted proteins precipitated from the cell lysate. Selected fractions between "A/4" to "A/60" and "B/11" represent fractions that were collected during the elution gradient from 0.08 M up to 0.7 M sodium chloride.

Proteins can be eluted by changes in pH or sodium chloride on ion-exchange resins. Theoretically, a pH lower than VP6's pI (6.65) would render a net positive charge, causing the like-charged molecules (VP6 and the Sepharose beads) to repeal each other. After protein loading and column wash procedures using Buffer B, the proteins were eluted using an elution gradient between Buffer B against Buffer B, pH 5.0, and 0.1 M sodium chloride. At the end of the gradient VP6 was not eluted off the column and was only eluted after 1 M sodium chloride buffer was exposed to the column (Figure 3-14 A and B.). The combination of a low pH and a low sodium chloride concentration was not able to eluting VP6 off the DEAE column.

More protein was expressed in KRX cells, suspended in Buffer B, and was applied to the DEAE Sepharose column, which was then washed with the same buffer before loading 2 × CV of Buffer B at pH 6, followed by 2 × CV of Buffer B at pH 5.5, then another 2 × CV of Buffer B at pH 5. This was done to determine the pH which can be used to elute VP6 off a DEAE column. The column was then regenerated with 1 M sodium chloride buffer. None of the buffers at pHs of 6; 5.5 or 5.0 were able to elute VP6 (Figure 3-15); nor did they elute other bacterial cellular proteins to further purify VP6. VP6 was present in fractions A/3 to A/5 (Figure 3-15 B). The experiment confirmed that VP6 was not eluted off the DEAE column by reducing the pH environment of the protein. The theoretical pI of the protein is based solely on the amino acid sequence, and the pH could have induced changes that only altered the tertiary or quaternary structure of the protein, resulting in the behaviour in question. It was found that an elution gradient of up to 0.7 M of sodium chloride can elute VP6 off a DEAE column when purifying with a sodium phosphate buffer at pH 7.04 (Figure 3-13). The lowest sodium chloride concentration required for eluting VP6 has not been established, which is essential for creating better separation of eluted proteins, thus increasing the purity of VP6.

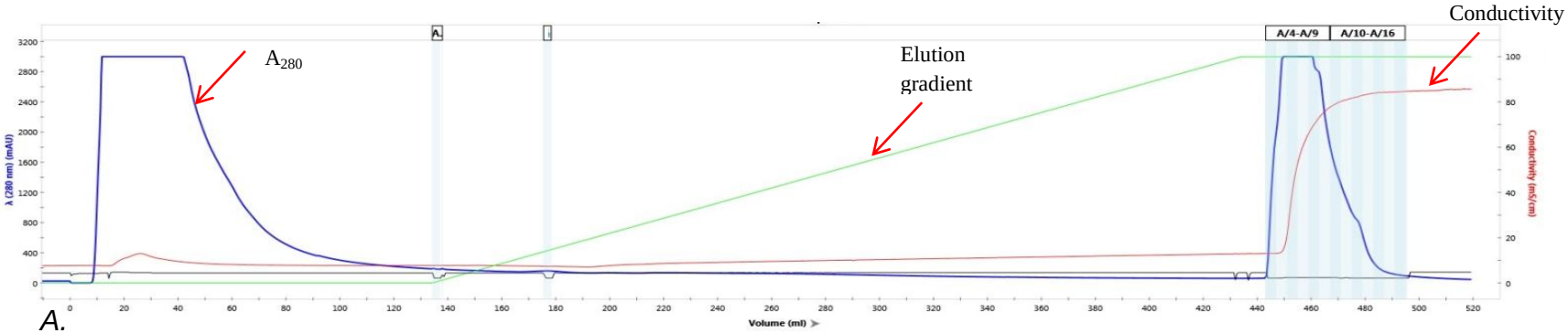

A.

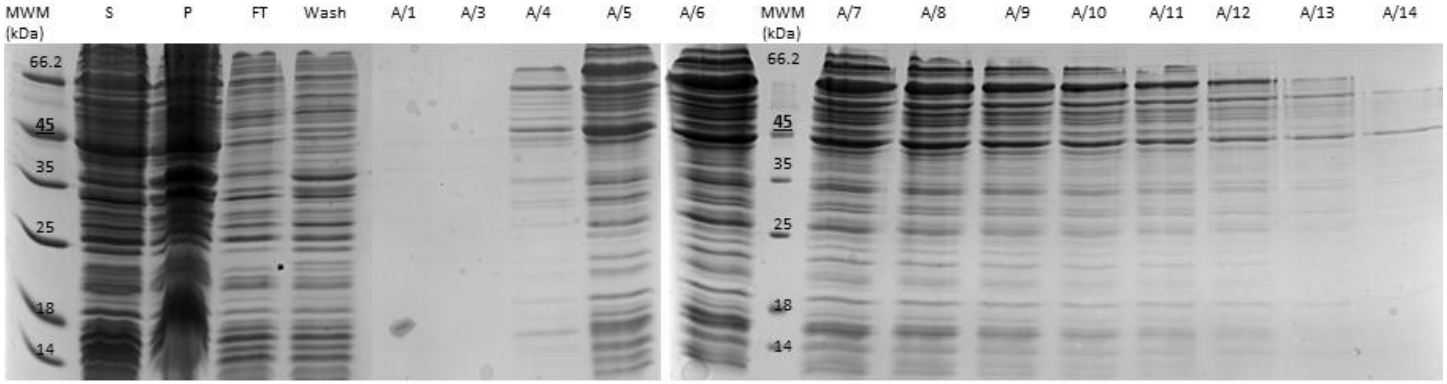

B.

Figure 3-14: Anion (DEAE Sepharose) exchange chromatography purification of VP6 using a sodium phosphate buffer and a gradient elution of up to 0.1 M sodium chloride at pH 5.0.

A. The elution chromatographic profile illustrates the absorbance at 280 nm (blue line), conductivity (red line) and elution gradient (green line). B. SDS-PAGE gel indicates the lane "MWM" which represents the molecular weight marker in kDa. The lane marked "S" represents the soluble proteins obtained from the supernatant of the cell lysate loaded onto the column. "P" represents the pelleted proteins precipitated from the cell lysate. The lane labelled "FT" represents the flow-through protein sample that did not bind, but passed through the column during sample loading. The lane marked "Wash" represents the proteins washed from column during the wash step. Selected fractions between "A/1" and "A/3" represent fractions that were collected during the elution gradient from 0.08 M up to 0.1 M sodium chloride at pH 5.0. Fractions labelled "A/4" to "A/14" represent fractions that were collected during column regeneration with a 1 M sodium chloride buffer.

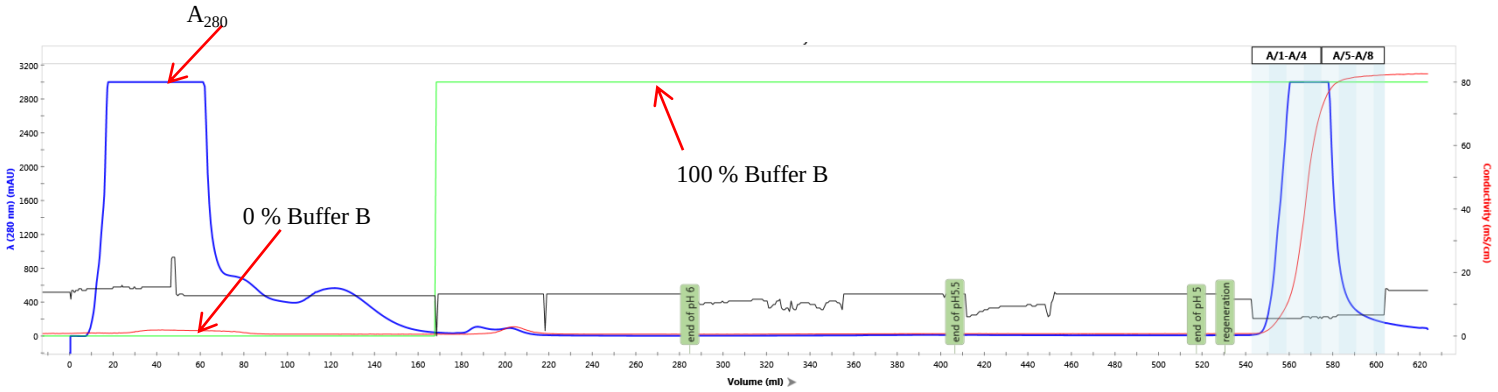

A.

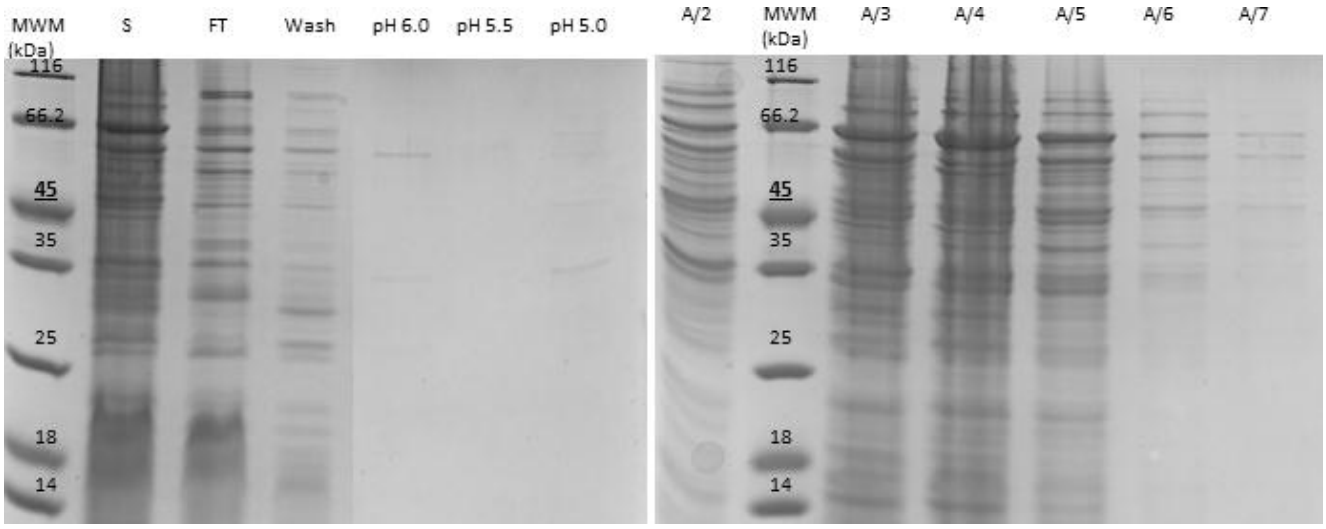

B.

Figure 3-15: Anion (DEAE Sepharose) exchange chromatography purification of VP6 using a sodium phosphate buffer and varying pH for elution

A. The elution chromatographic profile illustrates the absorbance at 280 nm (blue line), conductivity (red line) and the percentage of 0.05 M sodium phosphate buffer, pH 7.04, containing 0.08 M sodium chloride is represented as a green line. Buffers used were 0.05 M sodium phosphate buffers prepared at pH 6.0; 5.5; and at 5.0. B. SDS-PAGE gel indicating the lane "MWM" represents the molecular weight marker in kDa. The lane marked "S" represents the soluble proteins obtained from the supernatant of the cell lysate loaded onto the column. The lane labelled "FT" represents the flow-through protein sample that did not bind, but passed through the column during sample loading. The lane marked "Wash" represents the proteins washed from column during the wash step, with Buffer B at pH 7.04. Lanes marked "pH 6.0"; "pH 5.5"; and "pH 5.0" were proteins fractions collected during their respective pH buffer. Selected fractions between "A/2" and "A/7" represent fractions that were collected during column regeneration with 1 M sodium chloride.

To determine a better sodium chloride concentration required to isolate VP6 required an experiment that involves washing the column containing VP6 with increasing sodium chloride concentrations of Buffer B. The selected sodium chloride buffers are 0.2 M, 0.3 M, 0.5 M and 0.7 M. The first elution wash was with 0.2 M sodium chloride; followed by a 0.3 M sodium chloride; then a 0.5 M sodium chloride, and lastly a 0.7 M sodium chloride buffer (Figure 3-16 A.). Each elution was performed using 2 x CV of the sodium chloride buffer. VP6 was eluted at 0.2 M, 0.3 M and 0.5 M sodium chloride concentration but most of VP6 was eluted at the lowest sodium chloride concentration (Figure 3-16 B.). From the results it was deduced that an elution gradient of up to 0.2 M sodium chloride is essential to successfully eluting VP6 off a DEAE column and is low enough to create better separation between VP6 and other cellular proteins.

The modified conditions for purifying VP6 on a DEAE column using an elution gradient were tested with an elution gradient from 0.08 M up to 0.2 M sodium chloride. The supernatant containing VP6 was loaded to the column, and washed with 4 × CV of Buffer B before the elution gradient was initiated. During elution fractions were collected and analysed on an SDS-PAGE gel (Figure 3-17 B.). VP6 was eluted with the elution gradient of 0.08 M to 0.2 M sodium chloride. VP6 was present in fractions A/18 to A/24 (which was eluted by a sodium chloride concentration of approximately 0.15 M).

Results obtained from purifying VP6 using DEAE column chromatography showed that most bacterial cellular proteins are separated from VP6. The absence of VP6 in the unbound protein sample and regeneration with 1 M sodium chloride after a gradient elution of up to 0.2 M sodium chloride concentration indicates that there is little loss of VP6 during the anion exchange chromatography purification (Figure 3-18 B.). A second purification was still required as VP6 was not purified from other bacterial protein species.

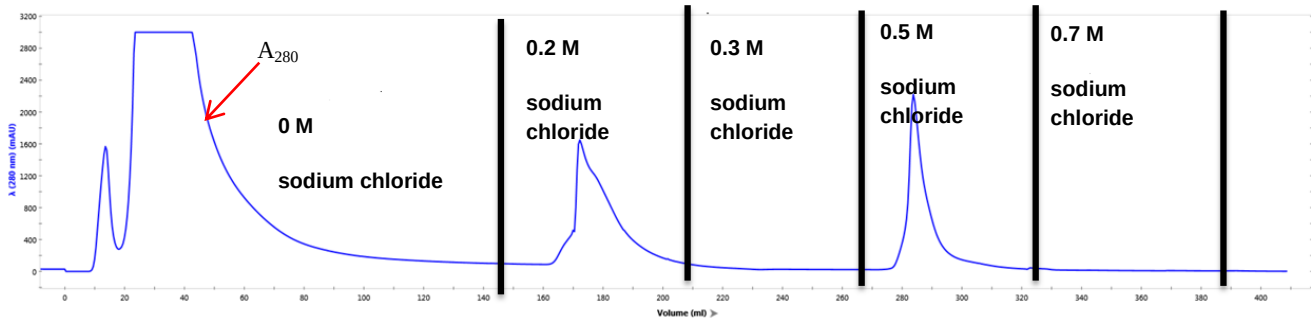

A.

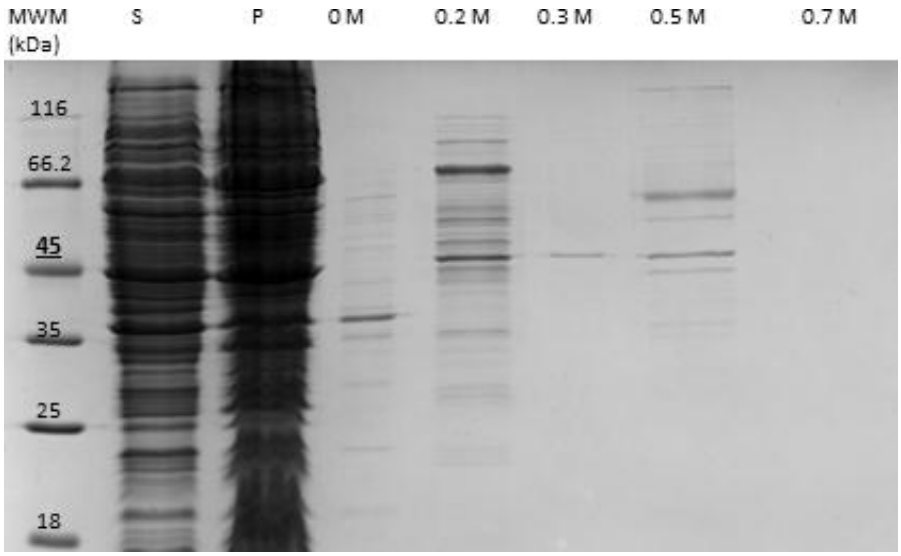

B.

Figure 3-16: Anion (DEAE Sepharose) exchange chromatography purification of VP6 using a sodium phosphate buffer and sodium chloride elution using 0.2 M, 0.3 M, 0.5 M and 0.7 M concentrations

A. The elution chromatographic profile illustrates the absorbance at 280 nm read at different sodium chloride concentrations of 0 M; 0.2 M; 0.3 M; 0.5 M and 0.7 M. B. SDS-PAGE gel indicates the lane "MWM" which represents the molecular weight marker in kDa. The lane marked "S" represents the soluble proteins obtained from the supernatant of the cell lysate loaded onto the column. "P" represents the pelleted proteins precipitated from the cell lysate. Lanes marked "0 M"; "0.2 M"; "0.3 M"; "0.5 M", and "0.7 M" represents protein fractions collected in their respective sodium chloride concentration.

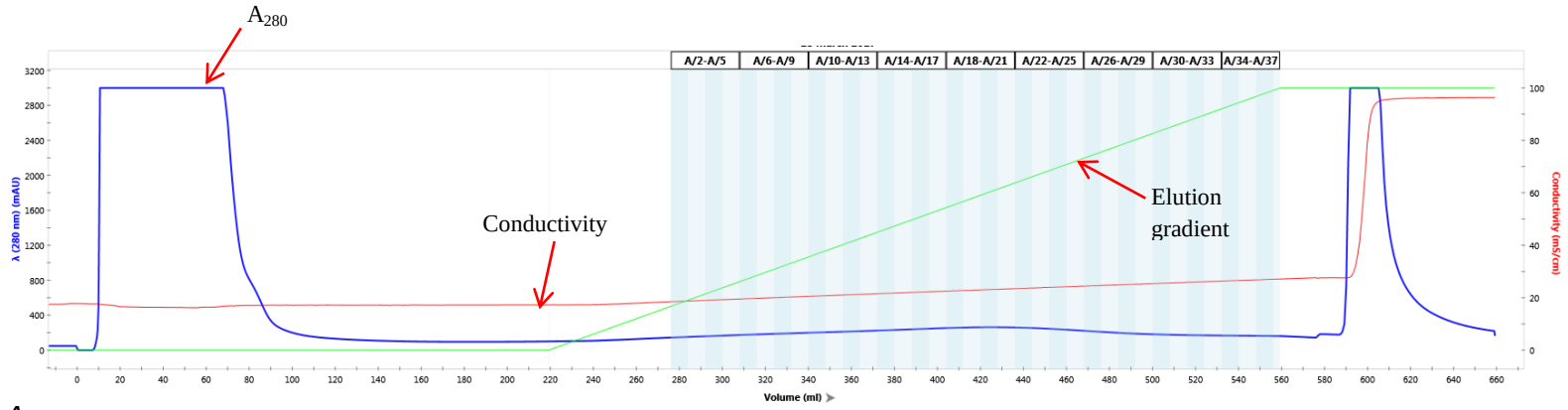

A.

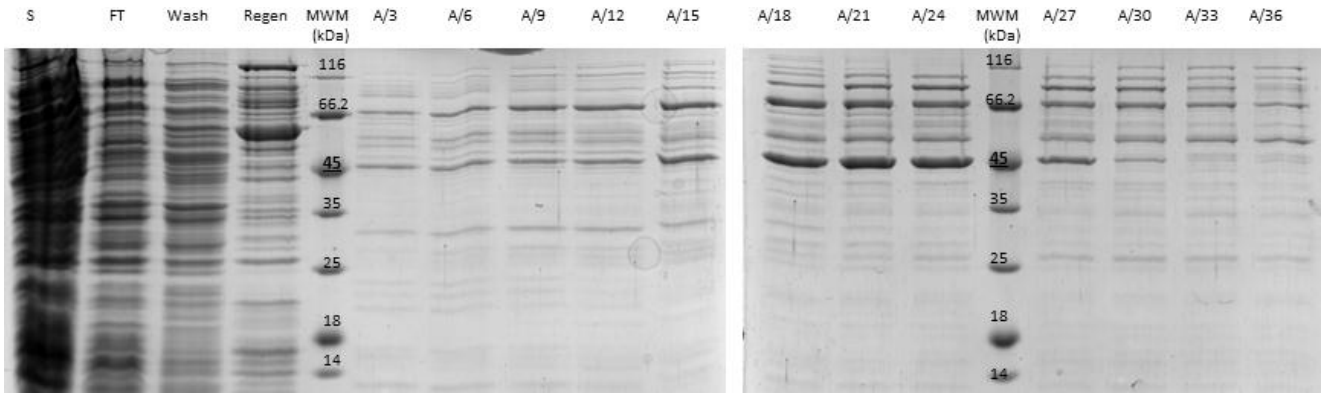

B.

Figure 3-17: Anion (DEAE Sepharose) exchange chromatography purification of VP6 using a sodium phosphate buffer and a gradient elution of up to 0.2 M sodium chloride

A. The elution chromatographic profile illustrates the absorbance at 280 nm (blue line), conductivity (red line) and elution gradient (green line). B. SDS-PAGE gel indicates the lane "MWM" which represents the molecular weight marker in kDa. The lane marked "S" represents the soluble proteins obtained from the supernatant of the cell lysate loaded onto the column. The lane labelled "FT" represents the flow-through protein sample that did not bind, but passed through the column during sample loading. The lane marked "Wash" represents the proteins washed from column during the wash step. "Regen" represents regeneration which signifies the protein collected during 1 M sodium chloride column wash. Selected fractions between "A/18" to "A/24" represent fractions that were collected during the elution gradient from 0.08 M up to 0.2 M sodium chloride.

Taraporewala *et al*. (2006) and Zhang *et al*. (2017) purified their target proteins using two different chromatography techniques to help achieve a higher level of purity by combining affinity and ion exchange chromatography. Seth *et al*. (2017) utilised three column chromatography purification techniques which included an initial purification using affinity chromatography (Ni^{2+} column), then an anion (Q Sepharose column) and then a cation (SP Sepharose column) exchange chromatography to further remove endotoxins, host cell proteins and residual DNA.

3.2.4 Purification using affinity and ion exchange chromatography

Seth *et al*. (2017); and Zhang *et al*. (2017) used affinity chromatography initially to partially purify their specific proteins of interest, followed by an ion exchange chromatography to complete the purification.

In the current study an anion exchange chromatography was selected as an ideal technique to be used as a first step of partially purifying VP6, this was because the DEAE column had a high resin volume of 36 ml ensuring that the binding capacity is high.

Supernatant containing VP6 was loaded onto the column, and then washed with 4 × CV of Buffer B before a gradient elution from 0.08 M sodium chloride to 0.2 M sodium chloride. Fractions were collected during elution, and were analysed on an SDS-PAGE gel (Figure 3-18 B.). The fractions that were visualised to have VP6 were pooled, and a 0.01 M imidazole was added along with 3 M urea to the pooled fractions. A lower 3 M urea was used in order to prevent complete unfolding of VP6 and other cellular proteins. Affinity chromatography was performed on a 5 ml HisTrap column which was equilibrated with Buffer A.

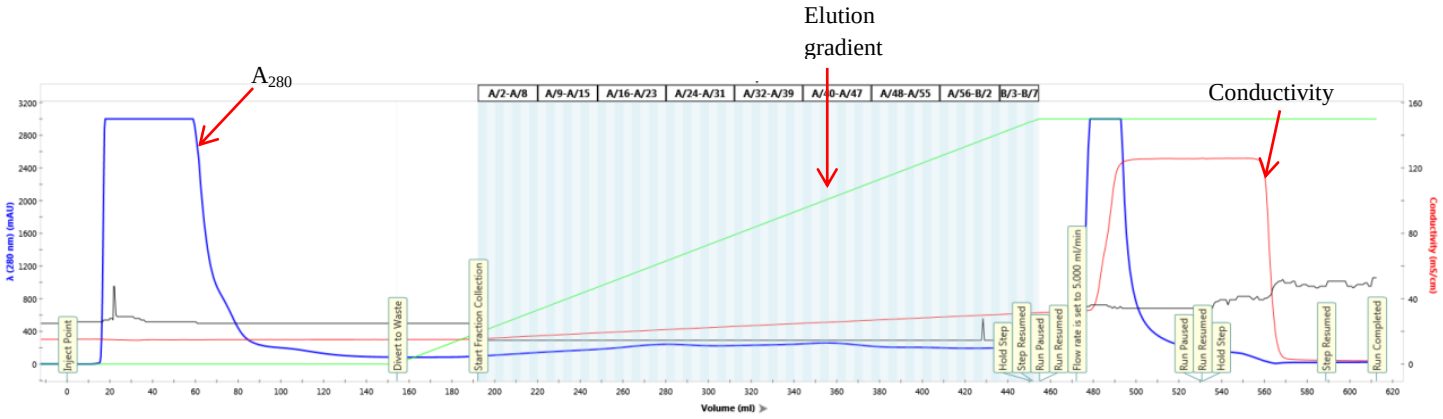

A.

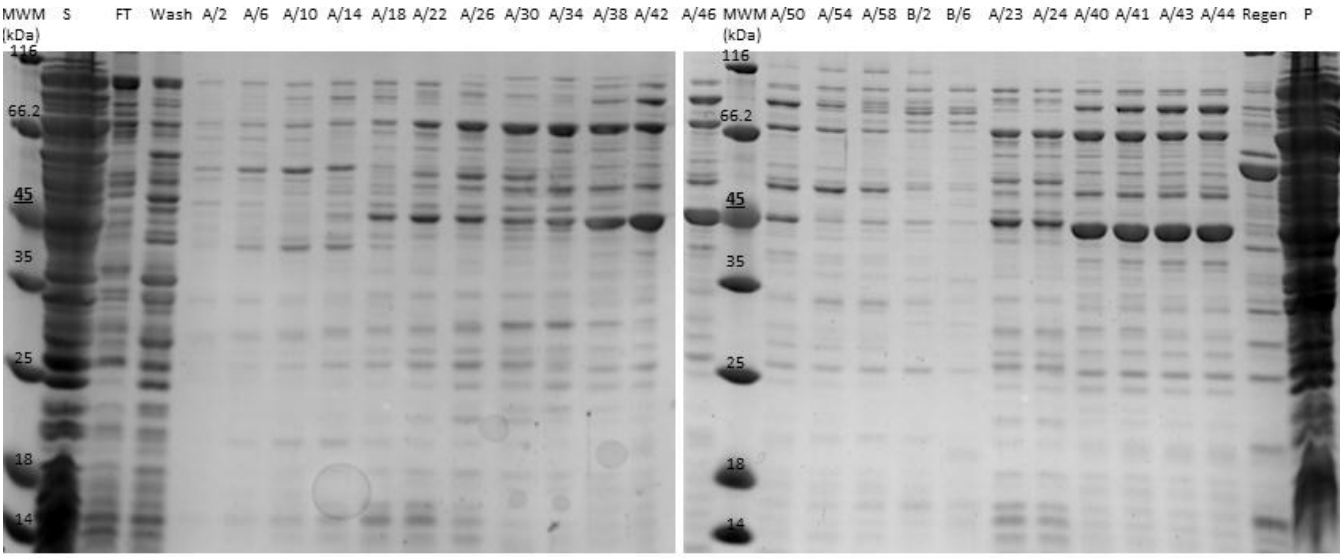

B.

Figure 3-18: Partial purification of VP6 using anion (DEAE Sepharose) exchange chromatography with a gradient elution of up to 0.2 M sodium chloride

A. The elution chromatographic profile illustrates the absorbance at 280 nm (blue line), conductivity (red line) and elution gradient (green line). B. SDS-PAGE gel indicates the lane "MWM" which represents the molecular weight marker in kDa. The lane marked "S" represents the soluble proteins obtained from the supernatant of the cell lysate loaded on the column. The lane labelled "FT" represents the flow-through protein sample that did not bind, but passed through the column during sample loading. The lane marked "Wash" represents the proteins washed from column during the wash step. "Regen" represents regeneration which signifies the protein collected during 1 M sodium chloride column wash. Selected fractions between "A/18" to "A/24" represent fractions that were collected during the elution gradient from 0.08 M up to 0.2 M sodium chloride.

The column was washed with Buffer A, and elution gradient used started from 0.01 M and ended with 0.2 M imidazole.

The presence of VP6 in the fractions collected during the elution confirmed that there was VP6 that remained bound to the column during sample application (Figure 3-19 B).

VP6 was not pure and, therefore, another HisTag affinity chromatography was conducted using fractions obtained from the experiment represented in Figure 3-19. The fractions were pooled and then diluted with the binding buffer without imidazole to give the pooled fractions containing imidazole a final concentration of approximately 0.01 M. The sample was then reloaded on the HisTrap column which was pre-equilibrated with 4 × CV of Buffer A which also used to wash the column after sample application. The elution gradient was between Buffer A against Buffer with 0.1 M imidazole. In this instance VP6 did completely bind to the Ni^{2+} resin and was present in the fractions collected during the elution gradient (Figure 3-20), but bacterial cellular proteins were still detected along with VP6.

Fractions from the experiment represented in Figure 3-20 were pooled, and imidazole concentration was diluted to approximately 0.01 M using Buffer A with no imidazole. The diluted sample was applied to a HisTrap column pre-equilibrated with Buffer A, and then the column was washed with the same buffer and eluted with a modified elution volume that was increased from 10 × CV to 15 × CV, and the elution gradient was shortened from 0.2 M to 0.1 M imidazole, this was an attempt to further separate the proteins during elution. Fractions A/3 to A/13 contained a low, but pure yield of VP6 (Figure 3-21). The protein yield was observed to be low and was repeated with a culture volume of 1300 ml instead of 500 ml in previous purifications.

KRX cells were grown and induced using optimised expression conditions described in section 3.1. Supernatant containing VP6 was obtained from KRX cells using the method described in section 2.3. The supernatant was loaded onto a DEAE column pre-equilibrated with Buffer B. An elution gradient from 0.08 M up to 0.2 M sodium chloride was used to elute VP6. After a 4 × CV wash with Buffer B VP6 was present fractions A/7 to A/9 (Figure 3-22).

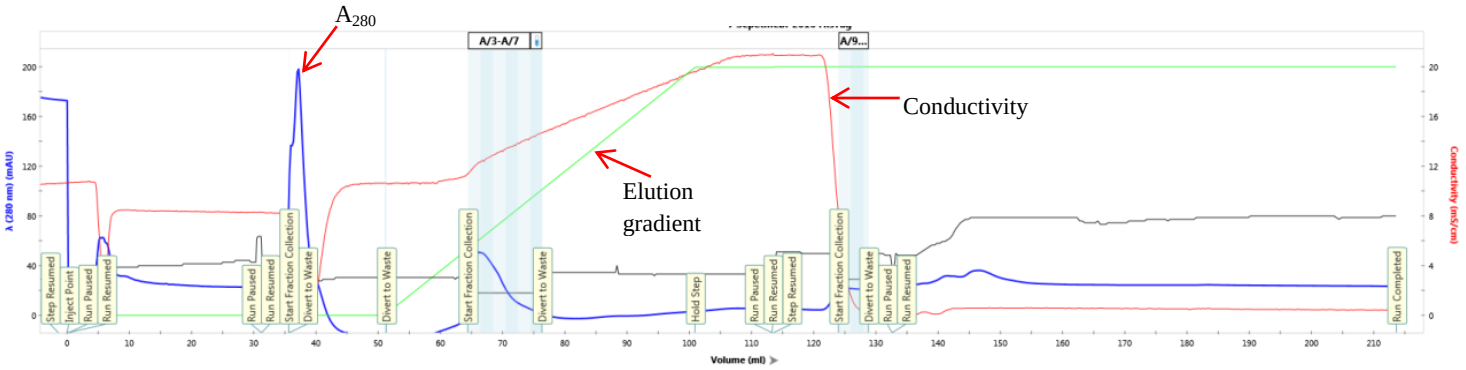

A.

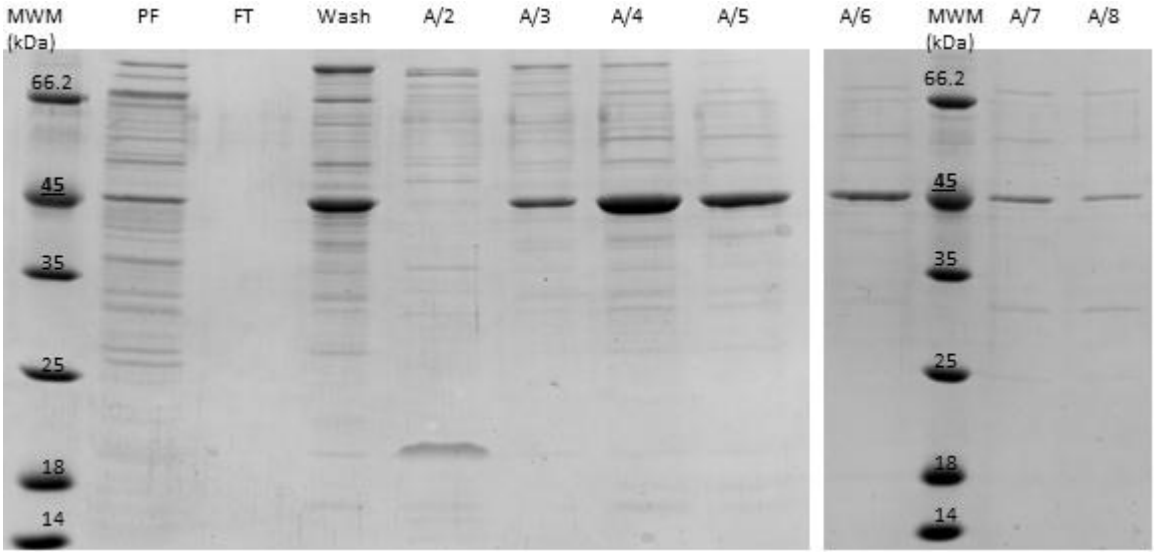

B.

Figure 3-19: Affinity (HisTag) chromatography purification of VP6 using a sodium phosphate buffer and a gradient elution from 0.01 M up to 0.2 M imidazole

A. The elution chromatographic profile illustrates the absorbance at 280 nm (blue line), conductivity (red line) and elution gradient (green line). B. SDS-PAGE gel indicating the lane "MWM" which represents the molecular weight marker in kDa. The lane marked "PF" represents the pooled fractions containing VP6 from the anion exchange chromatography represented in Figure 3-18. The lane labelled "FT" represents the flow-through protein sample that did not bind, but passed through the column during sample loading. The lane marked "Wash" represents the proteins washed from column during the wash step. Selected fractions between "A/2" to "A/8" represent the fractions that were collected during the elution gradient from 0.01 M up to 0.2 M of imidazole.

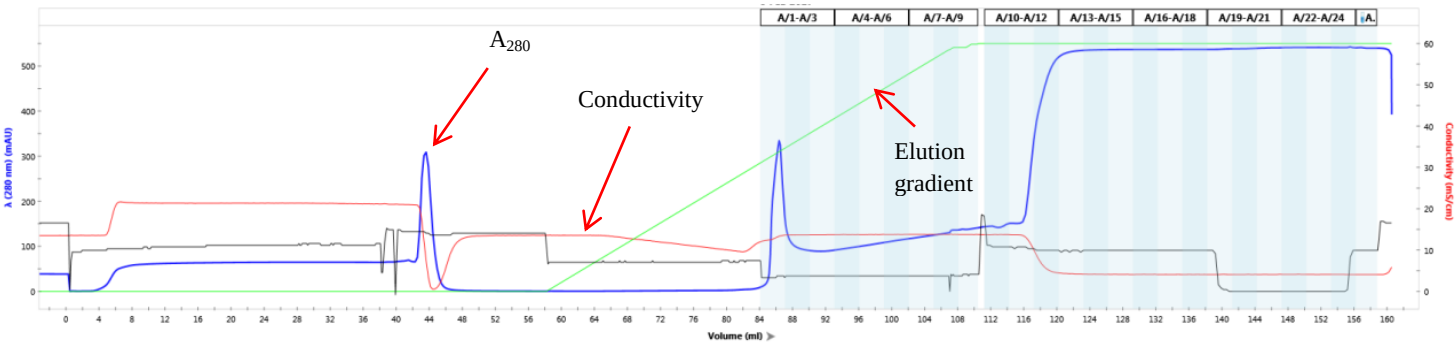

A.

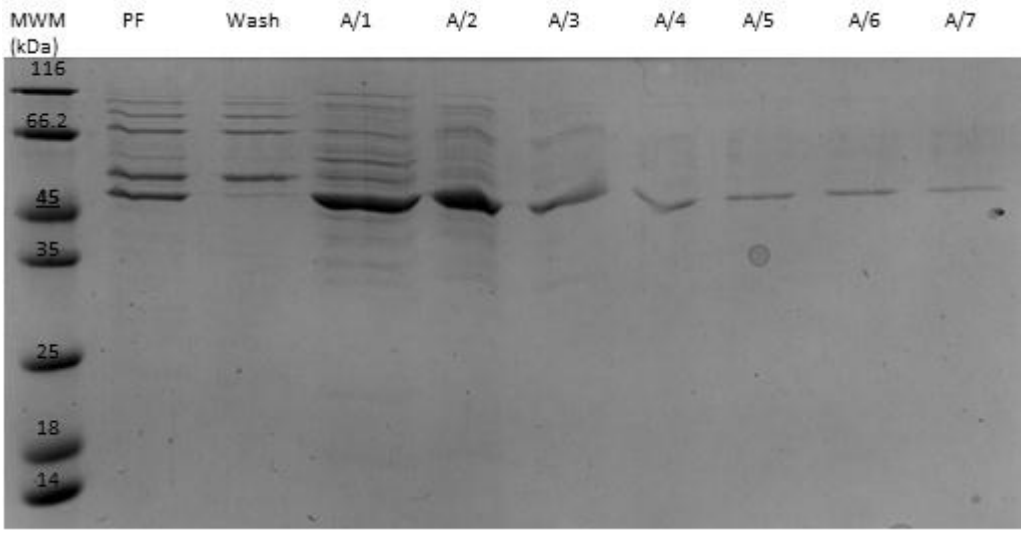

B.

Figure 3-20: Affinity (HisTag) chromatography purification of VP6 using a sodium phosphate buffer and a gradient elution from 0.01 M up to 0.1 M imidazole

A. The elution chromatographic profile illustrates the absorbance at 280 nm (blue line), conductivity (red line) and elution gradient (green line). B. SDS-PAGE gel indicating the lane "MWM" which represents the molecular weight marker in kDa. The lane marked "PF" represents the pooled fractions containing VP6 from affinity chromatography experiment (Figure 3-19). The lane marked "Wash" represents the proteins washed from column during the wash step. Selected fractions between "A/"1 to "A/7" represents the fractions that were collected during the elution gradient from 0.01 M up to 0.1 M imidazole concentration.

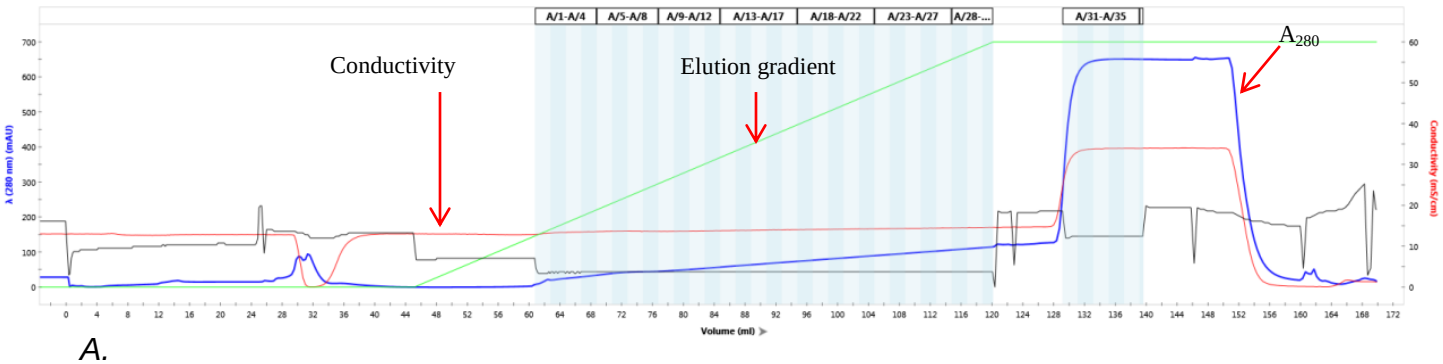

A.

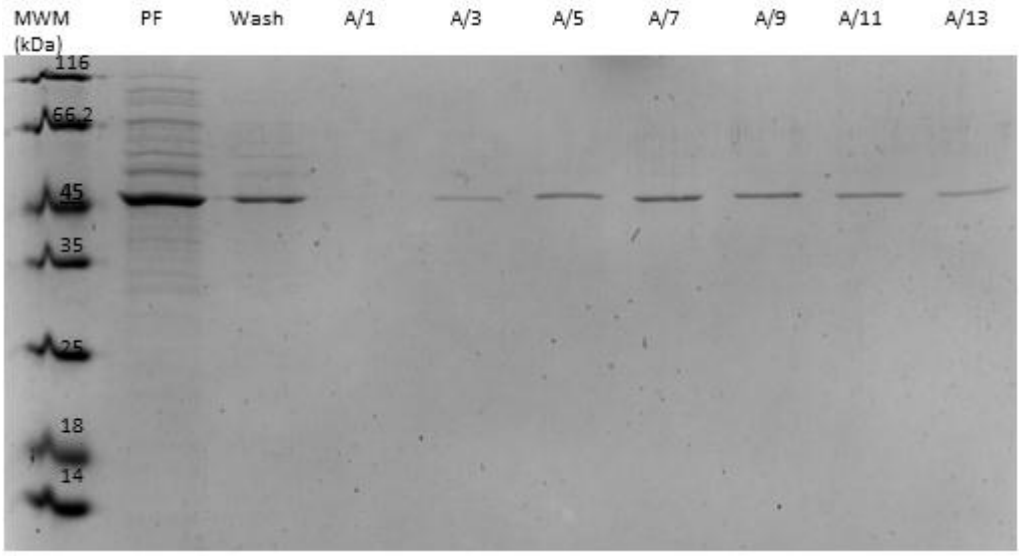

B.

Figure 3-21: Affinity (HisTag) chromatography purification of VP6 using a sodium phosphate buffer and a 15 column volumes gradient elution from 0.01 M up to 0.1 M imidazole

A. The elution chromatographic profile illustrates the absorbance at 280 nm (blue line), conductivity (red line) and elution gradient (green line). B. SDS-PAGE gel indicates the lane "MWM" which represents the molecular weight marker in kDa. The lane marked "PF" represents the pooled fractions containing VP6 from the previous HisTag VP6 purification. The lane marked "Wash" represents the proteins washed from column during the wash step. The selected fractions between "A/1" to "A/13" represents the fractions that were collected during the elution gradient from 0.01 M up to 0.1 M imidazole concentration.

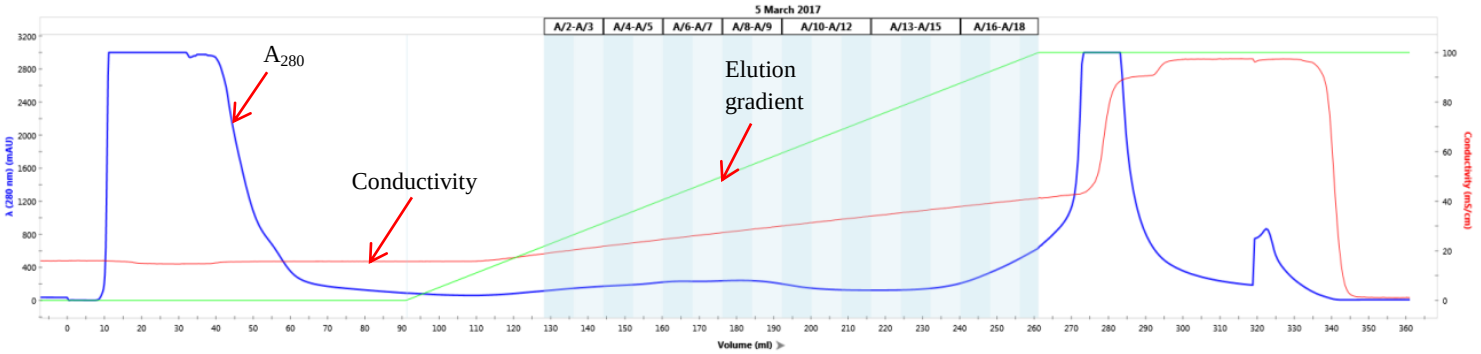

A.

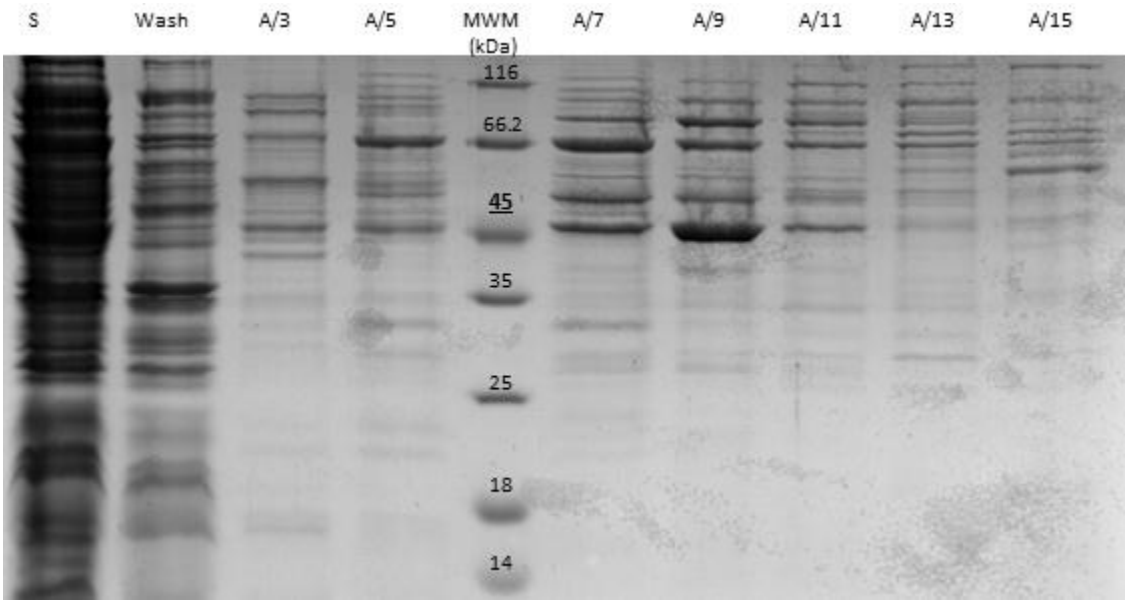

B.

Figure 3-22: Anion (DEAE Sepharose) exchange chromatography partial purification of VP6 using a gradient elution of up to 0.2 M sodium chloride, trial 2

A. The elution chromatographic profile illustrates the absorbance at 280 nm (blue line), conductivity (red line) and elution gradient (green line). B. SDS-PAGE gel indicates the lane "MWM" which represents the molecular weight marker in kDa. The lane marked "S" represents the soluble proteins obtained from the supernatant of the cell lysate loaded onto the column. The lane marked "Wash" represents the proteins washed from column during the wash step. Selected fractions between "A/3" and "A/15" represent fractions that were collected during the elution gradient from 0.08 M up to 0.2 M sodium chloride.

The VP6 containing fractions were pooled, and imidazole was added to a final concentration of 0.01 M, before being applied to a HisTrap column which was pre-equilibrated with Buffer A. The column was washed with 4 × CV of the same buffer; VP6 was completely bound to the column resin and was eluted during the elution gradient (Figure 3-23) spanning from 0.01 to 0.1 M imidazole concentration.

Fractions A/2 to A/11 were pooled, diluted with Buffer A to reduce the imidazole concentration to approximately 0.01 M, and then again loaded on a HisTrap column to ensure that VP6 reached a higher purity level. The purification was performed with the same conditions as the previous affinity chromatography experiment, but in this instance the elution gradient was reduced to 0.055 M which was calculated by deriving 55% (the point on the elution gradient where VP6 was eluted) from 0.1 M imidazole (final concentration of imidazole on the elution gradient), the elution volume was increased from 15 to 20 × CV. Fractions A/4 to A/11 contained more VP6 and no contaminant proteins (Figure 3-24).

In this study it was observed that the HisTrap column was not capable of binding all of the VP6 and the cellular proteins present in the supernatant, most of the proteins are washed off the column (Figure 3-8, Figure 3-9 and Figure 3-19). Thus, a 20 ml HisPrep column was used in experiments shown in Figures 3-23 and Figure 3-24.

Initially the HisTag affinity chromatography was not efficient in separating VP6 from other contaminating bacterial cellular proteins, but it was found that by narrowing the final gradient elution from 0.2 M to 0.1 M imidazole concentration, and increasing the elution volume from 10 to 20 × CV helped promote separation of VP6 from the contaminating proteins (Figure 3-24)

VP6 obtained from the affinity chromatography fractions contain 3 M urea, and approximately 0.05 M imidazole when pooled together, these chemicals affect the structure and absorbance reading of the protein, thus the protein has to be buffer exchanged into Buffer D prior to concentration determination and structural determination tests. The fractions containing pure VP6 were pooled, concentrated and loaded onto a HiPrep (50 ml) desalting column from GE, which was pre-equilibrated with Buffer D

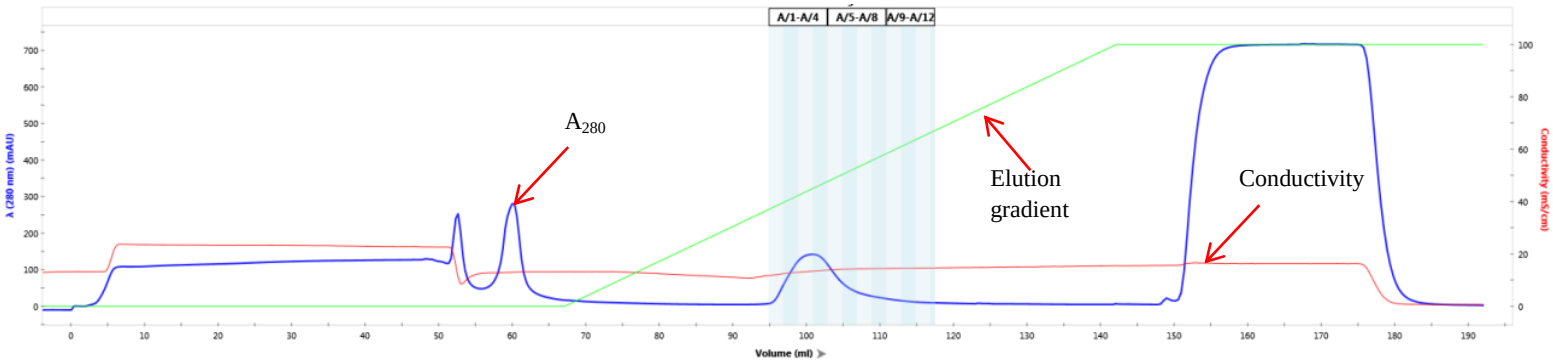

A.

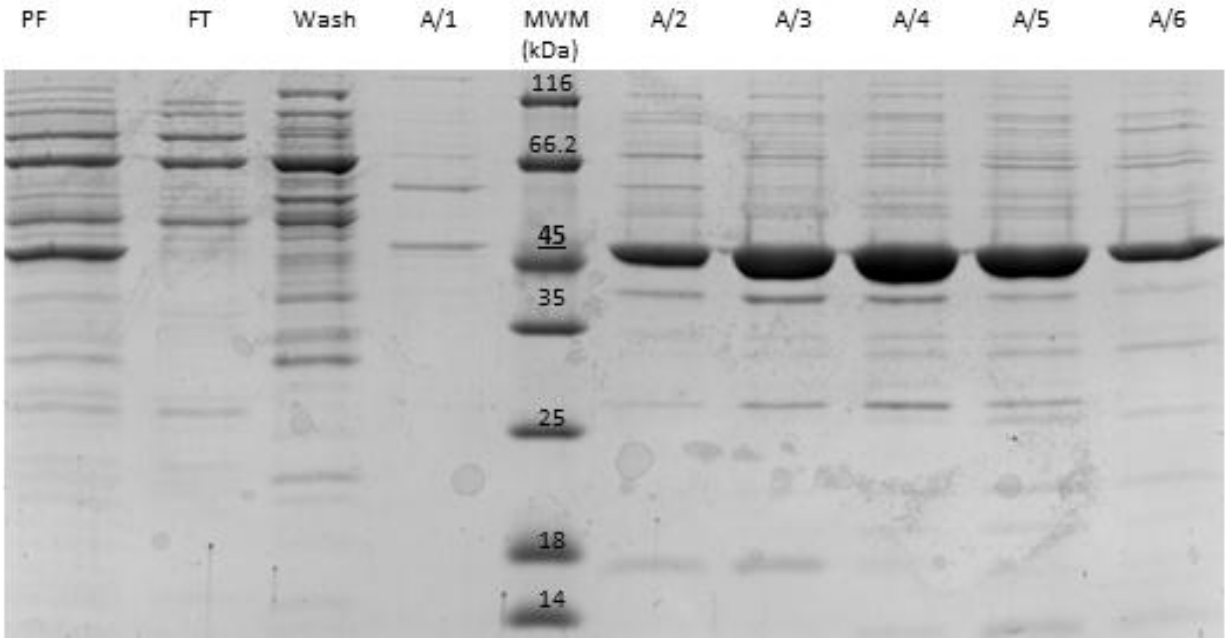

B.

Figure 3-23: Affinity (HisTag) chromatography purification of VP6 using a sodium phosphate buffer and a 15 column volume gradient elution from 0.01 M up to 0.1 M imidazole, trial 2

A. The elution chromatographic profile illustrates the absorbance at 280 nm (blue line), conductivity (red line) and elution gradient (green line). B. SDS-PAGE gel indicating the lane "MWM" which represents the molecular weight marker in kDa. The lane marked "PF" represents the pooled fractions containing VP6 from the ion exchange chromatography (Figure 3-22). The lane marked "Wash" represents the proteins washed from column during the wash step. Selected fractions "A/1" to "A/6" represent the fractions that were collected during the elution gradient from 0.01 M up to 0.1 M imidazole concentration.

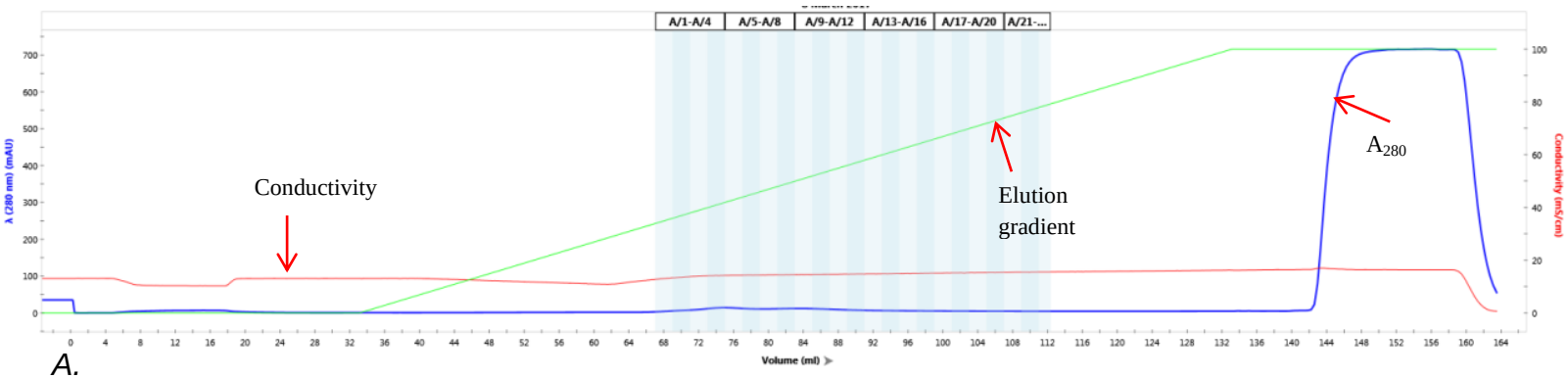

A.

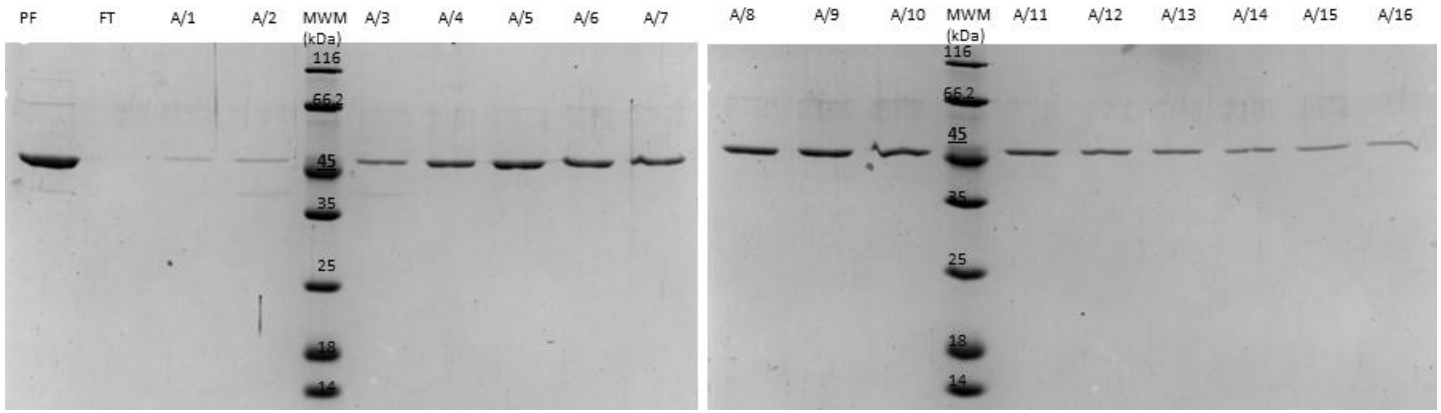

B.

Figure 3-24: Affinity (HisTag) chromatography purification of VP6 using a sodium phosphate buffer and a 20 column volumes gradient elution from 0.01 M up to 0.055 M imidazole

A. The elution chromatographic profile illustrates the absorbance at 280 nm (blue line), conductivity (red line) and elution gradient (green line). B. SDS-PAGE gel indicates the lane "MWM" which represents the molecular weight marker in kDa. The lane marked "PF" represents the pooled fractions containing VP6 from the HisTag affinity chromatography (Figure 3-23). Selected fractions between "A/1" to "A/16" represent fractions that were collected during the elution gradient from 0.01 M up to 0.055 M imidazole concentration.

The proteins that passed through the column were collected in 5 ml fractions, and then electrophoresed on a SDS-PAGE gel (Figure 3-25) in order to identify fractions containing VP6. Fractions A/4 and A/5 were pooled, then used for concentration determination and structural characterisation.

3.3. Protein concentration determination

Analysis of the protein sample was conducted by scanning across an absorbance spectrum ranging from 340 nm to 220 nm to assess concentration and purity of the purified VP6. The A_{260} was found to be higher than A_{280} indicating that there were nucleotides present in the VP6 sample (Figure 3-26), the A_{280} reading was used to determine the concentration of the purified VP6 using the formula described in section 2.13 which gave 0.76 µM VP6 in 5 ml Buffer D. This meant that a 1000 ml culture yielded 0.17 mg of VP6. The concentration calculated for VP6 is low because of the low absorbance reading at 280 nm.

3.4. Purification of VP6 with removal of nucleotides

Induced KRX cells were resuspended in Buffer E which has a lower sodium phosphate and lower sodium chloride concentration which prevents interferences with absorbance readings during UV CD analysis. The Buffer E used resuspend the proteins prior to purification contains 0.1 g/ml of DNase 1; 0.05 M magnesium chloride and 0.0001 M phenylmethane sulfonyl fluoride (PMSF) which binds and inhibits protease activity, thus preventing protein degradation by proteases.

The cells were sonicated, then centrifuged to separate the supernatant from pellet. The supernatant was applied to a DEAE anion exchange column that was pre-equilibrated with Buffer E. The column was then washed with 5 × CV of Buffer E before initiating a gradient elution starting at 0.02 M sodium chloride and ending with 0.3 M sodium chloride. VP6 was successfully bound to the column, with fractions A/9 to A/16 having the highest amount of VP6 (Figure 3-27).

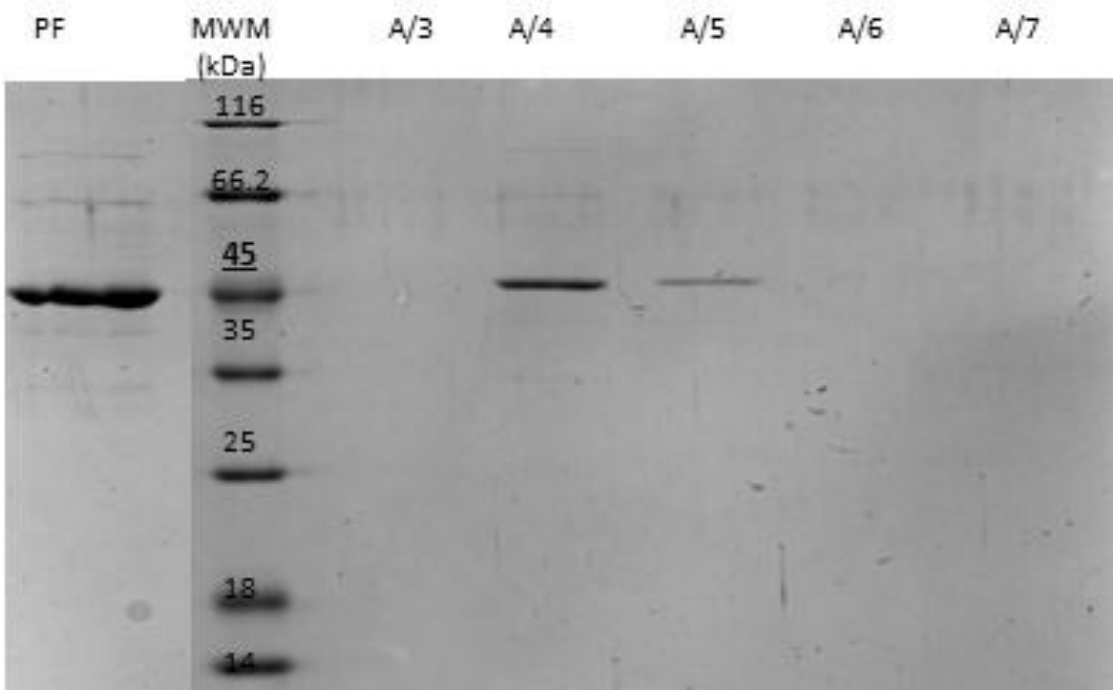

Figure 3-25: Buffer exchange using HiPrep desalting column

SDS-PAGE gel indicates the lane "MWM" which represents the molecular weight marker in kDa. The lane marked "PF" represents the pooled fractions containing VP6 from the HisTag affinity chromatography (Figure 3-24). The selected fractions between "A/3" to "A/7" represents the fractions that were collected after being applied on the HiPrep desalting column. Fractions "A/4" and "A/5" contain buffer exchanged VP6.

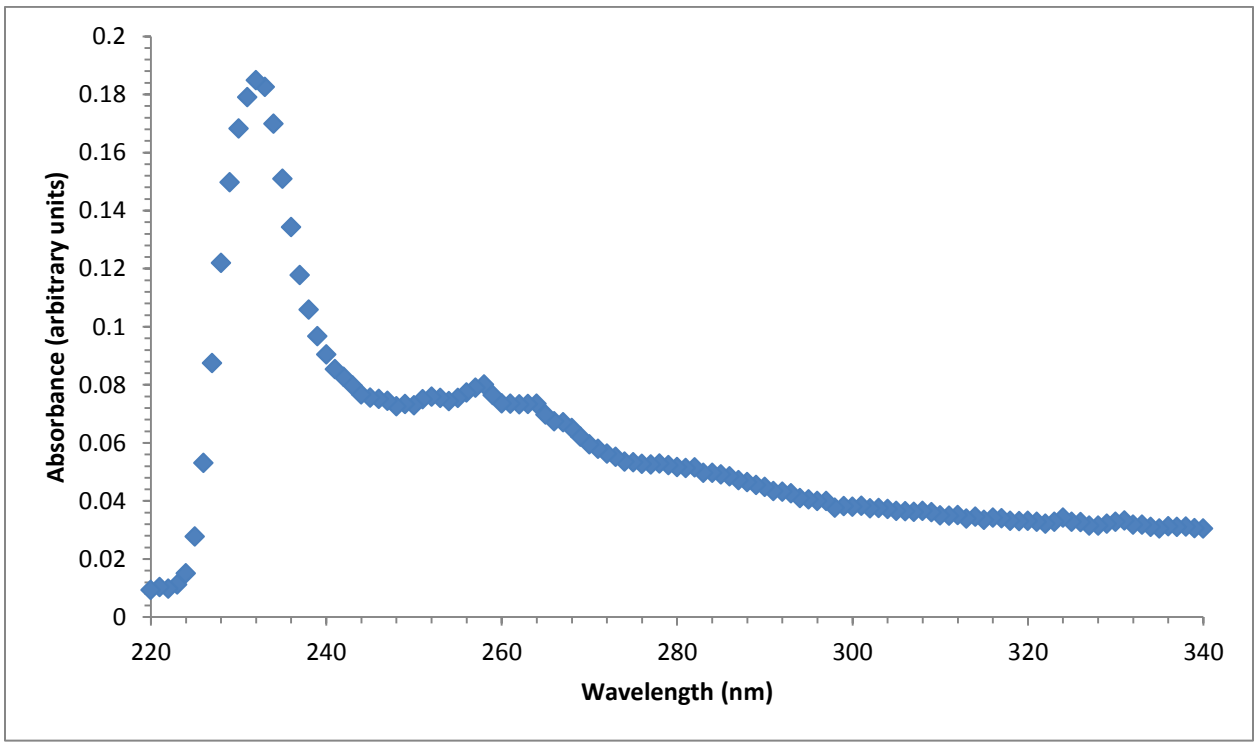

Figure 3-26: Absorbance spectrum of purified rotavirus VP6
The absorbance spectrum of VP6 was set from 340 nm to 220 nm. The spectrum was collected using 0.76 µM of VP6 buffer exchanged into 0.05 M sodium phosphate buffer, pH 7.04, containing 0.08 M sodium chloride over the length of 1 cm. The spectrum was collected at 1 nm per 0.5 s.

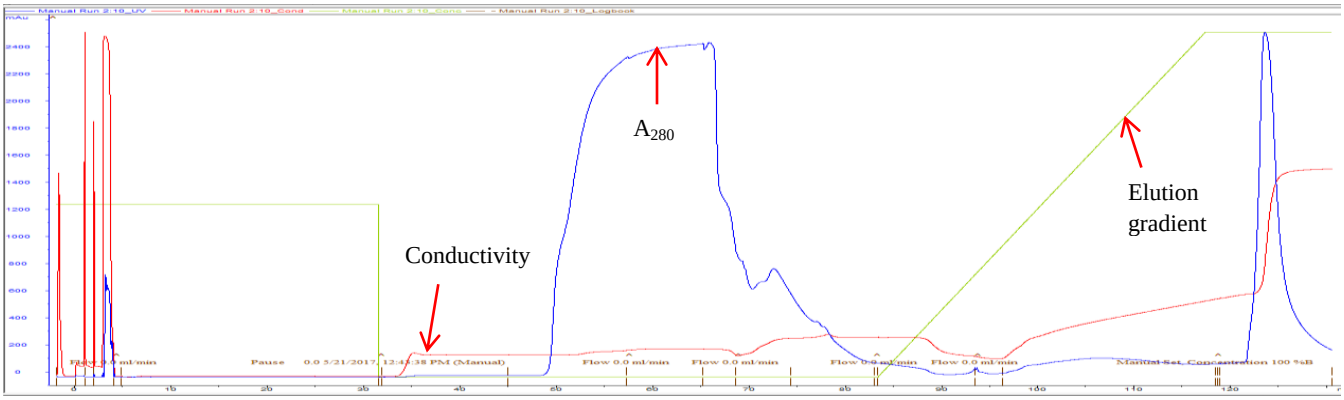

A.

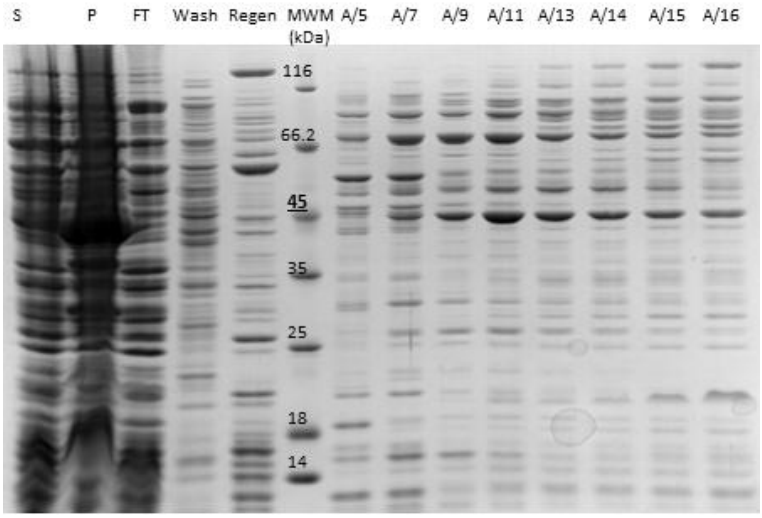

B.

Figure 3-27: Partial purification of VP6 using anion (DEAE Sepharose) exchange chromatography with a gradient elution of up to 0.3 M sodium chloride

A. The elution chromatographic profile illustrates the absorbance at 280 nm (blue line), conductivity (red line) and elution gradient (green line). B. SDS-PAGE gel indicating the lane "MWM" which represents the molecular weight marker in kDa. The lane marked "S" represents the soluble proteins obtained from the supernatant of the cell lysate loaded onto the column. "P" represents pelleted proteins precipitated from the cell lysate. The lane labelled "FT" represents the flow-through protein sample that did not bind, but passed through the column during sample loading. The lane marked "Wash" represents the proteins washed from column during the wash step. "Regen" represents regeneration which signifies the protein collected during 1 M sodium chloride column wash. Selected fractions between "A/5" and "A/15" represent fractions that were collected during the elution gradient from 0.02 M up to 0.3 M sodium chloride.

The fractions containing VP6 were pooled, concentrated, buffer exchanged to Buffer E containing 0.01 M imidazole, then loaded onto a HisPrep column pre-equilibrated with Buffer E containing 0.01 M imidazole, then VP6 was eluted with gradient of between Buffer E and Buffer E containing 0.055 M imidazole. Fractions A/1 to A/23 contained VP6 with only A/13 to A/23 containing pure VP6 (Figure 3-28 B).

Pure protein was obtained in fractions A/13 to A/23 which were then pooled, concentrated and buffer exchanged to Buffer E using a 5 ml desalting column. Using the A_{280} reading (Figure 3-29), from the absorbance spectrum VP6 concentration was calculated to be 1 µM (0.22 mg of VP6 from 1000 ml cell culture), A_{260}/A_{280} ratio was 0.91, which is lower than that obtained from the spectrum represented in Figure 3-26, which was 1.43. This indicated that there were less nucleotides present.

3.5. Structural characterisation of purified VP6

Far-UV CD was used on a 1 µM protein concentration in Buffer E with a path length of 1 mm. The CD spectra of VP6 (Figure 3-30 A), shows typical spectral characteristics of proteins that contains α-helices. This is signified by the trough at 208 nm and the trough at 222 nm that is also due to α-helices, counter-acted by the increase in ellipticity due to the presence of β-sheets (Sreerama & Woody, 2003). Far-UV CD can be used to assess changes in the protein's secondary structure when determining the stability of VP6 in different temperature, urea and sodium chloride concentrations.

Intrinsic fluorescence was used to identify the local tertiary environment around the tryptophan residues of the VP6 protein which can also provide a useful way of monitoring local conformational changes in the protein (Lakowicz, 2006). The RV VP6 has 5 tryptophan residues with 2 located on the β-sheet domain and three in the α-helical domain (Figure 1-4) (Zhao *et al.* 2011). The fluorescence intensity was recorded at 340 nm when excited at wavelengths of 295 nm and at 280 nm (Figure 3-30 B).

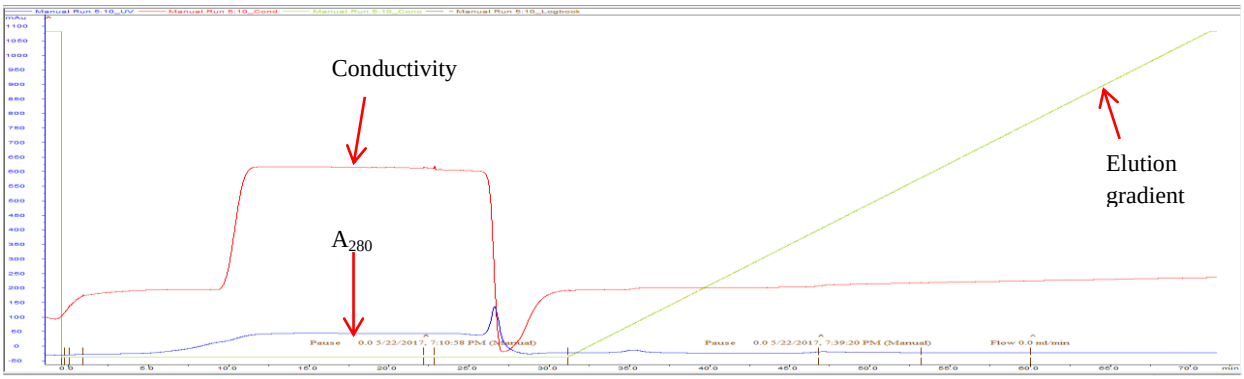

A.

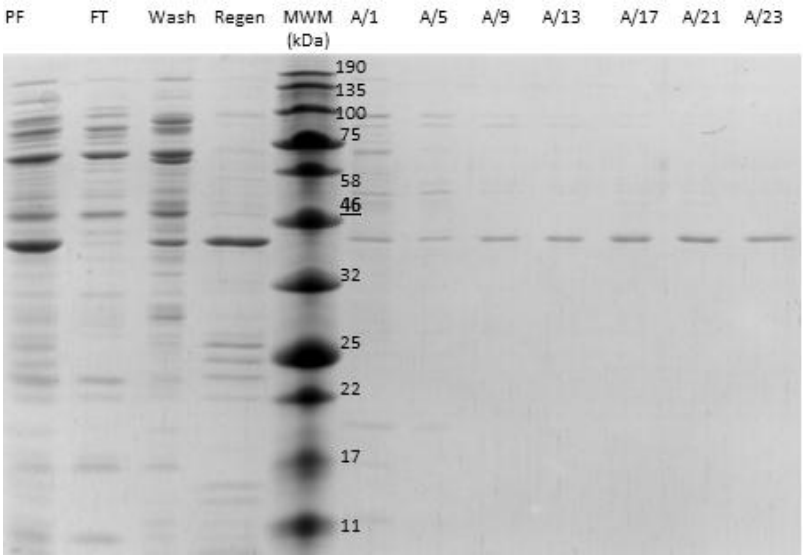

B.

Figure 3-28: Affinity (HisTag) chromatography purification of VP6 using a sodium phosphate buffer and a 20 column volumes gradient elution from 0.01 M up to 0.055 M imidazole, trial 2

A. The elution chromatographic profile illustrates the absorbance at 280 nm (blue line), conductivity (red line) and elution gradient (green line). B. SDS-PAGE gel indicating the lane "MWM" which represents the molecular weight marker in kDa. The lane marked "PF" represents the pooled fractions containing VP6 from the ion exchange chromatography (Figure 3-29). The lane labelled "FT" represents the flow-through protein sample that did not bind, but passed through the column during sample loading. The lane marked "Wash" represents the proteins washed from column during the wash step. "Regen" represents regeneration which signifies the protein collected during 0.5 M imidazole column wash. The selected fractions between "A/1" to "A/16" represents the fractions that were collected during the elution gradient from 0.01 M up to 0.055 M imidazole concentration.

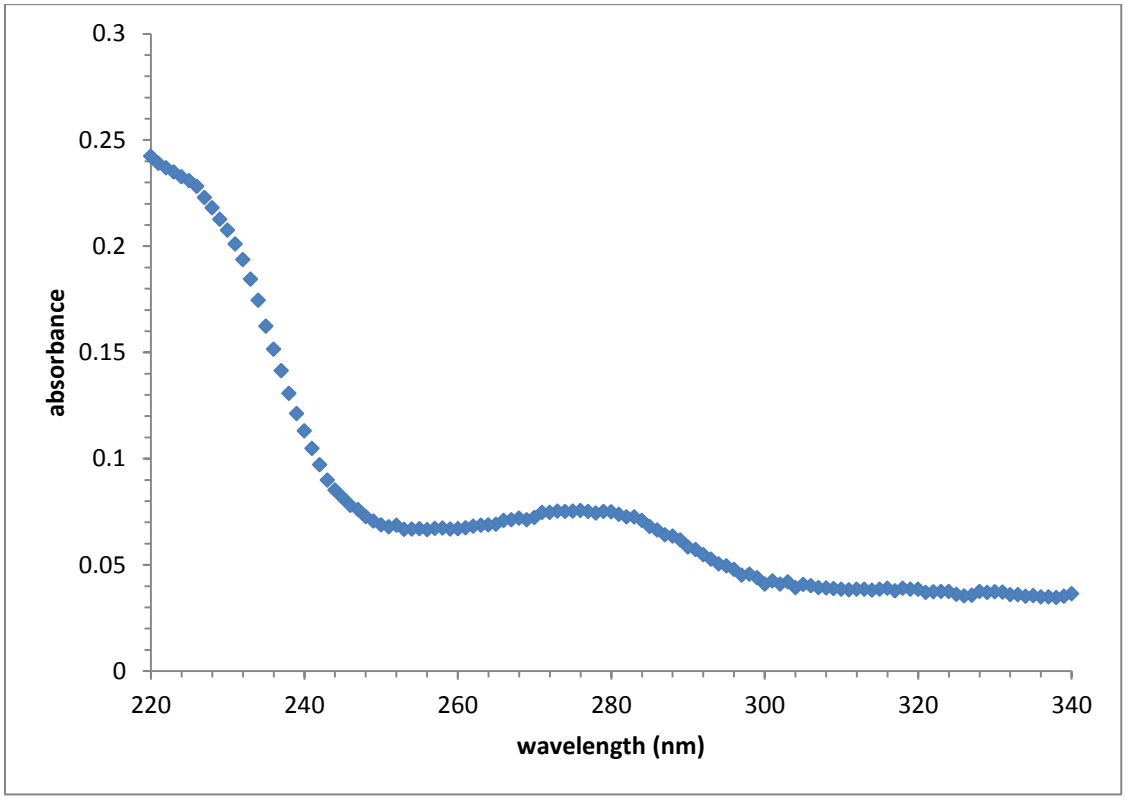

Figure 3-29: Absorbance spectrum of purified rotavirus VP6
Spectrum shown represents the absorbance of VP6 over wavelengths of 340 to 220 nm. The spectrum was collected using 1 µM VP6 in 0.02 M sodium phosphate buffer, pH 7.04, containing 0.02 M sodium chloride over a 1 cm pathlength. The spectrum was collected at 1 nm per 0.5 s.

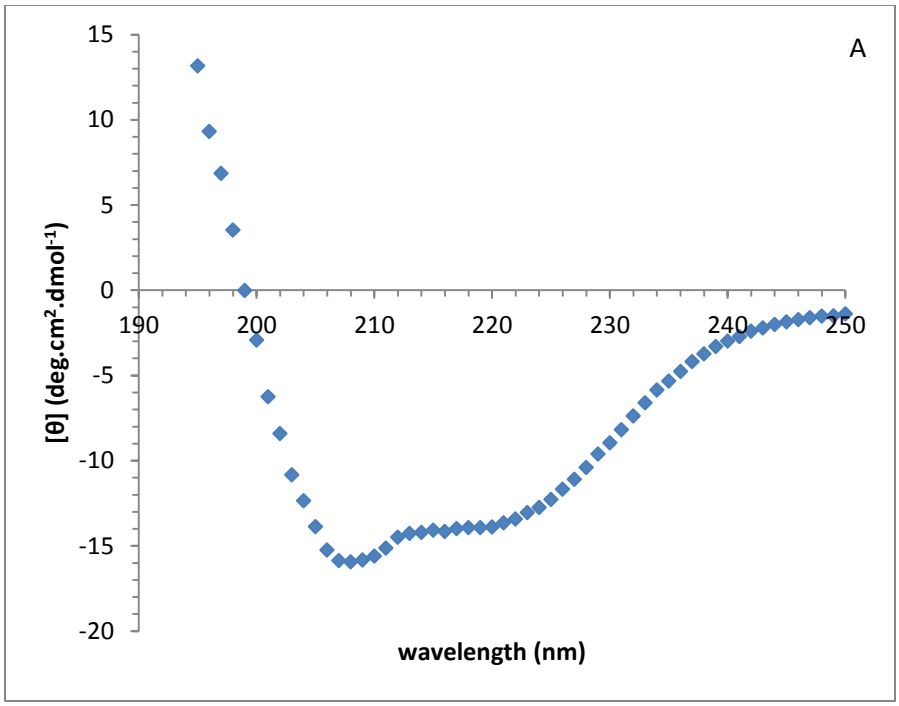

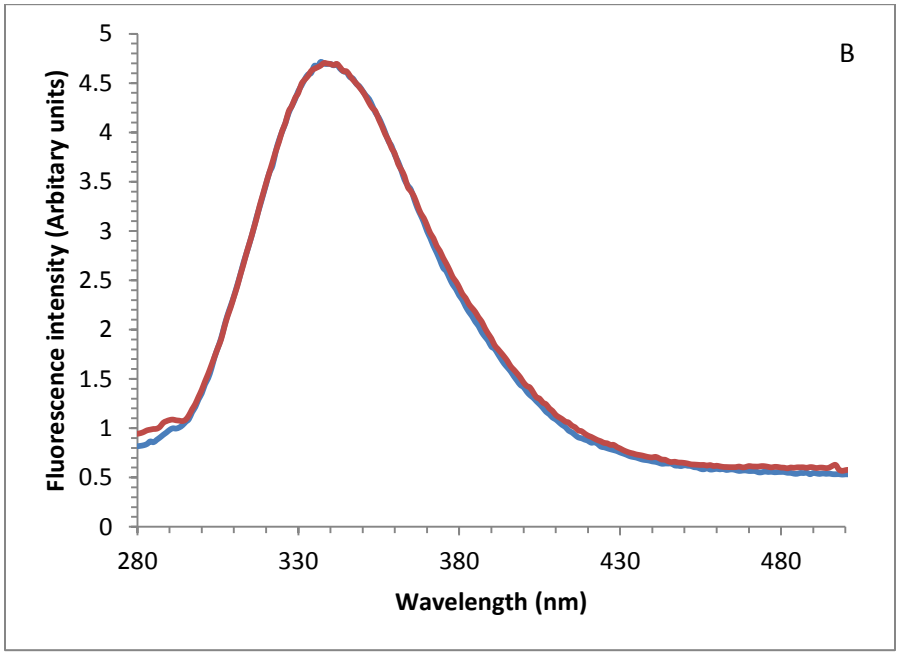

Figure 3-30: Native VP6 assessed by far-UV CD and Fluorescence
A. Far-UV circular dichroism spectrum of the native secondary structure of VP6, and B. fluorescence emission spectrum of rotavirus VP6 excited at 280 nm (red), and excited at 295 nm (blue). Both spectra were collected using 1 µM of VP6 in 0.02 M sodium phosphate buffer, pH 7.04, containing 0.02 M sodium chloride.

3.6 Thermal unfolding

Thermal unfolding was assessed using far-UV CD to monitor changes in the secondary structure of VP6 when exposed to 0.02 M sodium chloride (Appendix B i), and 0.2 M sodium chloride (Appendix B ii). VP6 that was in 0.02 M sodium phosphate buffer, pH 7.04 containing 0.02 M sodium chloride lost its α-helical properties as the temperature increased above 50°C; this is indicated by the increase in absorbance at 222 nm (Kelly *et al.* 2005; and Corrêa & Ramos, 2009). At 90°C VP6 displayed a loss in structure and therefore the value shifted to a lower minimum at 200 nm (Appendix B i) (Corrêa & Ramos, 2009).

Ellipticity at 222 nm versus temperature displayed a sigmoidal shape showing no change in the α-helical domain while between 20°C to 40°C, but showed an increase in ellipticity when temperature was increased above 40ºC (Figure 3-31 A red). There was a loss in the secondary structure particularly in the α-helices. There is a gradual loss of secondary structure between 40°C to 70°C displayed by an increase in ellipticity at 222 nm. VP6 in Buffer E displayed an increase in ellipticity at 222 nm indicating a loss in α-helical structure, but with less defined intermediate structures (Figure 3-31 A blue). The VP6 sample was diluted at a ratio of 1:1 with Buffer E, yielding a final concentration of 0.76 µM. Using the thermal unfolding data, an intrinsic fluorescence at 340 nm versus temperature graph was derived which indicated that the fluorescence intensity decreased as the temperature was increased from 20ºC to 40ºC (Figure 3-31 B blue). An intrinsic fluorescence versus wavelength graph shows that fluorescence intensity at 340 nm decreased as the temperature increased from 20°C to 90°C (Appendix C i).

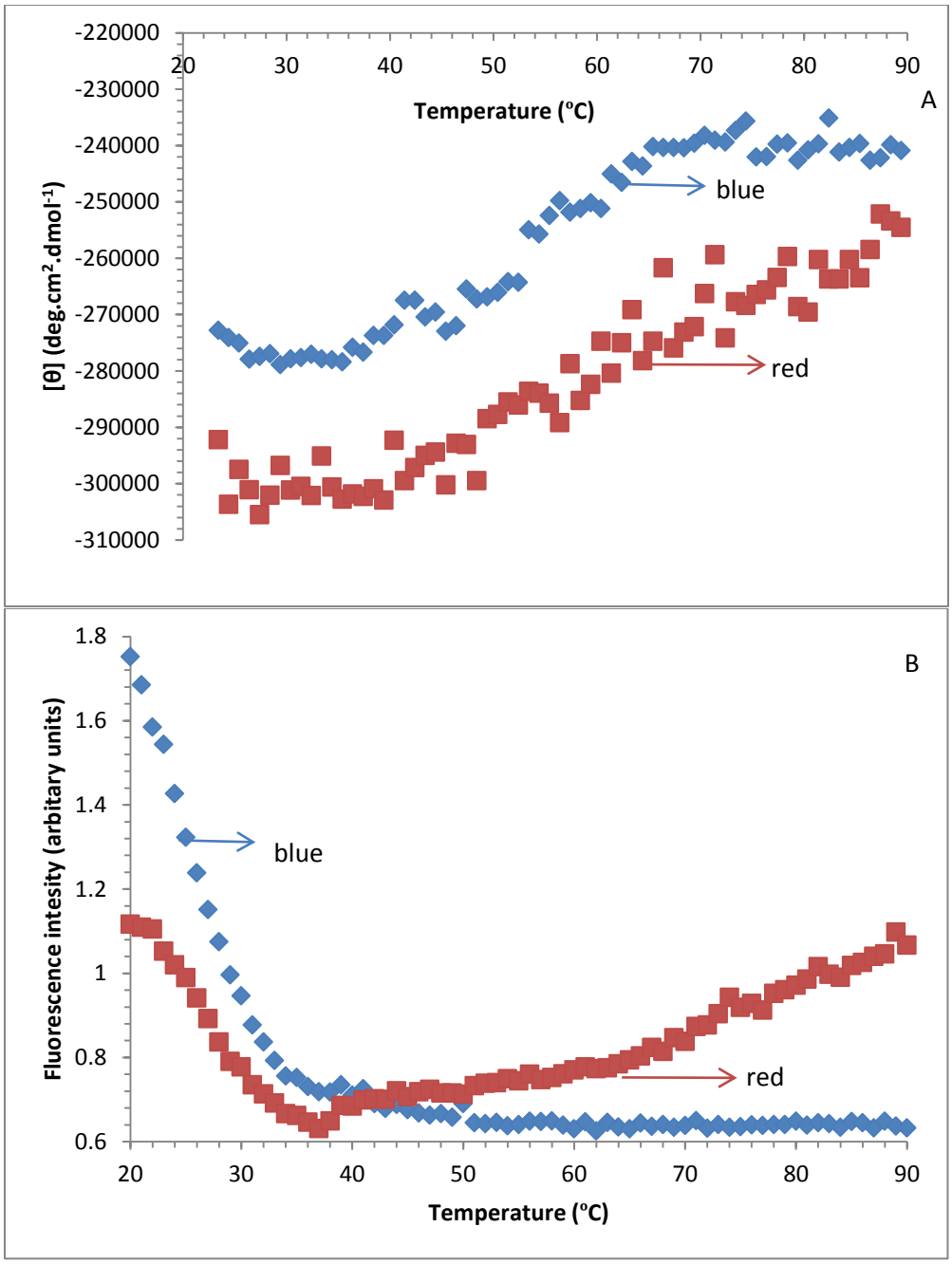

Figure 3-31: Thermal unfolding of VP6 monitored by far-UV CD and intrinsic fluorescence
A. Far-UV CD heat unfolding curve assessed using 1 µM VP6 in 0.02 M sodium phosphate buffer, pH 7.04 containing 0.02 M sodium chloride (blue). Heat unfolding curve of 0.35 µM VP6 in 0.02 M sodium phosphate buffer, pH 7.04 containing 0.2 M sodium chloride (red). Both the far-UV spectra were monitored at 222 nm during thermal ramping from 20°C to 90°C
B. Intrinsic fluorescence thermal unfolding was monitored using 0.78 µM protein in 0.02 M sodium phosphate pH 7.04 containing 0.02 M sodium chloride (blue), a thermal unfolding spectra of 0.35 µM VP6 in 0.02 M sodium phosphate pH 7.04 containing 0.2 M sodium chloride (red). Both the fluorescence emission spectra were monitored at 340 nm during thermal ramping from 20°C to 90°C.

These findings of reduction in fluorescence intensity are associated with quenching most probably by peptide bonds (Lakowicz, 2006), histidine was also reported to be capable of quenching.

Thermal unfolding was monitored using intrinsic fluorescence with 0.35 µM protein (0.08 mg VP6 from 1000 ml cell culture) in Buffer E containing 0.2 M sodium chloride. The fluorescence intensity at 340 nm dropped to its lowest when temperature reached 37ºC, then continued to rise until 90ºC (Figure 3-31 B red). The temperature versus intrinsic fluorescence emission graph indicates that there was a blue shift in the emission peak from 340 nm at 20ºC to 319 nm at 90ºC (Appendix C ii).

VP6 was allowed to cool down and refold back to its tertiary structure at 20°C. The emission intensity was recorded to be 0.78 (Figure 3-32 B blue) which shows that the structural changes that promoted quenching were still favoured.

Structural analysis of VP6 was performed in the presence of 0.2 M sodium chloride to evaluate any difference in VP6's structure and conformational stability on exposure to that sodium chloride concentration.

The thermally unfolded VP6 sample used for CD thermal denaturation assessment was allowed to return to room temperature then again assessed by far-UV CD to monitor the refolded state of the protein. VP6 refolded back into its native state, this was indicated by an ellipticity minima at 208 nm (Figure 3-32 A red). The ellipticity at 217 nm to 222 nm is constant indicating the counter absorptive action of decrease in ellipticity caused by the α-helices and the increase in ellipticity caused by β-sheet.

Intrinsic fluorescence was used to monitor tertiary structural changes during heat denaturation, the emission of light by intrinsic fluorophores is dependent on the local tertiary environment of the protein (Lakowicz, 2006).

3.7 Effect of urea and sodium chloride on the secondary and tertiary structure of VP6

A 3 M urea concentration was used during affinity HisTag chromatography to ensure that the HisTag was not buried within the protein. The 3 M urea was preferred as to prevent complete unfolding of the protein.

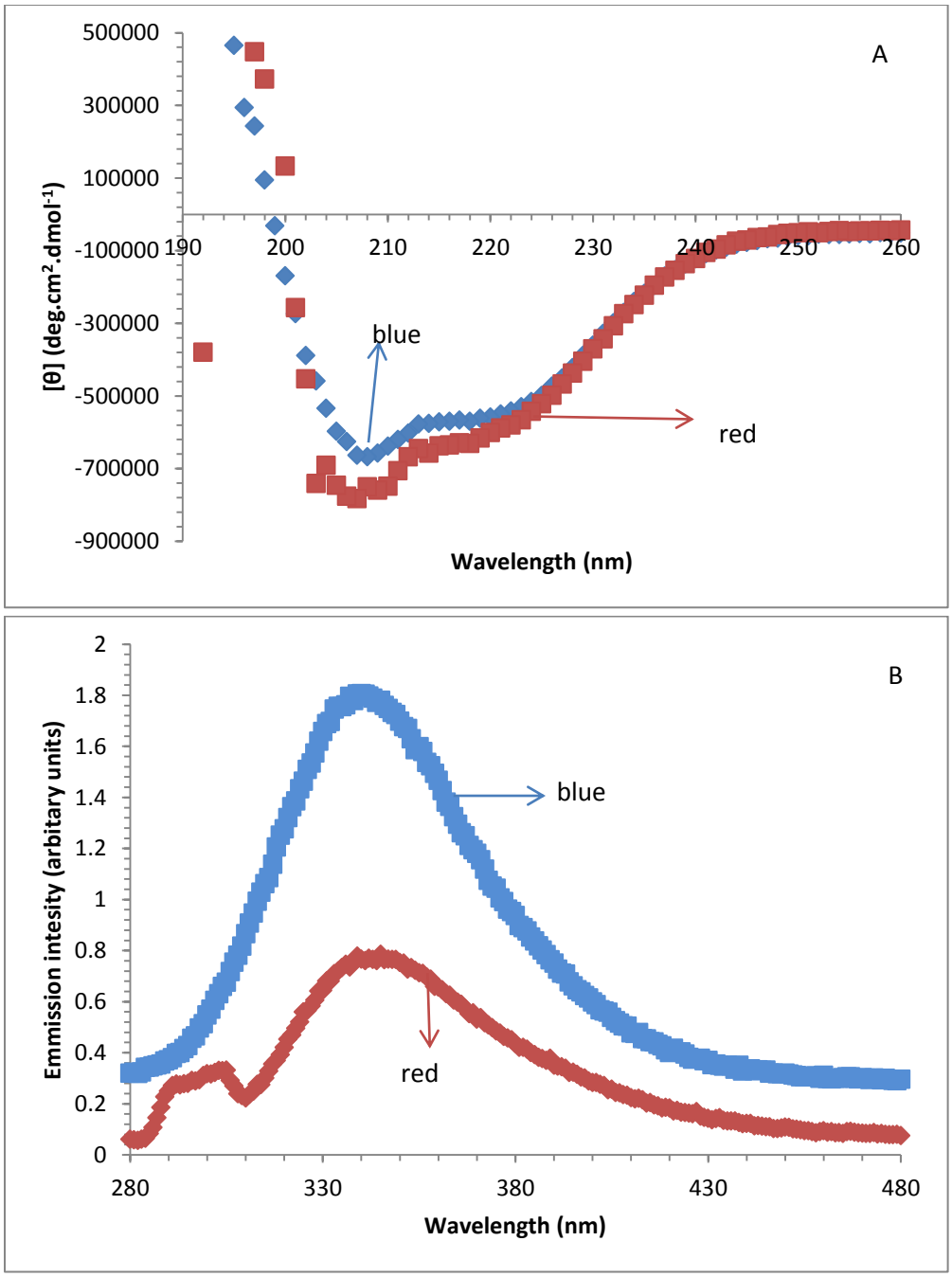

Figure 3-32: Reversibility of thermally unfolded VP6 monitored by Far-UV circular dichroism and intrinsic fluorescence

A. The far-UV CD spectrum for the native folded form of VP6 (blue), and the spectrum for the refolded form of the protein after thermal denaturation at 90ºC (red). The spectra were collected using 1 µM protein in 0.02 M sodium phosphate buffer, pH 7.04, containing 0.02 M sodium chloride. B. Intrinsic fluorescence emission spectrum for the native VP6 form (blue), and refolded form of VP6 (red), after a thermal denaturation at 90ºC. Fluorescence spectra for VP6 refolded after thermal unfolding up to 90°C using 0.78 µM protein in 0.02 M sodium phosphate buffer, pH 7.04, containing 0.02 M sodium chloride.

Far-UV CD and intrinsic fluorescence were used to monitor the secondary and tertiary structural changes caused by 3 M urea.

Far-UV CD revealed that the mean residue ellipticity at 222 nm still maintained a high negative value (Figure 3-33 A green) implying that the β-sheets and α-helices of VP6 were not unfolded by 3 M urea.

Intrinsic fluorescence spectra of VP6 with 3M urea displayed a maximum at 340 nm (Figure 3-33 B green), thus showing no red-shift that is typically observed when fluorophores are shifted from proteinic to aqueous environment. Instead there is quenching indicating that there was structural rearrangements that brought the quencher close to the tryptophan residue.

There was no observable difference in VP6s secondary structure when exposed to 0.02 M sodium chloride from when it was exposed to 0.2 M sodium chloride (Figure 3-33 A).

The presence of 0.2 M sodium chloride caused tertiary structural rearrangements that promoted quenching (Figure 3-33 B red) as compared to a higher fluorescence emission intensity when VP6 was exposed to a lower sodium chloride concentration of 0.02 M (Figure 3-33 B blue).

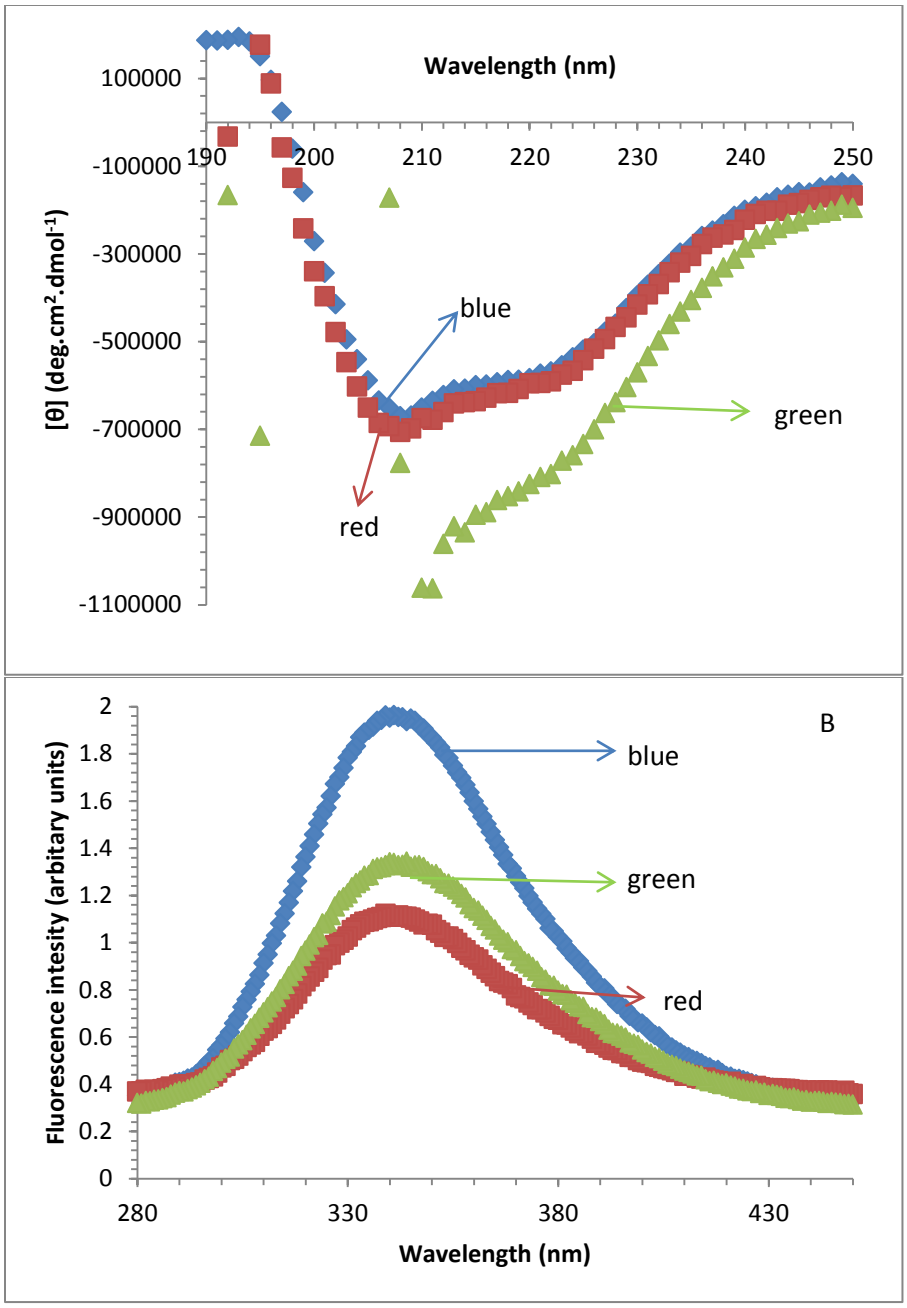

Figure 3-33: Effect of urea and sodium chloride on the secondary and tertiary structure of VP6

A. Far-UV circular dichroism spectra using 0.40 µM native VP6 in 0.02 M sodium phosphate buffer, pH 7.04, containing 0.02 M sodium chloride, (blue); 0.35 µM VP6 in 0.02 M sodium phosphate buffer at pH 7.04, containing 0.2 M sodium chloride (red), and 0.35 µM VP6 in 0.02 M sodium phosphate buffer at pH 7.04, containing 0.02 M sodium chloride and 3 M urea (green). B. Intrinsic fluorescence spectra of 0.40 µM native VP6 in 0.02 M sodium phosphate buffer, pH 7.04, containing 0.02 M sodium chloride (blue); 0.35 µM VP6 in 0.02 M sodium phosphate buffer at pH 7.04, containing 0.2 M sodium chloride (red), and 0.35 µM VP6 in 0.02 M sodium phosphate buffer at pH 7.04, containing 0.02 M sodium chloride and 3 M urea (green).

Chapter 4: Discussion

Over-expressed soluble VP6 was highly expressed in KRX cells when induced with 0.0001 M IPTG and 0.05% *L*-rhamnose, for a period of 6 h while incubated at 25°C (Figure 3-2). BL21 cells proved to be efficient in expressing VP6 at a higher yield than KRX cells, but the ratio of soluble to insoluble VP6 was low. The expression efficiency of proteins by the KRX cells was also described by Hartnett *et al.* (2006) who found that these cells express soluble active enzyme (firefly luciferase) when compared to the BL21 cells, which express non-functional, misfolded enzymes with low enzyme activity. KRX cells have a suppressed T7 RNA polymerase expression which is under the control of *rhaP*$_{BAD}$ promoter induced by *L*-rhamnose (Studier & Moffat, 1986; Narita & Tokuda, 2009). This provides a more controllable expression of proteins by reducing the rate of expression, which in turn prevents protein from misfolding into inclusion bodies (Villaverde & Carrio, 2003; Sørensen & Mortensen, 2005). A study by Zhao *et al.* (2011) used BL21 cells with a pET vector to express RV VP6 which used insoluble, pelleted protein as no soluble proteins were obtained, Bredell *et al.* (2016) compared the expression of RV VP6 in *E.coli* BL21 cells to yeast cells which reported that the yeast cells expressed soluble protein while the BL21 cells failed to accomplish this. Esteban *et al.* (2013) carried out a study to express RV VP6 using *Lactococcus lactis* which failed to express VP6 in a soluble form. Eukaryotic human embryonic kidney cells proved to be efficient in expressing soluble non-degraded VP6 compared to the insect cell-baculovirus system which had a higher VP6 yield in insoluble form (da Silva *et al.* 2012)

The use of a denaturant (Seth *et al.* 2017) while purifying a protein may vary the outcome of the experiment whereby the charged regions are fully exposed allowing for binding onto the resin. This prevents aggregation of the proteins due to exposure to a pH environment outside its stable pH range (Chi *et al.* 2003)[a].

Failure of VP6 to be eluted off a weak anion exchanger column (DEAE Sepharose) after exposing the protein to sodium phosphate buffer at pH 5 reveals that VP6 was not protonated by the buffer with a pH that is a unit lower than its pI (6.65), or it could be that the expressed VP6 had a different pI from the theoretical pI of 6.42.

Rotavirus VP6 is affected by pH and ionic strength as shown by Lepault *et al.* (2001). A MOPS buffer was used to purify VP6 using an anion (DEAE Sepharose) exchanger column. A 0.03 M MOPS buffer has an ionic strength of 0.99. Lepault *et al.* (2001) indicated that RV VP6 is affected by the ionic strength of the solution and, thus, a buffer with a greater ionic strength than sodium phosphate (which is 0.42) was used in order to increase the stability of the protein. This was to eliminate the formation of small protein aggregates that occur when exposed to a buffer with an ionic strength below 0.1 (Lepault *et al.* 2001). RV VP6 has been shown to exist as tubular structures when exposed to an aqueous environment at pH 6 to 8 with a buffer with an ionic strength above 1. Purification using a MOPS buffer and a DEAE column did not produce good results (Figure 3-11). The reason the MOPS buffer was not ideal for VP6 purification on a DEAE column was because there were proteins that were found to be present at different elution fractions in the gradient, and those proteins had a similar size as VP6 when compared against the MWM. This indicates that VP6 existed in different structural conformations when it was suspended in 0.03 M MOPS buffer. The effect of ionic strength having an effect on VP6's conformation is seen in Figure 3-33 B where the presence of 0.2 M sodium chloride caused tertiary structural rearrangements that promoted quenching (Figure 3-33 B red) as compared to a higher fluorescence emission intensity when VP6 was exposed to a lower sodium chloride concentration of 0.02 M (Figure 3-33 B blue).

A thermal unfolding study of VP6 was performed to monitor the structural behaviour of VP6 in increasing temperature when exposed to 0.02 M sodium chloride and when exposed to a higher sodium chloride concentration of 0.2 M. When the temperature was raised from 20°C to 37°C fluorescence emission signal was gradually reduced in proteins exposed to 0.02 M and 0.2 M of sodium chloride, this indicated that there were conformational changes that promoted quenching (Appendix C i and Appendix C ii). When the temperature was further increased above 50°C, the VP6 exposed to 0.2 M of sodium chloride started displaying an increase in its fluorescence emission intensity, which indicated that there were conformational changes in the protein that caused quenchers to move away from the fluorophores, the fluorescence emission continued to rise until 90°C was reached (Appendix C ii). There was also a blue-shift when the

temperature was increased from 57ºC to 90ºC which shows that there were tertiary structural changes that occurred, which further buried the fluorophores within the protein (Appendix C ii). The VP6 exposed to 0.02 M of sodium chloride only experienced a further drop in fluorescence emission until 90°C was reached, with no shift in the emission peak from all the spectrum collected (Appendix C i).

Purification using sodium phosphate at pH 7.04 improved the purity of VP6, even though the protein was not pure there was better isolation of the target protein whereby it was separated from lower molecular weight proteins (Figures 3-13; 3-17, and Figure 3-18). It was also observed that VP6 purification using HisTag affinity chromatography mostly separated proteins with a higher molecular weight from VP6 (Figure 3-9).

A dual purification procedure was adopted with anion exchange chromatography used as the first purification technique then followed by HisTag affinity chromatography. When a protein sample containing VP6 was applied to a HisPrep affinity chromatography column, it was observed that VP6 was found in the fraction containing unbound proteins from the column wash, indicating that it did not bind to the column (Figure 3-8). The 3 M urea appeared to affect the tertiary structure of VP6 as seen in Figure 3-33 to facilitate exposure of the histidine residues and allow binding of VP6 to the HisPrep column.

When VP6 was partially purified using DEAE anion exchange chromatography (Figure 3-27) it no longer required to be unfolded using urea in order to bind to the HisPrep affinity chromatography column (Figure 3-28). This was suspected to have occurred because of the decrease in competing for binding sites due to the decrease in bacterial cellular proteins and the increased in resin bed.

Far-UV CD and intrinsic fluorescence were used as secondary and tertiary structural probes for VP6. The far-UV CD readings agree with findings by Zhao *et al.* (2011), that illustrated that VP6 has the highest negative value at 208 nm (Figure 3-30 A), and the minimum at 222 nm value that was counteracted by the presence of β-sheets (Figure 1-4) (Kelly & Price, 2000).

A study by Zhao *et al.* (2011) who characterised RV VP6 found that VP6 displayed a fluorescence emission peak of 341 nm which is in agreement with the fluorescence data

from the current study (Figure 3-30 B). Appendix D shows a globular structure of a VP6 monomer with the five tryptophan residues buried within the protein, hence, explaining why the emission peak was recorded at a wavelength of 340 nm (Lakowicz, 2006).

A 0.2 M sodium chloride concentration was used to elute VP6 off a DEAE column, this condition was assessed to observe the structural (secondary or tertiary) effects that it has on VP6. There was no observable difference in VP6's secondary structure when exposed to 0.02 M sodium chloride from when it was exposed to 0.2 M sodium chloride (Figure 3-33 A), but ellipticity at 222 nm monitoring thermal unfolding showed that there were two distinct intermediate phases to the secondary structure that occur at temperatures 20ºC to 40ºC, and 70ºC to 90ºC (Figure 3-31 A red). Thermal unfolding of VP6 in 0.2 M sodium chloride did not display distinct intermediate secondary structure phases (Figure 3-31 A blue); this is because a protein spectrum from a lower protein concentration has a low signal making it difficult to identify the intermediate phases on the spectra. VP6 was able to refold back to its secondary structure when cooled to 20ºC after exposure to 90ºC (Figure 3-32 A), but the tertiary structure did not return to its native conformation when assessed using intrinsic fluorescence (Figure 3-32 B). Chi *et al.* (2003)[b] stated that certain proteins can permanently aggregate and not refold after being thermally denatured. During thermal denaturation VP6 displayed a reduction in fluorescence emission at a peak of 340 nm, when heated up to 90°C (Appendix C i); whereas it is described that during protein unfolding (chemical or thermal), an intrinsic fluorescence spectral peak experiences a red-shift; this occurs when the fluorophores shift from proteinic to the aqueous environment (Lakowicz, 2006). This gives the impression that VP6 was not unfolding with the increase in temperature, but merely being quenched. Tryptophan emission can be affected by quenchers that include nearby peptide bonds, which undergo alignment changes that occur because of "small motions" in amino acid side chains or protein backbone. Reduced emission intensity by tryptophan may come as a result of quenching caused by small motions in amino acid side chains or backbone (Lakowicz, 2006). The presence of two histidine tags expressed on either side of VP6 can be affected by these "small motions", allowing the tags to move close to the tryptophan residues, and acting as quenchers.

Appendix C ii shows that there was a blue-shift in the emission intensity when thermal unfolding was monitored in the presence of 0.2 M sodium chloride. The emission intensity was highest at 320 nm when the temperature reached 90ºC, this emission intensity is characterised by the primary fluorophore tryptophan being placed in a less aqueous environment, (Lakowicz, 2006). The shift in the emission peak to a lower wavelength was not observed when VP6 was in 0.02 M sodium chloride (Appendix C i), indicating that sodium chloride had an influence in the tertiary conformation of the protein during changing temperatures.

Far-UV CD spectra of VP6 exposed to 3 M urea did not affect the secondary structure of the protein (Figure 3-33 A green) but changes in the tertiary structure assessed by intrinsic fluorescence indicated that the emission maximum on the intrinsic fluorescence spectrum of VP6 in 3 M urea was still observed at 340 nm with a lower emission unit of 1.34 (Figure 3-33 B green), which comes as a result of low VP6 concentration which was calculated to be 0.4 µM when assessing the native protein, and 0.35 µM when assessing the denatured VP6. Addition of 3 M urea did not affect the secondary structure (Figure 3-33 A), and the tertiary structure (Figure 3-33 B) of VP6.

Chapter 5: Conclusion

The goal of this study was to develop a swift and cost effective method of expressing soluble RV VP6. Purification proved to be difficult when binding VP6 to a DEAE Sepharose column using MOPS buffer. A phosphate buffer was used to purify VP6 on an anion exchange column along with HisTag affinity chromatography. The expressed VP6 was found to have a correctly folded secondary structure characterised by an ellipticity minima at 208 nm, and an ellipticity value that was affected by the presence of the β-sheet making a constant reading between 222 nm and 215 nm, as determined by Far-UV CD. Intrinsic fluorescence of VP6 revealed that the protein had buried tryptophan residues as indicated by its emission peak at 340 nm. High sodium chloride concentrations of 0.2 M had no effect on VP6's secondary structure, but it altered the tertiary structure of the protein by causing motions that caused quenchers to move closer to the tryptophan residues, thus decreasing the emission signal (Figure 3-33 B red). Exposing VP6 to increasing temperatures of up to 90ºC when the protein was in a buffer containing a sodium chloride concentration of 0.02 M indicated that VP6 was resistant to unfolding at those temperatures, but the emission signal was reduced showing that it had undergone structural changes that caused quenchers to move closer the fluorophores (Figure 3-31 B blue; & Appendix C i). When VP6 was In the presence of 0.2 M sodium chloride, the emission from the fluorophores was gradually decreased, but when the temperature reaches 50ºC there was an increase in the emission intensity indicating that there were structural changes that caused the fluorophores and quenchers to move away from each other (explained by the gradual increase in emission signal), this was also accompanied by further burying of the tryptophan residues explained by the shift in emission peak to shorter wavelengths (Figure 3-31 B red; & Appendix C ii). This indicated that there are variations in VP6's amino acids that are exposed depending on the ionic strength of the buffer, this further explains why successful binding of VP6 to a DEAE Sepharose column was achieved when using a phosphate buffer, but failed to bind when a higher ionic strength MOPS buffer was used.

Chapter 6: References

Aiyegbo, M.S., Sapparapu, G., Spiller, B.W., Eli, I.M., Williams, D.R., Kim, R., Lee, D.E., Liu, T., Li, S., Woods, V.L., Nannemann, D.P., Meile, J., Stewart, P.L. & Crowe, J.E., 2013. Human rotavirus VP6-specific antibodies mediate intracellular neutralization by binding to a quaternary structure in the transcriptional pore. *PloS one*, 8 (5), e61101.

Amerein, K.E., Takacs, B., Stieger, M., Molnos, J., Flint, N.A. & Burn, P., 1995. Purification and characterization of recombinant human p50csk protein-tyrosine kinase from an *Escherichia coli* system overproducing the bacterial chaperones GroES and GroEL. *Proceedings of the National Academy of Sciences of the United States of America*, 92 (4), pp.1048-1052.

Atherly-John, Y.C., Cunningham, S.J. & Crain, E.F., 2002. A randomized trial of oral vs intravenous rehydration in a pediatric emergency department. *Archives of Pediatrics & Adolescent Medicine*, 156 (12), pp.1240–3.

Badillo-Godinez, O., Gutierrez-Xicotencatl, L., Plett-Torres, T., Pedroza-Saavedrac, A., Gonzalez-Jaimes, A., Chihu-Amparanc, L., Maldonado-Gamac, M., Espino-Solis, G., Bonifaz, L.C., EsquiveL-Guadarrama, F., 2015. Targeting of rotavirus VP6 to DEC-205 induces protection against the infection in mice. *Vaccine*, 33, pp.4228-4237

Barth, H.G., Boyes, B.E. & Jackson, C., 1996. Size exclusion chromatography. *Analytical Chemistry*, 68, pp.445-466.

Bertolotti-Ciarlet, A., Ciarlet, M., Crawford, S.E., Conner, M.E. & Estes, M.K., 2003. Immunogenicity and protective efficacy of rotavirus 2/6-virus-like particles produced by a dual baculovirus expression vector and administered intramuscularly, intranasally, or orally to mice. *Vaccine*, 21(25-26), pp.3885–3900.

Bornhorst, J.A. & Falke, J.J., 2000. Purification of proteins using polyhistidine affinity tags. *Methods Enzymology*, 326, pp.245-254.

Bredell, H., Smith, J.J., Prins, W.A., Gorgens, J.F. & van Zyl, W.H., 2016. Expression of rotavirus VP6 protein: A comparison amongst *Escherichia coli*, Pichia pastoris and Hansenula polymorpha. *FEMS Yeast Research Advance Access*, http://femsyr.oxfordjournals.org/.

Bugli, F., Caprettini, V., Cacaci, M., Martini, C., Sterbini, F.P., Torelli, R., Longa S.D., Papi, M., Palmieri, V., Giardina, B., Posteraro, B., Sanguinetti, M. & Arcovito, A., 2014. Synthesis and characterization of different immunogenic viral nanoconstructs from rotavirus VP6 inner capsid protein. *International Journal of Nanomedicine*, 9, pp.2727-2739.

Chakrabarti, S., Barrow, C.J., Kanwar, R.K., Ramana, V, & Kanwar, J.R., 2016. Studies to prevent degradation of recombinant Fc-fusion protein expressed in mammalian cell line and protein characterization. *International Journal of Molecular Sciences*, 17, pp.913-935

a. Chi, E.Y., Krishman, S., Randolph, T.W. & Carpenter J.F., 2003. Physical stability of proteins in aqueous solution: mechanism and driving forces in nonnative protein aggregation. *Pharmaceutical Research*, 20 (9), pp.1325-1336.

b. Chi, E.Y., Krishnan, S., Kendrick, B.S., Chang, B.S., Carpenter, J.F. & Randolph, T.W., 2003. Roles of conformational stability and colloidal stability in the aggregation of recombinant human granulocyte colony-stimulating factor. *Protein Science*, 12, pp.903–913.

Choi, A.H., Basu, M., McNeal, M.M., Clements, J.D. & Ward R.L., 1999. Antibody-independent protection against rotavirus infection of mice stimulated by intranasal immunization with chimeric VP4 or VP6 protein. *Journal of virology*, 73 (9), pp.7574-7581.

Choi, A.H., Basu, M., McNeal, M.M., Flint, J., Van Cott, J.L., Clements, J.D. & Ward RL., 2000. Functional mapping of protective domains and epitopes in the rotavirus VP6 protein. *Journal of virology*, 74 (24), pp.11574–11580.

Choi, A.H., McNeal, M.M., Basu, M., Flint, J.A., Stone, S.C., Clements, J.D., Bean, J.A., Poe, S.A., Van Cott, J.L. & Ward, R.L., 2002. Intranasal or oral immunization of inbred and outbred mice with murine or human rotavirus VP6 proteins protects against viral shedding after challenge with murine rotaviruses. *Vaccine*, 20 (27-28), pp.3310–21.

Collins, P.J., Mulherin, E., O'Shea, H., Cashman, O., Lennon, G., Pidgeon, E., Coughlan, S., Hall, W. & Fanning, S., 2015. Changing patterns of rotavirus strains circulating in Ireland: Re-emergence of G2P[4] and identification of novel genotypes in Ireland. *Journal of Medical Virology*, 87, pp.764–773

Corrêa, D.H.A. & Ramos, C.H.I., 2009. The use of circular dichroism spectroscopy to study protein folding, form and function. *African Journal of Biochemistry Research*, 3 (5), pp.164-173

Corthesy, B., Benureau, Y., Perrier, C., Fourgeux, C., Parez, N., Greenberg, H. & Schwartz-Cornil, I., 2006. Rotavirus anti-VP6 secretory immunoglobulin A contributes to protection via intracellular neutralization but not via immune exclusion. *Journal of Virology*, 80, pp.10692-10699.

Coskun, O., 2016. Separation techniques: Chromatography. *Northern Clinics of Istanbul*, 3 (2), pp.156-160.

Coulson, B.S., 2012. Importance of host cell receptor specificity and immune responses in rotavirus pathogenesis. *Under the Microscope*, pp.67–69.

Crawford, S.E. Mukherjee, S.K., Estes, M.L., Lawton, J.A., Shaw, A.L., Ramig, R.F. & Prasad B.V.V., 2001. Trypsin cleavage stabilizes the rotavirus VP4 spike. *Journal of virology*, 75(13), pp.6052–6061.

Cuatrecasas, P., Wilchek, M, & Anfinsen, C.B., 1968. Selective enzyme purification by affinity chromatography. *Proceedings of the National Academy of Sciences of the United States of America*, 61, pp.636–643.

Cunliffe, N.A., Bresee, J.S. & Hart, C.A., 2002. Rotavirus vaccines: development, current issues and future prospects. *The Journal of infection*, 45 (1), pp.1–9.

Da Silva, H.C., da Silva e Mouta, S., de Mendonca, L., de Souza Pereira, M.C., da Rocha Nogueira, A., de Azevedo, M.L.B., Leite, J.P.G. & de Moraes, M.T.B., 2012. Comparison of two eukaryotic systems for the expression of VP6 protein of rotavirus specie A: transient gene expression in HEK293-T cells and insect cell-baculovirus system. *Biotechnology Letters*, 34, pp. 1623–1627

De Vos, B., Vesikari, T., Linhares, A.C., Salinas, B., Pe´rez-Schael, I., Ruiz-Palacios, G.M., Guerrero, M.L., Phua, K.B., Delem, A. & Hardt, K., 2004. A rotavirus vaccine for prophylaxis of infants against rotavirus gastroenteritis. *Pediactrics Infectious Disease Journal*, 23, pp.179-182.

Desselberger, U. & Huppertz, H.I., 2011. Immune responses to rotavirus infection and vaccination and associated correlates of protection. *Journal of Infectious Diseases,* 203, pp.188–195

Dunn, J.J., Studier, F.W. & Gottesman, M., 1983. Complete nucleotide sequence of bacteriophage T7 DNA and the locations of T7 genetic elements. *Journal of Molecular Biology*, 166, pp.477-535

Erk, I., Huet, J., Duarte, M., Duquerroy, S., Rey, F., Cohen, J. & Lepault, J., 2003. Zinc ion controls assembly and stability of the major capsid protein of rotavirus. *Journal of virology*, 77 (6), pp.3595-3601.

Espejo, R.T., Lopez, S. & Arias, C., 1981. Structural polypeptides of simian rotavirus SA11 and the effect of trypsin. *Journal of virology*, 37 (1), pp.1–6.

Esteban, L.E., Temprana, C.F., Argüelles, M.H., Glikmann, G. & Castello, A.A., 2013. Antigenicity and immunogenicity of rotavirus VP6 protein expressed on the surface of lactococcus lactis. *BioMed Research International*, pp.1-8.

Estes, M.K. & Cohen, J., 1989. Rotavirus gene structure and function. *Microbiological Reviews*, 53 (4), pp.410–449.

Estes, M.L. & Kapikian, A.Z., 2007. Rotaviruses. *Virology*, 2, pp.1917-1974.

Fabbretti, E. Afrikanova, I., Vascotto, F. & Burrone, O.R., 1999. Two non-structural rotavirus proteins, NSP2 and NSP5, form viroplasm-like structures in vivo. *The Journal of general virology*, 80 (2), pp.333–9.

Fahnert, B., Lilie, H. & Neubauer, P., 2004. Inclusion Bodies: Formation and utilisation. *Advances in Biochemical Engineering/Biotechnology*, 89, pp.93-142.

Fountoulakis, M., 2001. Proteomics: Current technologies and applications in neurological disorders and toxicology. *Amino Acids*, 21, pp.363-381

Garaicoechea, L., Olichon, A., Marcoppido, G., Wigdorovitz, A., Mozgovoj, M., Saif, L., Surrey, T. & Parreno, V., 2008. Llama-derived single-chain antibody fragments directed to rotavirus VP6 protein possess broad neutralizing activity in vitro and confer protection against diarrhea in mice. *Journal of Virology*; 82, pp.9753-64.

Gasteiger, E., Hoogland, C., Gattiker, A., Duvaud, S., Wilkins, M.R., Appel, R.D. & Bairoch, A., 2005. Protein identification and analysis tools on the ExPASy server. *The Proteomics Protocols Handbook.*

Georges-Courbot, M.C., Beraud, A.M., Beards, G.M., Campell, A.D., Gonzalez, J.P., Georges, A.J. & Flewet, T.H., 1988. Subgroups, serotypes, and electrophoretypes of rotavirus isolated from children in Bangui, Central African Republic. *Journal of clinical microbiology*, 26 (4), pp.668–671.

Georgiou, G, & Valax, P., 1996. Expression of correctly folded proteins in *Escherichia coli*. *Current Opinion in Biotechnology*, 7, pp.190-197.

Gerberding, S.J, & Byers, C.H., 1998. Preparative ion-exchange chromatography of proteins from dairy whey. *Journal of Chromatography A*, 808, pp.141–151.

Geyer, A., Sebata, T., Peenze, I. & Steele, A.D., 1996. Group Band C porcine rotaviruses identified for the first time in South Africa. *Journal of the South African Veterinary Association*, 67 (3), pp.115-116.

González, R., Torres-Vega, M.A., López, S. & Arias, C.F., 1998. In vivo interactions among rotavirus nonstructural proteins. *Archives of virology*, 143 (5), pp.981–96.

Gorziglia, M. Larralde, G., Kapikian, A.Z. & Chanock, RM., 1990. Antigenic relationships among human rotaviruses as determined by outer capsid protein VP4. *Proceedings of the National Academy of Sciences of the United States of America*, 87(18), pp.7155–7159.

Gottesman, S., 1996. Proteases and their targets in *Escherichia coli*. *Annual Review of Genetics*, 30, pp.465–506.

Graham, K.L. Halasz, P., Tan, Y., Hewish, M.J., Takada, Y., Mackow, E.R., Robinson, M.K. & Coulson, B.S., 2003. Integrin-using rotaviruses bind alpha2beta1 integrin alpha2 I domain via VP4 DGE sequence and recognize alphaXbeta2 and alphaVbeta3 by using VP7 during cell entry. *Journal of virology*, 77 (18), pp.9969–9978.

Green, A.A. & Hughes, W.L., 1955. Protein solubility on the basis of solubility in the aqueous solutions of salt and organic solvents. *Methods Enzymology*, 1, pp.67-90.

Greenfield, N.L., 1996. Methods to estimate the conformation of proteins and polypeptides from circular dichroism data. *Analytical Biochemistry*, 235, pp.1-10.

Gutierrez, M.P.I., Sanchez-San, C.J., Perez-Vargas, J., Espinosa, R., Arias, C.F. & Lopez., 2010. Different rotavirus strains enter MA104 cells through different endocytic pathways: the role of clathrin-mediated endocytosis. *Journal of Virology*, 84 (18), pp. 9161–9169.

Hartnett, J., Gracyalny, J. & Slater, M.R., 2006. The single step (KRX) competent cells: efficient cloning and high protein yields. *Protein Expression*, 94, pp.27-30

Heaton, P.M., Goveia, M.G., Miller, J.M., Offit, P. & Clark, H.F., 2005. Development of a pentavalent rotavirus vaccine against prevalent serotypes of rotavirus gastroenteritis. *The Journal of Infectious Diseases*, 192, pp.17-21

Hoffmann, F. & Rinas, U., 2000. Kinetics of heat-shock response and inclusion body formation during temperature-induced production of basic fibroblast growth factor in high-cell-density cultures of recombinant *Escherichia coli*. *Biotechnology Progress,* 16, pp.1000–1007

Hu, L., Crawford, S.E., Hyser, J.M., Estes, M.K. & Prasad, B.V., 2012. Rotavirus non-structural proteins: structure and function. *Current opinion in virology*, 2(4), pp.380–388.

Hyser, J.M., Collinson-Pautz, M.R., Utama, B. & Estes, M.K., 2010. Rotavirus disrupts calcium homeostasis by NSP4 viroporin activity. *mBio*, 1 (5), pp.36–43.

Iturriza-Gómara, M., Dallman, T., Bányai, K., Böttiger, B., Buesa, J., Diedrich, S., Fiore, L., Johansen, K., Koopmans, M., Korsun, N., Koukou, D., Kroneman, A., László,B., Lappalainen, M., Maunula, L., Marques, A.M., Matthijnssens, J., Midgley, S., Mladenova, Z., Nawaz, S., Poljsak-Prijatelj, M., Pothier, P., Ruggeri, F.M., Sanchez-Fauquier, A., Steyer, A., Sidaraviciute-Ivaskeviciene, I., Syriopoulou, V., Tran, A.N., Usonis, V., Rougemont, A. & Gray, J., 2011. Rotavirus genotypesco-circulating in Europe between 2006 and 2009 as determined by EuroRotaNet, a pan-European collaborative strain surveillance network. *Epidemiology and Infection,* 139 (6), pp.895–909.

Jayaram, H., Estes, M.K. & Prasad, B.V. V, 2004. Emerging themes in rotavirus cell entry, genome organization, transcription and replication. *Virus Research*, 101 (1), pp.67–81.

Jiang, L., He, L. & Fountoulakis, M., 2004. Comparison of protein precipitation methods for sample preparation prior to proteomic analysis. *Journal of Chromatography A*, 1023, pp. 317–320.

Johnson, J., Lin, T., & Lomonossoff, G., 1997. Presentation of heterologous peptides on plant viruses: Genetics, structure, and function. *Annual Review of Phytopathology*, 35, pp.67-86.

Johnson, W.C, 1999. Analysing protein circular dichroism spectra for accurate secondary structures. Proteins: *Structure, Function, and Genetics*, 35, pp307-312.

Jonasson, P., Liljeqvist, S., Nygren, P.A. & Stahl, S., 2002. Genetic design for facilitated production and recovery of recombinant proteins in *Escherichia coli*. *Biotechnology Applications and Biochemistry,* 35, pp.91–105.

Jungbauer, A. & Hahn, R., 2009. Ion-exchange chromatography. *Methods in Enzymology*, 463, pp.349-371.

Kang, G., Desai, R., Arora, R., Chitamabar, S., Naik, T.N., Krishnan, T., Deshpande, J., Gupte, M.D., Venkatasubramaniam, S., Gentsch, J.R. & Parashar, U.D., 2013. Indian Rotavirus Strain Surveillance Network, Mathew, A., Anita, S.R., Ramani, S., Sowmynarayanan, T.V., Moses, P.D., Agarwal, I., Simon, A., Bose, A., Arora, R., Chhabra, P., Fadnis, P., Bhatt, J., Shetty, S.J., Saxena, V.K., Mathur, M., Jadhav, A., Roy, S., Mukherjee, A. & Singh, N.B., 2013. Diversity of circulating rotavirus strains in children hospitalized with diarrhea in India, 2005–2009. *Vaccine*, 31 (27), pp.2879–2883.

Kapikian, A.Z, 2001: A rotavirus vaccine for prevention of severe diarrhoea in infants and young children. *Norvatis Found Symptoms*, 238, pp.153-171.

Kelly, S.M. & Price, N.C., 2000. The use of circular dichroism in the investigation of protein structure and function. *Current protein & peptide science*, 1(4), pp.349–384.

Kelly, S.M., Jess, T.J. & Price, N.C., 2005. How to study proteins by circular dichroism. *Biochemica et Biophysica*, 1751, pp.119-139.

Kirkwood, C.D., Boniface, K., Barnes, G.L. & Bishop, R.F., 2011. Distribution of rotavirus genotypes after introduction of rotavirus vaccines, Rotarix® and RotaTeq®, into the national i immunization program of Australia. *The Pediatric Infectious Disease Journal*, 30 (1), pp.48–53.

Kopaciewicz, W., Rounds, M.A., Fausnaugh, J. & Regnier, F.E., 1983. Retention model for high performance ion-exchange chromatography. *Journal of Chromatography,* 266, pp.3-21.

Kruger, N, & Stingl, K., 2011. Two steps away from novelty – principles of bacterial DNA uptake. *Molecular Microbiology*, 80 (4), pp.860–867

Laemmli, U.K., 1970. Cleavage of structural proteins during the assembly of the head of bacteriophage T4. *Nature,* 227, pp.680-685.

Lakowicz, J.R., (2006). Principles of fluorescence spectroscopy, Protein fluorescence, pp.445-465. Plenum Publishers, USA.

Lanata, C.F., Fischer-Walker, C.L., Olascoaga, A.C., Torres, C.X., Aryee, M.J. & Black, R.E., 2013. Global causes of diarrhoeal disease mortality in children <5 years age: A systematic review. *PLoS ONE,* 8 (9), e0072788.

Lepault, J., Petitpas, I., Erk, I., Navaza, J., Bigot, D., Dona, M., Vachette, P., Cohen, J, & Rey F.A., 2001. Structural polymorphism of the major capsid protein of rotavirus. *The European Molecular Biology Organization Journal*, 20 (7), pp.1498-1507.

Lappalainen, S., Pastor, A.R., Malm, M., Lo´pez-Guerrero, V., Esquivel-Guadarrama, F., Palomares, L.A., Vesikari, T. & Blazevic, V., 2015. Protection against live rotavirus challenge in mice induced by parenteral and mucosal delivery of VP6 subunit rotavirus vaccine. *Archives of Virology*, 160, pp.2075-2078.

a. Lawton, J.A., Estes, M.K. & Prasad, B.V., 1997. Three-dimensional visualization of mRNA release from actively transcribing rotavirus particles. *National Structural and Molecular Biology*, 4, pp.118–121.

b. Lawton, J.A., Zeng, C.Q., Mukherjee, S.K., Cohen, J., Estes M.K. & Prasad B.V.V., 1997. Three-dimensional structural analysis of recombinant rotavirus-like particles with intact and amino-terminal-deleted VP2: Implications for the architecture of the VP2 capsid layer. *Journal of virology*, 71 (10), pp. 7353–7360.

Li, T., Lin, H., Zhanga, Y., Wanga, M.L.D., Chea, Y., Zhua, Y., Li, S., Zhanga, J., Gea, S., Zhao, Q. & Xia, N., 2014. Improved characteristics and protective efficacy in an animal model of *E.coli*-derived recombinant double-layered rotavirus virus-like particles. *Vaccine*, 32 (17), pp.1921–1931.

Lilie, H., Schwarz, E. and Rudolph, R., 1998. Advances in refolding of proteins produced in *E.coli*. *Current Opinion in Biotechnology*, (9), pp.497-501

Linhares, A.C. Velázquez, F.R., Pérez-Schael, I., Sáez-Llorens X., Abate, H., Espinoza, F., López, P., Macías-Parra, M., Ortega-Barría, E., Rivera-Medina, D.M., Pavía-Ruz, N., Nuñez, E.O., Damaso, S., Ruiz-Palacios G., De Vos, B., O'Ryan, M., Gillard, P. & Bouckenooghe, A., 2008. Efficacy and safety of an oral live attenuated human rotavirus vaccine against rotavirus gastroenteritis during the first 2 years of life in Latin American infants: a randomised, double-blind, placebo-controlled phase III study. *Lancet*, 371(9619), pp.1181–1189.

Lobstein, J., Emrich, C.A., Jeans, C., Faulkner, M., Riggs, P. & Berkmen, M., 2012. Shuffle, a novel *Escherichia coli* protein expression strain capable of correctly folding disulfide bonded proteins in its cytoplasm. *Microbiology Cell Factories*, 11, pp.56.

Los, G.V. &Wood, K., 2008. HaloTag: a novel protein labelling technology for cell imaging and protein analysis. *ACS chemical biology*, 3 (6),pp.373–82.

Luchs, A. & Timenetsky, M.C., 2014. G8P[6] rotaviruses isolated from Amerindian children in Mato Grosso do Sul, Brazil, during 2009: close relationship of the Gand P genes with those of bovine and bat strains. *Journal of General Virology*, 95 (3), pp.627–641.

Madore, H.P., Estes, M.K., Zarley, C.D., Hu, B., Parsons, S., Digravio, D., Greiner, S., Smith, R., Jiang, B., Corsaro, B., Barniak, V., Crawford, S. & Conner, M.E., 1999. Biochemical and i immunologic comparison of virus-like particles for a rotavirus subunit vaccine. *Vaccine*, 17 (19), pp.2461–71.

Magdeldin, S. & Moser, A., 2012. Affinity chromatography: Principles and Applications, Affinity chromatography: Dr. Sameh Magdeldin (Ed.), ISBN: 978-953-51-0325-7, InTech, Available from: http://www.intechopen.com/books/affinity-chromatography/affinity-chromatography-principles-and-applicationshttp://www.intechopen.com/books/affinity-chromatography/affinity-chromatography-principles-and-applications

Maranga, L., Cruz, P.E., Aunins, J.G. & Carrondo, M.J.T., 2002. Production of core and virus-like particles with baculovirus infected insect cells. *Advances in biochemical engineering/biotechnology*, 74 (1), pp.183–206.

Mascarenhas, J.D.P., Arias, C.F., Padilla-Noriega, L., López, S., Gusmão, R.H.P., Gabbay, Y.B. & Linhares, A.C., 1997. Characterization of rotavirus strains with unusual electrophoretic profiles. *Rio de Janeiro*, 92 (6), pp.771-774.

Mason, H.S, & Arntzen, C.J., 1995. Transgenic plants as vaccine production systems. *Manipulating Metabolism*, 13, pp.388-392.

Mathieu, M., Petitpas, I., Navaza, J., Lepault, J., Kohli, E., Pothier, P., Prasad, B.V.V., Cohen, J. & Rey, F.A., 2001. Atomic structure of the major capsid protein of rotavirus: implications for the architecture of the virion. *The EMBO journal*, 20(7), pp.1485–1497.

Matthijnssens, J., Ciarlet, M., McDonald, S.M., Attoui, H., Bányai, K., Brister, J.R., Buesa, J., Esona, M.D., Estes, M.K., Gentsch, J.R., Iturriza-Gómara, M., Johne, R., Kirkwood, C.D., Martella, V., Mertens, P.P., Nakagomi, O., Parre˜no, V., Rahman, M., Ruggeri, F.M., Saif, L.J., Santos, N., Steyer, A., Taniguchi, K., Patton, J.T., Desselberger, U. & Van Ranst, M., 2011. Uniformity of rotavirus strain nomenclature proposed by the Rotavirus Classification Working Group (RCWG). *Archives of Virology*, 156 (8), pp.1397-1413.

Mini, K.D., Mathew K. & Mathew, J., 2017. Purification of keratinase from Aspergillus flavus S125. *Journal of Microbiology and Biotechnology Research*, 6 (1), pp.17-21.

Mwenda, J.M., Ntoto, K.M., Abebe, A., Enweronu-Laryea, C., Amina, I., Mchomvu, J., Kisakye, A., Mpabalwani, E.M., Pazvakavambwa, I., Armah, Seheri, L.M., Kiulia, N.M., Page, N., Widdowson, M. & Steele, A.D., 2010. Burden and epidemiology of rotavirus diarrhea in selected African countries: Preliminary results from the African Rotavirus Surveillance Network. *The Journal of Infectious Diseases*, 202 (1), pp. 5-11.

Narita, S. & Tokuda, H., 2009. Biochemical characterization of an ABC transporter LptBFGC complex required for the outer membrane sorting of lipopolysaccharides. *FEBS Letters*, 583, pp.2160-2164.

Nava, P. López, S., Arias, C.F., Islas, S. & González-Mariscal, L., 2004. The rotavirus surface protein VP8 modulates the gate and fence function of tight junctions in epithelial cells. *Journal of cell science*, 117 (23), pp.5509–5519.

Nyaga, M.M., Jere, K.C., Esona, M.D., Seheri, M.L., Stucker, K.M., Halpin, R.A., Akopov, A., Stockwell, T.B., Peenze, I., Diop, A., Ndiaye, K., Boula, A., Maphalala, G., Berejana, C., Mwenda, J.M., Steele, A.D., Wentworth, D.E. & Mphahlele M.J., 2015. Whole genome detection of rotavirus mixed infections in human, porcine and bovine samples co-infected with various rotavirus strains collected from sub-Saharan Africa. *Infection, Genetics and Evolution,* 31, pp.321-334.

O'Brien, Bryant, C.J., Voogd, C., Greenberg, H.B., Gardner, R.C. & Bellamy, A.R., 2000. Rotavirus VP6 expressed by PVX vectors in Nicotiana benthamiana coats PVX rods and also assembles into viruslike particles. *Virology*, 270, pp.444-453.

Offit, P.A. & Blavat, G., 1986. Identification of the two rotavirus genes determining neutralization specificities. *Journal of Virology*, 57, pp.376–378

Oldfield, S., Adachi, A., Urakawa, T., Hirasawa, T, & Roy, P., 1990. Purification and characterization of the major group-specific core antigen VP7 of bluetongue virus synthesized by a recombinant baculovirus. *Journal of General Virology*, 71, pp.2649-2656.

Ousingsawat, J., Mirza, M., Tian, Y., Roussa, E., Schreiber, R., Cook, D.I. & Kunzelmann, K., 2011. Rotavirus toxin NSP4 induces diarrhea by activation of TMEM16A and inhibition of Na(+) absorption. *Pflugers Archiv,* 461, pp.579–589.

Palomares, L.& Ramírez, O.T., 2009. Challenges for the production of virus-like particles in insect cells: The case of rotavirus-like particles. *Biochemical Engineering Journal*, 45 (3), pp.158–167.

Parashar, U.D., Hummelman, E.G., Bresee, J.S., Miller, M.A. & Glass, R.I., 2003. Global illness and deaths caused by rotavirus disease in children. *Emerging infectious diseases*, 9 (5), pp.565–72.

Parashar, U.D., Pedreira, C., De Oliveira, L., Tate, J., Orozco, M., Mercado, J., Gonzalez, A., Malespin, O., Amador, J.J., Umaña, J., Balmaseda, A., Perez, M.C., Gentsch, J., Kerin, T., Hull, J., Mijatovic, S., Andrus, J. & Parashar, U., 2006. Rotavirus and severe childhood diarrhea. *Emerging Infectious Diseases*, 12 (2), pp.304–306.

Parbhoo, N., Dewar, J.B. & Gildenhuys, S., 2016. Sequence analysis and structural implications of rotavirus capsid proteins. *Acta virologica*, 60, pp.260-270.

Parez, P., 2008. Rotavirus gastroenteritis: Why to back up the development of new vaccines? *Comparative Immunology, Microbiology & Infectious Disease* 31, pp.253–269.

Patel, N.C., Hertel, P.M., Estes, M.K., de la Morena, M., Petru, A.M., Noroski, L.M., Revell, P.A., Hanson, I.C., Paul, M.E., Rosenblatt, H.M. & Abramson, S.L., 2010. Vaccine-acquired rotavirus in infants with severe combined immunodeficiency. *The New England journal of medicine*, 362 (4), pp.314–319.

Patton, J.T., Jones., Kalbach, He, T. & Xiaobo J., 1997. Rotavirus RNA polymerase requires the core shell protein to synthesize the double-stranded RNA genome. Rotavirus RNA polymerase requires the core shell protein to synthesize the double-stranded RNA genome. *Journal of virology*, 71 (12), pp.9618–9626.

Patton, J.T. & Spencer, E., 2000. Genome replication and packaging of segmented double-stranded RNA viruses. *Virology*, 277, pp.217–225.

Payne, D.C., Edwards, K.M., Bowen, M.D., Keckley, E., Peters, J., Esona, M.D., Teel, E.N., Kent, D., Parashar, U.D., Gentsch, J.R., 2010. Sibling transmission of vaccine-derived rotavirus (RotaTeq) associated with rotavirus gastroenteritis. *Pediatrics*, 125(2), pp.438–441.

Polson, C., Starkar, P., Incledon, B., Raguvaran V. & Grant, R., 2003. Optimization of protein precipitation based upon effectiveness of protein removal and ionization effect in the liquid chromatography-tandem mass spectrometry. *Journal of Chromatography B,* 785 (2), pp.263-275.

Prasad B.V.V. & Estes M.K., 1997. Molecular basis of rotavirus replication: structure-function correlations, pp.239–268.

Program, N.I., 2001. Correction: Intussusception among infants given an oral rotavirus vaccine. *The New England journal of medicine*, 344 (20), p.1564.

Riepenhoff-Talty, M., Gouvea, V., Evans, M.J., Svensson, L., Hoffenberg, E., Sokol, R.J., Uhnoo, I., Greenberg, S.J., Schakel, K., Zhaori, G., Fitzgerald, J., Chong, S., El-Yousef, M., Nemeth, A., Brown, M., Piccoli, D., Hyams, J., Ruffin, D. & Rossi, T., 1996. Detection of group C rotavirus in infants with extrahepatic biliary atresia. *The Journal of Infectious Diseases,* 174, pp.8-15.

Rixon, F., Taylor, P. & Desselberger, U., 1984. Rotavirus RNA segments sized by electron microscopy. *Journal of General Virology*, 65(1), pp.233-239.

Rosa, M.D., 1979. Four T7 RNA polymerase promoters contain an identical 23 bp sequence. *Cell*, 16, pp.815-825.

Rotavirus Classification Working Group, 6th meeting, Valencia, October 2013. Rubio, R.M., Mora, S.I., Romero, P., Arias, C.F. & López, S., 2013. Rotavirus prevents the expression of host responses by blocking the nucleocytoplasmic transport of polyadenylated mRNAs. *Journal of Virology,* 87 (11), pp.6336–6345

Ruiz-Palacios, G.M., Pérez-Schael, R., Velázquez, F.R., Abate, H., Breuer, T., Clemens, S.C., Cheuvart, B., Espinoza, F., Gillard, P., Innis, B.L., Cervantes, Y., Linhares, A.C., López, P., Macías-Parra, M., Ortega-Barría, E., Richardson, V., Rivera-Medina, D.M., Rivera, L., Salinas, B., Pavía-Ruz, N., Salmerón, J., Rüttimann, R., Tinoco, J.C., Rubio, P., Nuez, E., Guerrero, M.L., Yarzábal, J.P., Damaso, S., Tornieporth, N., Sáez-Llorens, X., Vergara, R.F., Vesikari, T., Bouckenooghe, A., Clemens, R., De Vos, B. & O'Ryan, M., 2006. Safety and efficacy of an attenuated vaccine against severe rotavirus gastroenteritis. *The New England Journal of Medicine*, 354, pp.11-22.

Saif, L.J. & Jiang, B., 1994. Nongroup A rotaviruses of humans and animals. *Current Topics in Microbiology and Immunology*, 185, pp.339–371.

Sánchez-San, M.C., López, T., Arias, C. F. & López, S., 2004. Characterization of rotavirus cell entry. *Journal of Virology*, 78, pp.2310-2318.

Santos, N. & Hoshino, Y., 2005. Global distribution of rotavirus serotypes/ genotypes and its implication for the development and implementation of an effective rotavirus vaccine. *Reviews in Medical Virology*, 15 (1), pp.29–56.

Sattar, B.Y.S.A., Lloyd-Evans, N. & Springthorpe, V.S., 1986. Institutional outbreaks of rota virus diarrhoea : potential role of fomites and environmental surfaces as vehicles for virus transmission. *Journal of Hygiene*, 96 (1), pp.277–289.

Schweder, T., Lin, H.Y., Jurgen, B., Breitenstein, A., Riemschneider, S., Khalameyzer, V., Gupta, A., Buttner, K. & Neubauer, P., 2002. Role of the general stress response during strong over-expression of a heterologous gene in *Escherichia coli*. *Application of Microbiology and. Biotechnology*. 58, pp.330–337.

Seth, L., Ferlez, K.M.B., Kaba, S.A., Musser, D.M., Emadi, S., Matyas, G.R., Beck, Z., Alving, C.R., Burkhard, P. & Lanar, D.E., 2017. Development of a self-assembling protein nanoparticle vaccine targeting Plasmodium falciparum Circumsporozoite Protein delivered in three Army Liposome Formulation adjuvants. *Vaccine*, 35 (41), pp.5448-5454

Sethia, P.P., Rao, K.K. & Noronha S.B., 2014. A dps promoter based expression system for improved solubility of expressed proteins in *Escherichia coli*. *Biotechnology and Bioprocess Engineering*, 19, pp.790-797.

Settembre, E.C., Chen, J.Z., Dormitzer, P.R., Grigorieff, N. & Harrison, S.C., 2011. Atomic model of an infectious rotavirus particle. *The EMBO journal*, 30(2), pp.408–416.

Shoja, Z., Tagliamonte, M., Jalilvand, S., Mollaei-Kandelous, Y., De Stradis, A., Tornesello, M.L., Buonaguro, F.M. & Buonaguro, L., 2014. Formation of self-assembled triple-layered rotavirus-like particles (tlRLPs) by constitutive co-expression of VP2, VP6, and VP7 in stably transfected high-five insect cell lines. *Journal of Medical Virology*, 87, pp.102-111.

Silvestri, L.S., Taraporewala, Z.F. & Patton, J.T., 2004. Rotavirus replication: plus-sense templates for double-stranded RNA synthesis are made in viroplasms. *Journal of virology*, 78 (14), pp.7763–7774.

Snelling, T.L., Andrews, R.M., Kirkwood, C.D., Culvenor, S. & Carapetis, J.R., 2011. Case-control evaluation of the effectiveness of the G1P[8] human rotavirus vaccine during an outbreak of rotavirus G2P[4] infection in central Australia. *Clinical infectious diseases*, 52 (2), pp.191–199.

Sørensen, H.P. & Mortensen, K.K., 2004. Advanced genetic strategies for recombinant protein expression in *Escherichia coli*. *Journal of Biotechnology*, 115, pp.113-128.

Sow, S.O., Tapia, M., Haidara, F.C., Ciarlet, M., Diallo, F., Kodio, M., Doumbia, M., Dembélé, R.D., Traoré, O., Onwuchekwa, U.U., Lewis, D.C., Victor, J.C., Steele, A.D., Neuzil, K.M., Kotloff, K.L. & Levine, M.M., 2012. Efficacy of the oral pentavalent rotavirus vaccine in Mali. *Vaccine*, 30 (1), pp.71–78.

Sreerama, N. & Woody, R.W., 2003. Structural composition of βI- and βII-proteins. *Protein Science*, 12, pp.384-388.

Studier, F.W., 2005. Protein production by auto-induction in high density shaking cultures. *Protein Expression and Purification*, 41, pp.207-234.

Studier, F.W. & Moffat, B.A., 1986. Use of bacteriophage T7 RNA polymerase to direct selective high-level expression of cloned genes. *Journal of Molecular Biology*, 189, pp.113–130.

Tabor, S. & Richardson, C.C., 1985. A bacteriophage T7 RNA polymerase/promoter system for controlled exclusive expression of specific genes. *Proceedings of National Academy of Science*, 82, pp.1074-1078.

Taraporewala, Z.F. Jiang, X., Carpio, R.V., Jayaram, H., Prasad, B.V.V. & Patton, J.T., 2006. Structure-function analysis of rotavirus NSP2 octamer by using a novel complementation system. *Journal of virology*, 80 (16), pp.7984–7994.

Tang, B., Gilbert, J.M., Matsui, S.M. & Greenberg, H.B., 1997. Comparison of the rotavirus gene 6 from different species by sequence analysis and localization of subgroup-specific epitopes using site-directed mutagenesis. *Virology*, 237, pp.89-96.

Tate, J.E., Burton, A.H., Boschi-Pinto, C., Steele, A.D., Duque, J. & Parashar, U.D., 2012. 2008 Estimate of worldwide rotavirus-associated mortality in children younger than 5 years before the introduction of universal rotavirus vaccination programmes: a systematic review and meta-analysis. *The Lancet Infectious Diseases*, 12 (2), pp.136–141.

Tihova, M., Dryden, K.A., Bellamy, A.R., Greenberg, H.B. and Yeager, M., 2001. Localization of membrane permeabilization and receptor binding sites on the VP4 hemagglutinin of rotavirus: implications for cell entry. *Journal of Molecular Biology*, 314 (1), pp.985–992

Thomas, J.G. & Baneyx, F., 1996. Protein misfolding and inclusion body formation in recombinant *Escherichia coli* cells overexpressing heat-shock proteins. *The Journal of Biological Chemistry*, 271 (19), pp.11141-11147.

Thomas, J.G. & Baneyx, F., 1997. Divergent effects of chaperone over-expression and ethanol supplementation on inclusion body formation in recombinant *Escherichia coli*. *Protein Expression and Purification*, 11, pp.289-296.

Trask, S.D., Ogden, K.M. & Patton, J.T., 2012. Interactions among capsid proteins orchestrate rotavirus particle functions. *Current opinion in virology*, 2 (4), pp.373–9.

Uhlén, M., Forsberg, G., Moks, T., Hartmanis, M. & Nilsson, B., 1992. Fusion proteins in biotechnology. *Current Opinion in Biotechnology*, 3, pp.363–369

Vesikari, T., Clark, H.F., Offit, P.A., Dallas, M.J., DiStefano, D.J., Goveia, M.G., Ward, R.L., Schodel, F., Karvonen, A., Drummond, J.E., DiNubile, M.J. & Heaton, P.M., 2006. Effects of the potency and composition of the multivalent human-bovine (WC3) reassortant rotavirus vaccine on efficacy, safety and immunogenicity in healthy infants. *Vaccine*, 24, pp.4821-4829.

Vicente, T., Sousa, M.F.Q., Peixoto, C., Mota J.P.B., Alves, P.M, & Carrondo M.J.T, 2008. Anion-exchange membrane chromatography for purification of rotavirus-like particles. *Journal of Membrane Science*, 311, pp.270-283.

Vieira, H.L.A., Estevao, C., Roldao, A., Peixoto, C.C., Sousa, M.F.Q., Cruz, P.E., Carrondo, M.J.T. & Alves, P.M., 2005. Triple layered rotavirus VLP production: Kinetics of vector replication, mRNA stability and recombinant protein production. *Journal of Biotechnology*, 120, pp.72-82.

Villaverde, A. & Carrio, M.M., 2003. Protein aggregation in recombinant bacteria: biological role of inclusion bodies. *Biotechnology Letters*, 25, pp.1385–1395

Vitour, D., Lindenbaum, P., Vende, P., Becker, M.M. & Poncet, D., 2004. RoXaN, a novel cellular protein containing TPR, LD, and zinc finger motifs, forms a ternary complex with eukaryotic initiation factor 4G and rotavirus NSP3. *Journal of virology*, 78 (8), pp.3851–3862.

Walker, C.L., Aryee, M.J., Boschi-Pinto, C. & Black, R.E., 2012. Estimating diarrhoea mortality among young children in low and middle income countries. *PLoS ONE,* 7, pp.e29151.

Ward, R.L., Bernstein, D.I., Knowlton, D.R., Sherwood, J.R., Young, E.C., Cusack, T.M., Rubino, J.R. & Schiff, G.M., 1991. Prevention of surface-to-human transmission of rotaviruses by treatment with disinfectant spray. *Journal of Clinical Microbiology*, 29 (9), pp.1991–1996.

Ward, R.L. & McNeal, M.M., 2010. VP6: A candidate rotavirus vaccine. *The Journal of Infectious Diseases*, 202 (1), pp.101–107.

Wilhelmi, I., Roman, E. & Sánchez-Fauquier., 2003. Viruses causing gastroenteritis. *Clinical Microbiology and Infection*, 9 (4), pp.247–262.

Wingfield, P.T., 2001. Protein precipitation using ammonium sulphate. *Current Protocols of Protein Science,* Appendix 3F

Xue, M., Yu, L., Che, T., Lin, H., Zeng, Y., Fang, M., Li, T., Ge, S, & Xia, N., 2015. Characterization and protective efficacy in an animal model of a noveltruncated rotavirus VP8 subunit parenteral vaccine candidate. *Vaccine*, 33, pp.2606-2613.

Zaman, K., Dang, D.A., Victor, J.C., Shin, S., Yunus, M., Dallas, M.J., Podder, G., Vu, D.T., Le, T.P., Luby, S.P., Le, H.T., Coia, M.L., Lewis, K., Rivers, S.B., Sack, D.A., Schodel, F., Steele, A.D., Neuzil, K.M. & Ciarlet, M., 2010. Efficacy of pentavalent rotavirus vaccine against severe rotavirus gastroenteritis in infants in developing countries in Asia: a randomised, double-blind, placebo-controlled trial. *Lancet*, 376 (9741), pp.615–623.

Zárate, S., Cuadras, M.A., Espinosa, R., Romero, P., Jua´rez, K.O., Camacho-Nuez, M., Arias, C.F. & Lo´pez, S., 2003. Interaction of rotaviruses with Hsc70 during cell entry is mediated by VP5. *Journal of virology*, 77 (13), pp.7254–7260.

Zeng, C.Q.Y., Estes, M.K., Charpilienne, A. & Cohen J., 1998. The N terminus of rotavirus VP2 is necessary for encapsidation of VP1 and VP3. *Journal of virology*, 72 (1), pp.201–208.

Zhang, Q., Lu, W. & Hua, Z., 2017. Expression, purification, and characterization of recombinant 8 kDa gelsolin fragment. *Protein Expression and Purification,* 135, pp.33-36

Zhao, Q., Chen, W., Chen, Y., Zhang, L., Zhang, J. & Zhang, Z., 2011. Self-assembled virus-like particles from rotavirus structural protein VP6 for targeted drug delivery. *Bioconjugate Chemistry*, 22, pp.346-352.

Chapter 7: Appendices

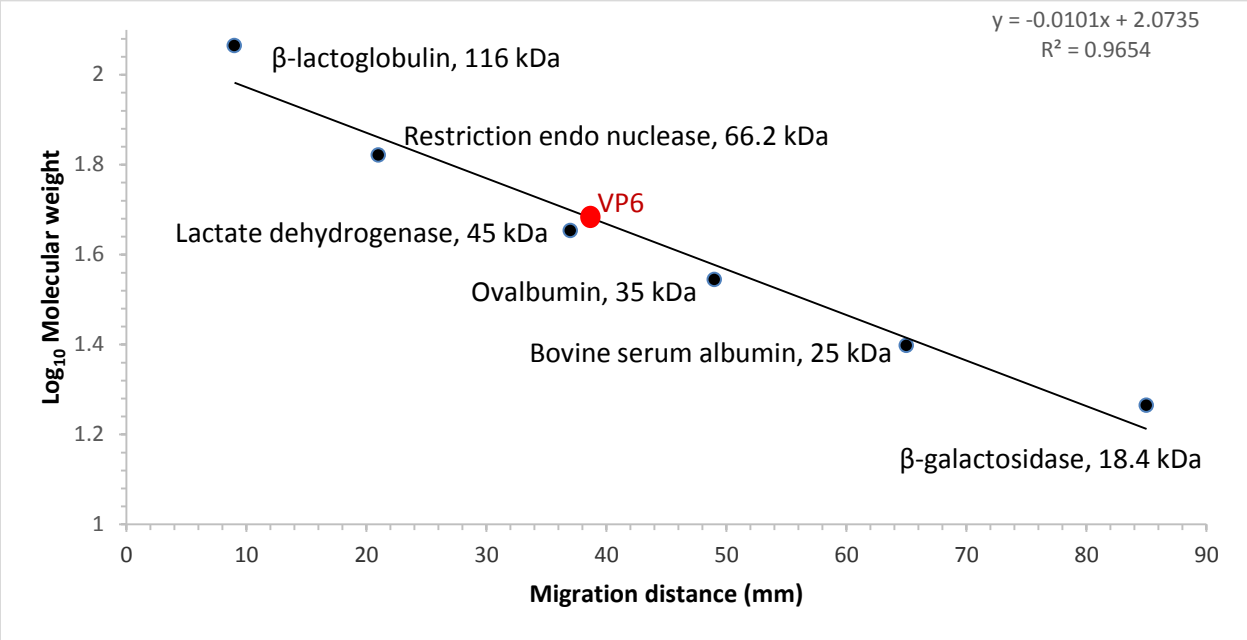

Appendix A: SDS-PAGE analysis of VP6

The calibration curve was used to calculate VP6's molecular weight which was found to be 50.12 kDa based on the straight line fit y = -0.0101x + 2.0735. This analysis is an example of how VP6's size was calculated from all SDS-PAGE gels.

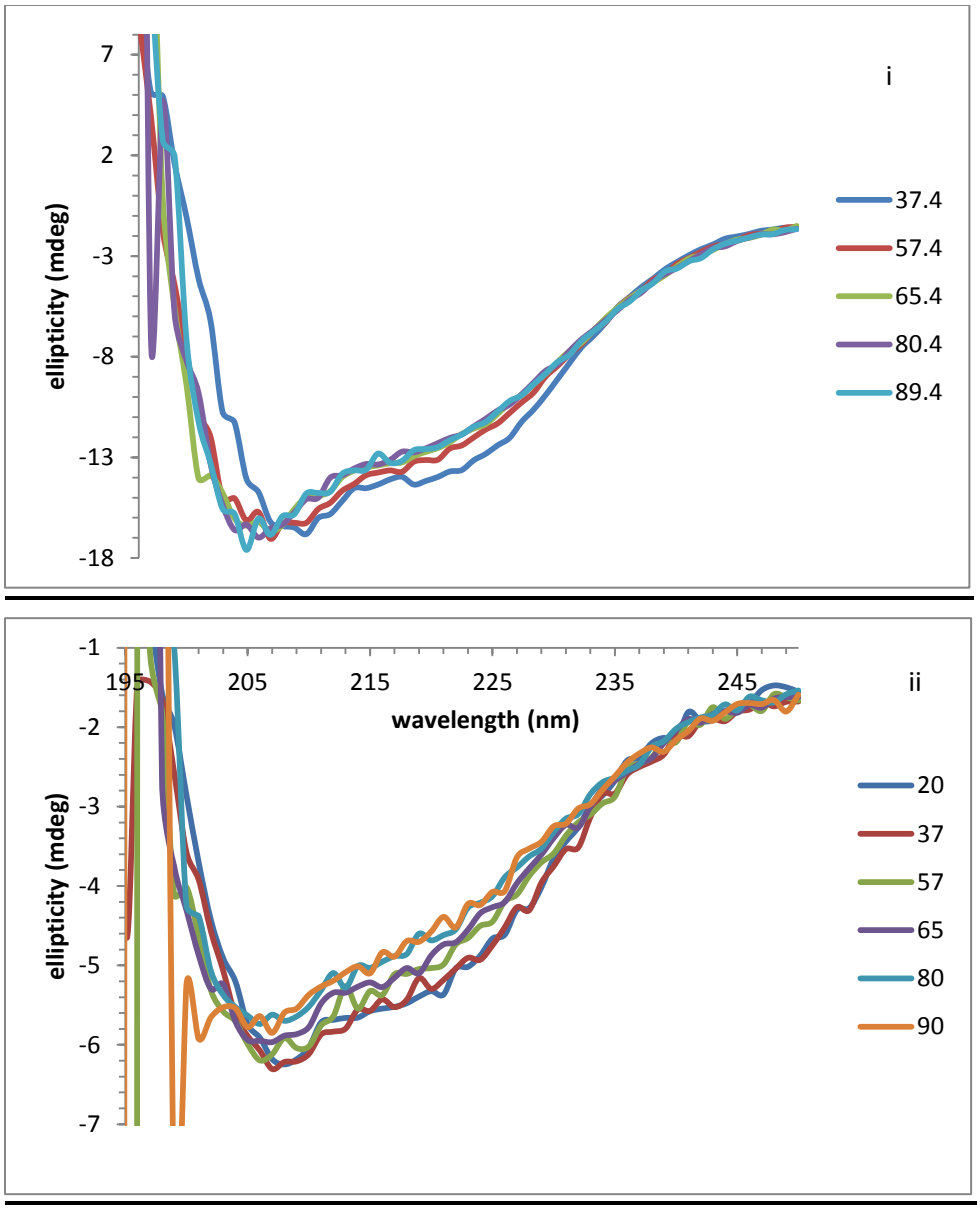

Appendix B: Circular dichroism during thermal unfolding of VP6

i. Far-UV circular dichroism spectrum recorded from 20ºC to 90ºC on 1 µM VP6 in 0.02 M sodium phosphate buffer, pH 7.04 containing 0.02 M sodium chloride. ii. Far-UV circular dichroism spectrum recorded from 20ºC to 90ºC on 0.35 µM VP6 in 0.02 M sodium phosphate buffer, pH 7.04 containing 0.2 M sodium chloride.

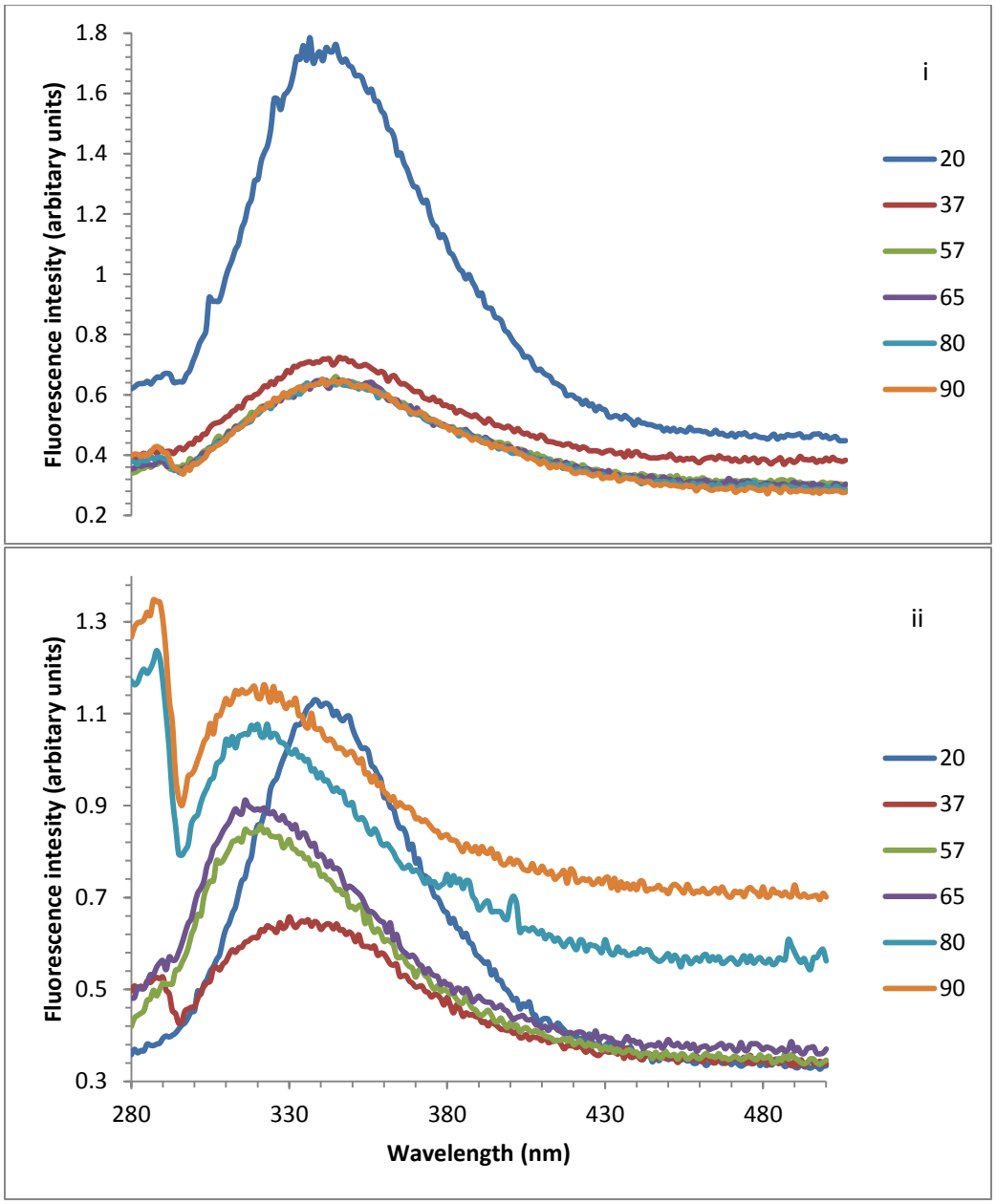

Appendix C: Fluorescence thermal unfolding of VP6 excited at 280 nm

Individual temperature spectra are selectively indicated between 20°C and 90°C, with each temperature having a fluorescence spectra read from 500 nm to 280 nm. i. Data was collected using 0.78 µM VP6 in 0.02 M sodium phosphate buffer, pH 7.04 containing 0.02 M sodium chloride. ii. Data was collected using 0.35 µM VP6 in 0.02 M sodium phosphate buffer, pH 7.04 containing 0.2 M sodium chloride.

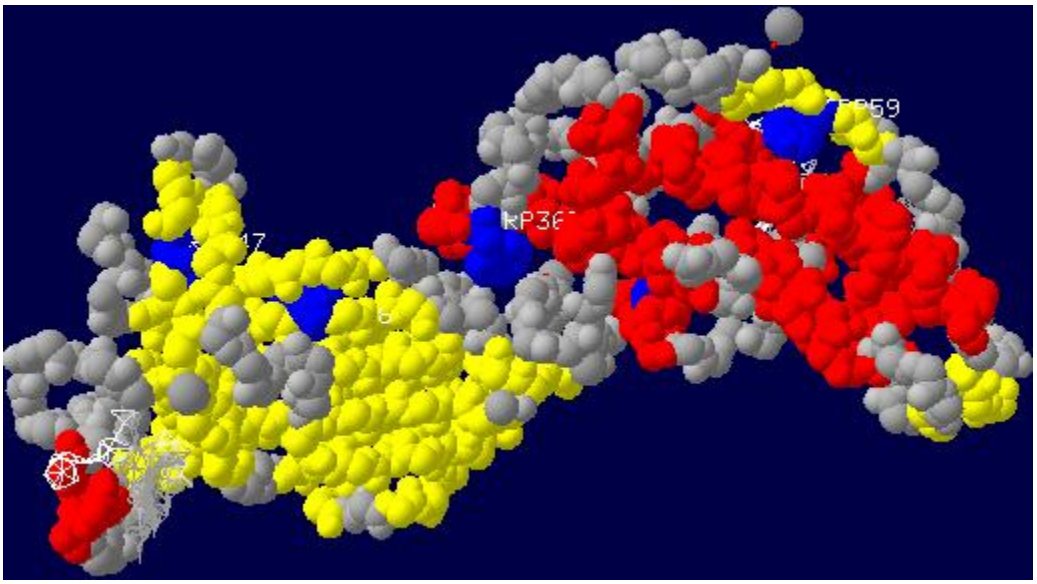

Appendix D: Globular diagram of rotavirus VP6

The 3-D globular structure of a rotavirus VP6 monomer was generated as part of the current study. VP6 comprises of five tryptophan residues (blue globules) (Mathieu *et al.* 2001). Image was generated using Swiss PDB Viewer (version 4.1.0) [Guex and Peitsch, 1997], from a rotavirus VP6 protein, PDB code: 1QHD.